Mario Mitter

Matrikelnr.: 0412516

Phases of Strongly-Interacting Matter
with Functional Methods

Dissertation

zur Erlangung des Doktorgrades der Naturwissenschaften

verfasst am Institut für Physik - FB Theoretische Physik
der Karl-Franzens-Universität Graz

Betreuer: Univ.-Prof. Dr.rer.nat. Reinhard Alkofer

Priv.-Doz. Dr.rer.nat. Bernd-Jochen Schaefer

November, 2012

Präambel

Ich, Mario Mitter, bestätige hiermit, dass die vorliegende Arbeit von mir selbstständig und unter Zuhilfenahme ausschließlich der angegebenen Hilfsmittel verfasst wurde.

Graz, im November 2012

Contents

CONTENTS

1. Introduction

It is a truth universally acknowledged, that Quantum Chromodynamics (QCD) is the theory of the strong interaction [1]. Its fundamental degrees of freedom are quark and gluon fields and it describes phenomena ranging from the formation of nucleons (protons and neutrons) in subatomic physics to neutron stars in astrophysics. QCD is a non-Abelian gauge theory, i.e., it is a relativistic quantum field theory (QFT) [2] with a local gauge symmetry as in electrodynamics. In contrast to the latter, its gauge group, $SU(3)$, is not commutative. This leads to self-interactions of the gauge fields which also carry the corresponding charge called color. Therefore, already the pure gauge theory without quarks is non-trivial, which is true for any non-Abelian gauge theory with general gauge group $SU(N)$ - called Yang-Mills theory. The interaction strength of such a Yang-Mills theory is described by a single gauge coupling g or, equivalently, $\alpha \equiv g^2/4\pi$ [3]. The strength of this interaction depends on the scale μ the theory is probed at, which leads to a scale-dependent or running gauge coupling $g(\mu)$. It is possible to describe the running coupling g by its beta function which only depends on g [1]

$$\mu \frac{d}{d\mu} g(\mu) = \beta(g) \ .$$

(1.1)

At small coupling g, the interaction can be treated as a perturbation. This allows the calculation of the beta function, which is found to be negative for QCD. Hence, when starting from a small value g and going to higher μ, the value of g will become even smaller. Therefore the interaction becomes very weak at small distances [4,5]. This asymptotic freedom of QCD is not spoiled as long as the number of quark flavors, N_f, does not exceed 33/2. On the other hand, perturbation theory predicts its own failure when going to large distances, as this implies a growing coupling constant. As soon as the coupling takes values of order unity, perturbation theory is not applicable anymore. The scale where the perturbative running coupling diverges is usually termed Λ_{QCD}. Its exact value depends e.g. on the renormalization scheme and the matter content and is given by $\Lambda_{QCD} \approx 200$ MeV in the modified MS scheme [6].

From this discussion it is clear that investigations of long range phenomena [2] require usually other methods than perturbation theory. Two very prominent properties of non-perturbative QCD - which also play a central role in this thesis - shall briefly be sketched.

Although QCD is formulated in terms of quark and gluon fields, no experiment has ever measured the corresponding particle excitations. The only thing observed in Nature are hadrons. These are colorless bound states of either a quark-antiquark pair (mesons) or three quarks (baryons). Other conceivable colorless excitations would be given by glueballs, but no unambiguous signs have been found in any experiments up to now. The absence of quarks

---

[1] In general, in presence of massive particles with mass m that interact with the gauge field, this is only true for $\mu \gg m$ [3].

[2] Here long range is meant in comparison to QCD scales, where momenta around $\Lambda_{QCD} = 200$ MeV correspond to 10^{-15} m.

and gluons from the particle spectrum, i.e. their confinement to hadrons is one of the main features of QCD, which is yet to be fully understood [7].

Quarks are described by Dirac spinors which would obey the Dirac equation in a quantum mechanical treatment. As in the Dirac equation, helicity becomes a good quantum number for massless quarks. In this case the theory becomes chirally symmetric before quantum fluctuations are taken into account. If chiral symmetry were also respected by the ground state of QCD, one would obtain parity partners for any hadron in the spectrum of QCD. Experimentally these parity partners are not found [8], which leads to the conclusion that the ground state does not respect the full symmetry. Therefore chiral symmetry is spontaneously broken, which implies the existence of massless bosons via Goldstone's theorem [9–11]. In nature, this symmetry is only approximate with the pions, kaons and η-meson as pseudo Goldstone bosons [3].

Confinement and spontaneous chiral symmetry breaking are not necessarily realized at very high-temperatures as e.g. prevalent at times shortly after the big bang. Temperature corresponds to energy and at sufficiently high temperatures one could expect a phase of quarks and gluons without spontaneous chiral symmetry breaking. By now it is clear from numerical simulations of QCD on discrete space-time lattices that a similar state is actually reached at temperatures $T \gtrsim 150$ MeV, which is termed quark-gluon plasma [12].

This thesis is mainly concerned with confinement and chiral symmetry breaking, especially at non-vanishing temperatures. These and related features are discussed in more detail in Ch. 2, which provides the context and relevant basics for the self-contained investigations in the subsequent chapters.

In Ch. 3 a special type of infrared singularity is assumed in the quark-antiquark interaction kernel. Such a singularity can be related to confinement in terms of a linearly rising potential. Consequences as well as consistency of this singularity are investigated.

A scalar version of QCD is used in Ch. 4 to investigate the center symmetry transition. Confinement of fundamentally charged matter can be related to this symmetry and a phase of spontaneously broken center symmetry corresponds to deconfinement. Order parameters for the transition are constructed from the scalar as well as the quark propagator and applied in numerical calculations.

The chiral transition to the phase of restored chiral symmetry is examined in an effective description in terms of quark and meson degrees of freedom with the functional renormalization group in Ch. 5. Special focus is put on the chiral anomaly in terms of a 't Hooft determinant, which plays a crucial role in the limit of vanishing quark masses. Additionally, the anomalous mass of the η'-meson is calculated at finite temperature.

The results are summarized at the and of each chapter. Additionally, a general conclusion together with an outlook for future investigations is given in Ch. 6. Conventions, lengthy calculations and numerical details have been put in the appendices A, B and C.

2. Strongly-Interacting Matter

Aspects of strongly-interacting matter as relevant for this thesis are discussed in this chapter. The main purpose of this discussion is to put the more special topics of the upcoming chapters into context. The first section is focused on non-perturbative properties of strongly-interacting matter at vanishing temperatures, which includes a brief discussion of some appropriate methods. In the second section, some aspects of Quantum Chromodynamics (QCD) at non-vanishing temperature and chemical potential are briefly touched upon. None of the material covered in this chapter is the work of the author and references are given either to reviews and textbooks for well-established topics or original literature where appropriate.

2.1. Non-Perturbative Quantum Chromodynamics

In order to accurately describe the physics of strongly-interacting matter it is necessary to use appropriate tools. Some of these will be briefly discussed in Sec. 2.1.1, before going on to QCD in Sec. 2.1.2 and effective descriptions of strongly-interacting matter in Sec. 2.1.3.

2.1.1. Quantum Field Theory with Non-Perturbative Methods

It has been argued in the introduction that an investigation of Quantum Chromodynamics close to, as well as below, its characteristic scale Λ_{QCD} requires non-perturbative methods due to the large (perturbative) running coupling. Here only a selection of non-perturbative approaches as relevant for the topics treated in this thesis shall be discussed.

In principle a quantum field theory is defined, as well as solved, if all its n-point functions [1] are known. The n-point functions are the vacuum expectations values of time-ordered products of n fields [2] present in the theory. Here, the vacuum is given by the ground state of the theory transforming trivially under the Poincaré group. Examples for important n-point functions of QCD are given by the gluon, ghost and quark propagators - which are 2-point functions - and the three-gluon, ghost-gluon and quark-gluon vertices - which are 3-point functions. There exist several hierarchies of n-point functions - including the full (time-ordered), the connected and the 1-particle irreducible (1PI) n-point functions. In this thesis the latter will be used almost exclusively. It has been shown in an axiomatic approach that from any of the equivalent hierarchies of n-point functions one can reconstruct the full quantum field theory, if some additional assumptions are fulfilled [13, 14].

---

[1] Although the term function is used frequently, the n-point functions are actually tempered distributions which are linear functionals defined on Schwartz space over $\mathbb{R}^{dn}$, where d is the number of space-time dimensions [13].

[2] The fields are operator valued distributions defined on d-dimensional space-time $\mathbb{R}^d$. This implies that their product is not necessarily well-defined on a single point, which reappears later as the need for regularization and renormalization of divergences at large momenta in the case of $d = 4$.

2. Strongly-Interacting Matter

It is useful to introduce generating functionals for these n-point functions, where the full n-point functions $G^{(n)}$ are obtained from [3]

$$Z[j] = \sum_n \frac{1}{n!} \int\limits_{x_1,\ldots,x_n \in \mathbb{R}^d} G^{(n)}(x_1,\ldots,x_n) j(x_1) \cdots j(x_n) \,. \tag{2.1}$$

If this generating functional were known, one could get the n-point functions as the kernels of the corresponding n^{th} (Fréchet) derivative evaluated at $j = 0$

$$G^{(n)}(x_1,\ldots,x_n) = \left. \frac{\delta^n}{\delta j(x_1) \cdots \delta j(x_n)} Z[j] \right|_{j=0} \,. \tag{2.2}$$

Therefore, a quantum field theory can be defined non-perturbatively by giving its generating functional. One way of doing so is via the path integral [2]

$$Z[j] = \int \mathscr{D}\phi \, \exp\left[iS[\phi] + \int\limits_{x \in \mathbb{R}^d} \phi(x) j(x) \right] \,, \tag{2.3}$$

where ϕ denotes the complete, c-numbered field content of the theory and S is the classical action. The path integral requires integration over all fields ϕ, which is denoted by the "measure" $\mathscr{D}\phi$, where a proper normalization has been assumed to be included in its definition. As the exponent $iS[\phi]$ leads to a highly oscillatory integrand, any attempts of solving the path integral use a Euclidean formulation [15]. This can be obtained by replacing the time coordinate x^0 with imaginary time $-ix^d$. Starting from a metric with signature $(1, -1, \ldots, -1)$ in Minkowski space one arrives at a completely negative Euclidean metric and the Euclidean generating functional is given by

$$Z_E[j] = \int \mathscr{D}\phi \, \exp\left[-S_E[\phi] + \int\limits_{x \in \mathbb{R}^d} \phi(x) j(x) \right] \,. \tag{2.4}$$

The Euclidean action S_E is positive definite and one stands a chance of defining a proper measure (at least) in this formulation. Of course, this generating functional also yields Euclidean n-point functions and it is necessary to define a procedure for regaining the theory in Minkowski space. It was found by Osterwalder and Schrader that there exists a set of assumptions for the Euclidean n-point functions which, if fulfilled, allow the reconstruction of the quantum field theory in Minkowski space-time [16, 17]. Such an imaginary time formulation is well-suited for investigations of ground state properties, whereas investigations of time-dependent phenomena are hard. As will become clear in Sec. 2.2, it is also straightforwardly generalized to finite temperature and equilibrium thermodynamics, which will be the main concern in this thesis. With this motivation, the Euclidean formulation will be used exclusively in the remainder of this thesis and the subscripts E will be dropped from now on. Unfortunately all rigorous attempts have found that for $d = 4$ only free theories can be defined in terms of the path integral without regularization and renormalization [15]. The

---

[3]Whenever the measure dx is not shown explicitly, the ordinary Lebesgue measure is assumed.

corresponding divergences that need regularization usually appear at very small distances. One straightforward way of regularization is to replace continuous space-time by a discrete lattice. In case of the strong interaction the corresponding field is called lattice QCD [18–23] which is one important non-perturbative approach. In lattice QFT $\mathscr{D}\phi$ is replaced by a product of ordinary integrals on each of the lattice sites with the goal of taking a well-defined continuum limit of vanishing lattice spacing a. In practice this amounts to showing independence of the obtained results from a for small enough lattice spacings. One obstacle in a direct evaluation of these multi-dimensional integrals is the fast growth of the computational effort with the number of lattice sites. Therefore, so-called Monte-Carlo methods are employed with the basic idea of approximating the expectation value of some random variable f with probability measure $\rho(x)$ on $[a,b]$ by a sum

$$\langle f \rangle = \int\limits_{x \in [a,b]} \rho(x)f(x) = \lim_{N \to \infty} \sum_{i=1}^{N} f(x_i) \ . \tag{2.5}$$

Here, it is necessary that the x_i are chosen randomly on $[a,b]$ with a probability corresponding to the measure $\rho(x)$. Choosing such randomly distributed x_i is a subject of its own, where often Metropolis algorithms [23] are applied. A signed or even complex measure $\rho(x)$ will lead to fluctuations which severely limit the applicability of the Monte-Carlo methods. In case of lattice QFT it is therefore preferable to have a positive definite measure $\exp[-S[\phi]]$ with $\S[\phi] \in \mathbb{R}$. Another relevant issue is the discretization of the action S, which defines the probability measure. The action usually involves derivatives, which have to be approximated. Furthermore, modern physical theories are constructed with the help of symmetries, which sometimes cannot be implemented uniquely such that the original symmetry is obtained in the continuum limit $a \to 0$. Nevertheless, lattice methods provide a powerful tool for the calculation of the expectation value of any observable $\mathcal{O}[\phi]$ via

$$\langle \mathcal{O}[\phi] \rangle = Z[0]^{-1} \int \mathscr{D}\phi \, \mathcal{O}[\phi] \exp\left[-S_E[\phi]\right] \ . \tag{2.6}$$

In particular this yields the n-point functions. In gauge theories, the evaluation of propagators and the like additionally requires gauge fixing, since all gauge-dependent quantities vanish without choosing a gauge.

Another approach is to use a continuum formulation and derive the defining equations for the n-point functions from the path integral. After a short detour via the effective action, two examples of the latter possibility will be introduced in the following.

Effective Action

Instead of the generating functional $Z[j]$ for the full n-point functions $G^{(n)}$ it is also possible to use its connected or 1PI counterpart. By the linked cluster theorem [14], the generating functional for the connected n-point functions is given by

$$W[j] = \log Z[j] \ , \tag{2.7a}$$

2. Strongly-Interacting Matter

$$W^{(n)}(x_1, \ldots, x_n) = \left. \frac{\delta^n}{\delta j(x_1) \cdots \delta j(x_n)} W[j] \right|_{j=0} . \tag{2.7b}$$

Via a Legendre transform, the effective action - the generating function of the 1PI n-point functions - can be obtained

$$\Gamma[\phi_{cl}] = \sup_j \left(-W[j] + \int_{x \in \mathbb{R}^d} \phi_{cl}(x) j(x) \right) , \tag{2.8a}$$

$$\Gamma^{(n)}(x_1, \ldots, x_n) = \left. \frac{\delta^n}{\delta \phi_{cl}(x_1) \cdots \delta \phi_{cl}(x_n)} \Gamma[\phi_{cl}] \right|_{\phi_{cl}[j=0]} . \tag{2.8b}$$

In the second line it has been assumed that for any ϕ_{cl} there is a unique j which maximizes the right hand side of Eq. (2.8a). By additionally assuming convexity and differentiability, this relation is explicitly given by

$$\phi_{cl}[j] = \frac{\delta}{\delta j} W[j] . \tag{2.9}$$

Using Eq. (2.7a), one obtains immediately $\phi_{cl}[0] = \langle \phi \rangle$. Inverting Eq. (2.9) allows to express the effective action as

$$\Gamma[\phi_{cl}] = -W[j[\phi_{cl}]] + \int_{x \in \mathbb{R}^d} \phi_{cl}(x) j[\phi_{cl}](x) , \tag{2.10}$$

with derivative

$$\frac{\delta}{\delta \phi_{cl}} \Gamma[\phi_{cl}] = j[\phi_{cl}] . \tag{2.11}$$

Therefore the effective action is stationary in the absence of currents, i.e. at $\phi_{cl}[j=0]$, which justifies its name. Important relations between connected and 1PI n-point functions can be derived by differentiation of Eq. (2.9), yielding e.g.

$$D(x_1, x_2) \equiv W^{(2)}(x_1, x_2) = \left(\Gamma^{(2)} \right)^{-1} (x_1, x_2) , \tag{2.12a}$$

$$W^{(3)}(x_1, x_2, x_3) = \int_{y_1, y_2, y_3 \in \mathbb{R}^d} D(x_1, y_1) D(x_2, y_2) D(x_3, y_3) \Gamma^{(3)}(y_1, y_2, y_3) , \tag{2.12b}$$

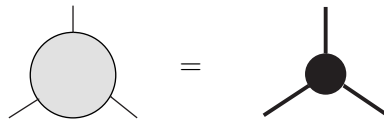Diagrammatically, the second relation can be represented as

Figure 2.1.: Relation between connected and 1PI 3-point function.

where gray blobs represent connected vertices, black dots represent 1PI vertices and thick lines represent the dressed propagator D. When connected to a vertex, thin lines represent the corresponding argument of the leg, whereas thin lines that stand alone or connect vertices represent the bare propagator defined by

$$D_0(x_1, x_2) \equiv \frac{\delta^2}{\delta\phi(x_1)\delta\phi(x_2)} S[\phi] \Big|_{\phi=0} . \tag{2.13}$$

One important quantity that can be derived from the effective action is the effective potential. For constant $\bar{\phi} \equiv \phi_{cl}$, the effective potential is defined as the function

$$U(\bar{\phi}) = \frac{\Gamma[\bar{\phi}]}{V_d} , \tag{2.14}$$

where V_d is the volume of d-dimensional space-time. Via variational methods one can show that this effective potential is the minimum of the expectation value of the energy density over all states Ω with field expectation value $\bar{\phi} = \langle \Omega, \phi\Omega \rangle$ [3]. This implies that the vacuum state minimizes the effective potential in the absence of currents.

Dyson-Schwinger Equations

The Dyson-Schwinger equations (DSEs) [24–29] are the equations of motion for the n-point functions. They provide an infinite set of coupled non-linear integral equations. The set of DSEs can be formulated for any hierarchy of n-point functions and the corresponding equations are usually obtained from some generating relation. The fastest way of obtaining this generating equation for the full n-point functions is via the generalized divergence theorem

$$0 = \int \mathscr{D}\phi \frac{\delta}{\delta\phi} \exp\left[-S[\phi] + \int_{x\in\mathbb{R}^d} \phi(x)j(x) \right] , \tag{2.15}$$

which works, if the integrand vanishes at the boundary of integration. In a compact notation this relation and the corresponding generating equations for connected and 1PI n-point functions can be written as [28]

$$0 = \left(-\frac{\delta S}{\delta\phi}\left[\frac{\delta}{\delta j}\right] + j \right) Z[j] , \tag{2.16a}$$

$$0 = -\frac{\delta S}{\delta\phi}\left[\frac{\delta W}{\delta j} + \frac{\delta}{\delta j}\right] + j , \tag{2.16b}$$

$$0 = \frac{\delta\Gamma}{\delta\phi_{cl}} - \frac{\delta S}{\delta\phi}\left[\phi_{cl} + W^{(2)}[j[\phi_{cl}]]\frac{\delta}{\delta\phi_{cl}}\right] + j[\phi_{cl}] . \tag{2.16c}$$

From either of these relations the equation for a specific n-point function can be obtained by $n-1$ functional differentiations and setting $j = 0$ or $\phi_{cl} = \phi_{cl}[j = 0]$ at the end.

The prototype of all DSEs is the one for the propagator. It is obtained from the functional

derivative of Eq. (2.16a) with respect to j at $j = 0$

$$0 = \int \mathscr{D}\phi \left(-\frac{\delta S}{\delta \phi(x)} \phi(y) + \delta^{(d)}(x-y) \right) \exp\left[-S[\phi] \right] , \qquad (2.17)$$

where x and y are generalized indices. Writing the action in terms of the bare propagator D_0 and an interaction term S_I as

$$S[\phi] = \frac{1}{2} \int\limits_{x,y\in\mathbb{R}^d} \phi(x) D_0^{-1}(x,y)\phi(y) + S_I[\phi] , \qquad (2.18)$$

allows to rewrite the DSE as

$$\delta^{(d)}(x-y) = \int\limits_{z\in\mathbb{R}^d} D_0^{-1}(x,z)\langle\phi(z)\phi(y)\rangle + \left\langle \frac{\delta S_I[\phi]}{\phi(x)}\phi(y) \right\rangle . \qquad (2.19)$$

Assuming that the 1-point function vanishes, i.e. $\langle\phi\rangle = 0$, the propagator is given by

$$D(x,y) = \langle\phi(x)\phi(y)\rangle . \qquad (2.20)$$

Multiplying Eq. (2.19) with the inverse propagator results in the corresponding DSE

$$D^{-1}(x,y) = D_0^{-1}(x,y) + \int\limits_{z\in\mathbb{R}^d} \left\langle \frac{\delta S_I[\phi]}{\phi(x)}\phi(z) \right\rangle D^{-1}(z,y) . \qquad (2.21)$$

The second term in this equation is the self-energy that provides all quantum corrections to the bare inverse propagator $D_0^{-1}(x,y)$. Obviously, the exact form of the self-energy term depends on the interactions present. If $S_I \neq 0$, it is at least cubic in the fields and therefore the self-energy term involves at least 3-point functions. This is an explicit example of the general dependence of DSEs on higher n-point functions.

Before going on, some general aspects of the DSEs shall be mentioned. As demonstrated by the propagator equation Eq. (2.21), the DSE for some n-point function will depend in general also on m-point functions with $m > n$. Furthermore, already the self-energy in the propagator DSE can include two-loop contributions. When deriving the equation for higher n-point functions, the order of differentiation of Eq. (2.16) is not unique, which can lead to different versions of the Dyson-Schwinger equations. The solution can, however, not depend on the formulation of the DSE and has to fulfill all equations. The different versions of the DSE for some n-point function will in general depend on different higher m-point functions $m > n$, which can be used to minimize truncation errors in numerical investigations. The Dyson-Schwinger equations contain bare vertices (see App. A.3 for their definition) and therefore the introduction of renormalization constants is necessary in general. Although the equations as such are fully non-perturbative, the renormalization procedure of the DSEs is close to perturbative renormalization in spirit. Additionally, from the appearance of the bare action in the defining Eq. (2.16), the treatment of quantum field theories which are only non-perturbatively renormalizable is at least hard, as the prior knowledge of the non-perturbative action would be required. On the other hand, the DSEs wash out truncation errors via the integration, which makes them eventually robust against approximations.

Functional Renormalization Group (FRG)

The renormalization group approach in the Wilsonian sense [30] integrates the path integral not in one big step, but in infinitesimal momentum shell contributions. In its original formulation this leads to an effective measure $\exp[-S_{eff}]$ for the integration of fields with non-vanishing Fourier modes only below some scale k. Therefore, S_{eff} can in principle be obtained from the bare theory by the integration of all Fourier modes larger than this scale k. The momentum shell approach to the renormalization group has been realized in a variety of ways [31–52].

In this thesis, Wetterich's formulation for the effective average action is used, which turns out to be especially well suited in numerical applications. It is formulated for the effective average action $\Gamma_k[\phi_{cl}]$, which additionally depends on the scale k. This scale indicates, which quantum fluctuations have been integrated already. The Wetterich equation describes the evolution of this effective average action when integrating an infinitesimal momentum shell by the flow $\partial_k \Gamma_k[\phi_{cl}]$. In the limit $k \to 0$ all quantum fluctuations are integrated and the effective action is approached

$$\Gamma[\phi_{cl}] = \lim_{k \to 0} \Gamma_k[\phi_{cl}] \ . \tag{2.22}$$

In principle a theory is therefore defined by its initial action $\Gamma_{\Lambda \to \infty}$, which together with the flow equation defines a trajectory in the space of all possible theories. This trajectory connects the initial action at $k = \Lambda \to \infty$ with the full quantum effective action at $k \to 0$.

Predictivity of the theory demands that the definition of the initial action can be given with the help of a finite number of parameters. This can be achieved, if the flow is characterized by some fixed point Γ^*

$$\partial_k \Gamma^*[\phi_{cl}] = 0 \ . \tag{2.23}$$

In general the space of all theories is highly non-trivial. Nevertheless, it will be assumed for the following argument that a basis can be chosen, which allows an expansion of Γ_k with a set of coefficients $\{g_i\}$ at least close to this fixed point. From the corresponding beta functions

$$\beta_j(\{g_i\}) \equiv k \partial_k g_j \ , \tag{2.24}$$

one can define a new basis, given by the eigenvectors of the stability matrix $\partial_{g_l} \beta_j(\{g_i^*\})$ at the fixed point $\{g_i^*\}$. The corresponding eigenvalues can furthermore be used to classify these eigenvectors into relevant (negative eigenvalue) and irrelevant (positive eigenvalue) operators [4]. In many cases, one can define the critical surface as the set of all actions that flow into the fixed point. The tangent space to this critical surface at the fixed point is then spanned by the irrelevant operators. Suppose that the above fixed point is actually the Gaussian fixed point corresponding to the free theory. In a perturbatively renormalizable theory, the relevant operators are then given exactly by the renormalizable interactions. Assume that one starts with some arbitrary initial action Γ_Λ, which might also include non-renormalizable/irrelevant couplings at large Λ. If the corresponding flow is still governed by the Gaussian fixed point, the non-renormalizable/irrelevant couplings will gradually die

---

[4]There exist also the possibility of a marginal operator (vanishing eigenvalue), which will be ignored in the following discussion.

out and only the renormalizable couplings survive. Therefore, the theory at scales $k \ll \Lambda$ is characterized only by a finite number of renormalizable couplings, as demanded by predictivity. In general it is necessary to start with an action Γ_Λ that lies in the basin of attraction of some fixed point with a finite number of relevant directions. When choosing an inital action Γ_Λ that is very close to such a critical surface, the flow will almost reach the fixed point before it is pushed into the subspace spanned by the relevant directions. Therefore any information about the irrelevant directions is lost and the theory is predictive. Obviously, this implies that the flow cannot be inverted, and therefore the renormalization group can at most be a semi-group.

In Wetterich's equation, a suppression of the integration of modes below some scale k is introduced by adding an additional term $\Delta S_k[\phi]$ in the measure

$$W_k[j] = \ln \int \mathscr{D}\phi \, \exp \left[-S_E[\phi] - \Delta S_k[\phi] + \int_{x \in \mathbb{R}^d} \phi(x) j(x) \right] . \tag{2.25}$$

Taking the additional term to be bilinear in ϕ it can be written as

$$\Delta S_k[\phi] = \frac{1}{2} \int_{x,y \in \mathbb{R}^d} \phi(x) R_k(x,y) \phi(y) . \tag{2.26}$$

By choosing the regulator function R_k in momentum space to be large at momenta $p \ll k$ and zero at $p \gg k$, an effective mass is introduced which leads to a decoupling of the low momentum modes [53]. A typical example for the regulator is shown in Fig. 2.2.
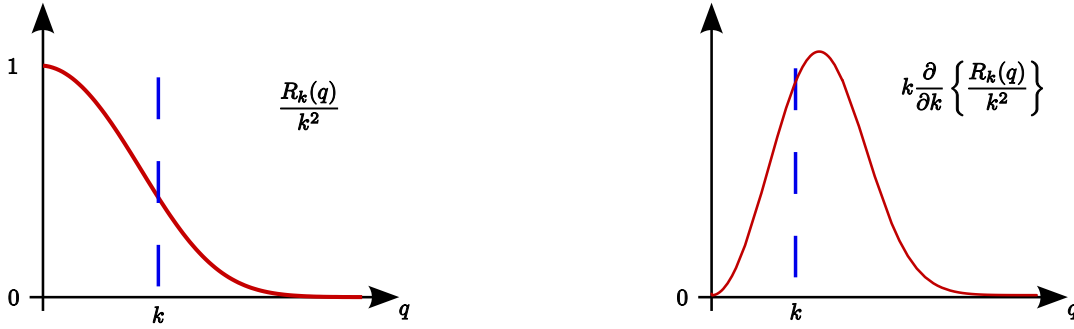

Figure 2.2.: Typical form of the regulator function R_k and its derivative (picture from [54]).

Therefore when performing the path integral, only modes with large momenta above $\sim k$ are integrated.

The (not necessarily convex) effective average action is defined as the modified Legendre transform

$$\Gamma_k[\phi_{cl}] = -W_k[j_k[\phi_{cl}]] + \int_{x \in \mathbb{R}^d} \phi_{cl}(x) j_k[\phi_{cl}](x) - \Delta S_k[\phi_{cl}] , \tag{2.27}$$

where the now k-dependent relation between ϕ_{cl} and j is again provided by the stationarity

condition

$$\phi_{cl,k}[j] = \frac{\delta W_k[j]}{\delta j} = \langle \phi \rangle_{k,j} \ . \tag{2.28}$$

Here, the trivial generalization of the expectation value Eq. (2.6) with non-vanishing source j and Eq. (2.25) is indicated by the subscript k, j. Therefore the flow of the effective action is given by

$$\begin{aligned}
\partial_k \Gamma_k[\phi_{cl}] &= -\partial_k W_k[j_k[\phi_{cl}]] - \partial_k \Delta S_k[\phi_{cl}] \\
&= \frac{1}{2} \int_{x,y \in \mathbb{R}^d} \left(\langle \phi(x)\phi(y) \rangle_{k,j_k[\phi_{cl}]} - \phi_{cl}(x)\phi_{cl}(y) \right) \partial_k R_k(x,y) \\
&= \frac{1}{2} \int_{x,y \in \mathbb{R}^d} W_k^{(2)}[j_k[\phi_{cl}]](y,x) \partial_k R_k(x,y) \ .
\end{aligned} \tag{2.29}$$

In the first line the cancellation of the derivatives $\partial_k j_k$, and in the second line $\phi_{cl} = \langle \phi \rangle_{k,j_k[\phi_{cl}]}$ together with

$$W_k^{(2)}[j] = \langle \phi\phi \rangle_{k,j} - \langle \phi \rangle_{k,j} \langle \phi \rangle_{k,j} \ , \tag{2.30}$$

and symmetry of R_k have been used. From Eq. (2.27) one obtains the generalization of Eq. (2.12a)

$$\begin{aligned}
W_k^{(2)}[j_k[\phi_{cl}]] &= \left(\frac{\delta^2}{\delta \phi_{cl} \delta \phi_{cl}} \left(\Gamma_k[\phi_{cl}] + \Delta S_k[\phi_{cl}] \right) \right)^{-1} \\
&= \left(\Gamma_k^{(2)}[\phi_{cl}] + R_k \right)^{-1} \ ,
\end{aligned} \tag{2.31}$$

and the resulting Wetterich equation [37] is given by

$$\partial_k \Gamma_k[\phi_{cl}] = \frac{1}{2} \, \mathrm{Tr} \left[\left(\Gamma_k^{(2)}[\phi_{cl}] + R_k \right)^{-1} \partial_k R_k \right] \ . \tag{2.32}$$

Diagrammatically this is often written as

$$\partial_k \Gamma_k[\phi_{cl}] \ = \ \frac{1}{2} \quad \bigcirc\!\!\!\!\otimes \quad ,$$

where the crossed circle represents $\partial_k R_k$ and the thick line stands for the partially dressed propagator. The trace has to be taken over continuous as well as possible discrete arguments. If more than one field type is present, the trace additionally includes a sum over the corresponding field types. If a given particle is not its antiparticle, the corresponding generalizations of the mass term Eq. (2.26) and relation Eq. (2.30) have to be used.

It is hard to solve the Wetterich equation Eq. (2.32) exactly due to the presence of func-

tional derivatives and usually truncations have to be employed. By functional differentiation and inserting $\phi_{cl,k}[j = 0]$ one obtains furthermore the flow equations for the higher n-point functions. It is clear that the equation for some n-point function will in general depend on m-point functions up to $m \leq n + 2$. Therefore the system never closes, as in case of the Dyson-Schwinger equations. In contrast to the DSEs, the equation has one-loop structure - also for higher n-point functions - but is not of one-loop order in the perturbative sense, since it is an exact equation. Additionally, only (partially) dressed n-point functions appear in the flow equation.

The details of the momentum shell integration are controlled by the choice of the regulator R_k. In order to guarantee, that the flow gives the correct limits in the ultraviolet and infrared, the regulator has to fulfill some technical conditions (see e.g. [45]). Apart from these limiting conditions any regulator would in principle do the job, where regulators that respect the symmetries of the theory are preferred. The flow in theory space depends on this choice as is illustrated in Fig. 2.3.
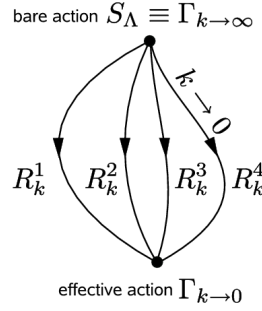

Figure 2.3.: Regulator dependent flow in theory space (picture from [54]).

Therefore, the regulator introduces a renormalization scheme dependence analogous to the scheme dependence in perturbative renormalization theory. It is very important that the physical predictions have to be independent of the renormalization scheme, i.e. the choice of the regulator. This is only true for the full flow and one cannot expect to find a regulator independence as soon as truncations are made. Additionally, in practice one starts at some finite initial scale Λ, and therefore the initial action Γ_Λ corresponding to a specific $\Gamma_{k=0}$ can also depend on the regulator. On the other hand, it is possible to use this scheme dependence to check the quality of a given truncation. Furthermore, for a given truncation one can find optimized regulators via the principle of minimal sensitivity [49, 55, 56].

Finally, some common truncations for the effective average action shall be sketched briefly. Very close to its nature as the generating functional of 1PI n-point functions is the expansion

$$\Gamma_k[\phi_{cl}] = \sum_n \frac{1}{n!} \int_{x_1,\ldots,x_n \in \mathbb{R}^d} \Gamma_k^{(n)}[\hat{\phi}](x_1,\ldots,x_n) \left(\phi_{cl}(x_1) - \hat{\phi}(x_1)\right) \cdots \left(\phi_{cl}(x_n) - \hat{\phi}(x_n)\right) \ , \ (2.33)$$

where one reasonable choice for the expansion point is $\hat{\phi} = \phi_{cl,k}[j = 0]$, as the Taylor coefficients $\Gamma_k^{(n)}[\hat{\phi}](x_1,\ldots,x_n)$ approach the 1PI n-point functions $\Gamma^{(n)}$ for $k \to 0$.

Another possibility, which puts emphasis on the effective potential, is an expansion in deriva-

tives

$$\Gamma_k[\phi_{cl}] = \int\limits_{x\in\mathbb{R}^d} \left\{ U_k(\phi_{cl}) + \frac{1}{2}Z_k(\phi_{cl})(\partial\phi_{cl})^2 + \dots \right\} ,\tag{2.34}$$

where the exact form of the contributions depend on the symmetries of the theory. This is an expansion in momenta and therefore well-suited for investigations of long-ranged phenomena as well as ground state properties from the effective potential.

The BMW approximation scheme [57, 58] to a given order s implements the full n-point functions up to $n \leq s$. Higher n-point functions are approximated by taking deriatives of the known n-point functions $n \leq s$ and neglecting the corresponding additional loop momentum dependence. At lowest order $s = 0$ this corresponds to the local potential approximation, i.e. the lowest order in the derivative expansion

$$\Gamma_k[\phi_{cl}] = \int\limits_{x\in\mathbb{R}^d} \left\{ U_k(\phi_{cl}) + \frac{1}{2}(\partial\phi_{cl})^2 \right\} .\tag{2.35}$$

Here any momentum dependence in the vertices [5] is ignored and for constant ϕ one obtains

$$\Gamma_k^{(n)}[\phi](p_1 = 0, \dots, p_n = 0) = \nabla_\phi^n U_k(\phi) .\tag{2.36}$$

For any truncation there are at least two sources of errors. The first error comes from the choice of the initial action Γ_Λ, such that the physics are reproduced correctly at $k = 0$ in the given truncation. The second contribution is due to the projection of the full flow on the subspace of theory space defined by the truncation.

Before going back to QCD, it should be mentioned that there exist also other non-perturbative approaches, where one is for example given by the nPI formalism which has been applied e.g. to the investigation of non-equilibrium phenomena [59].

2.1.2. Aspects of Quantum Chromodynamics

Quantum Chromodynamics can be characterized by its gauge invariant action

$$S = \int\limits_{\mathbb{R}^4} \bar{q} \left\{ (iD_\mu\gamma_\mu + Z_M M)\, q - \frac{1}{4}F_{\mu\nu}^a F_{\mu\nu}^a \right\} .\tag{2.37}$$

Here, the field strength tensor is given by $F_{\mu\nu}^a = \partial_\mu A_\nu^a - \partial_\nu A_\mu^a + g f^{abc} A_\mu^b A_\nu^c$. The gluon field is an element of the Lie algebra $A_\mu = A_\mu^a T^a$ with Hermitian generators T^a and structure constants f^{abc} for the gauge group $SU(3)$ as defined in App. A.2. The purely gluonic part of the action is invariant under local gauge transformations $G(x) \in SU(3)$

$$A_\mu(x) \to {}^G A_\mu(x) = G(x)A_\mu G^\dagger(x) - \frac{i}{g}\left(\partial_\mu G(x)\right) G^\dagger(x) ,\tag{2.38}$$

---

[5]The conventions for the Fourier transform are defined in App. A.3

which means that the gluon field is in the adjoint representation of $SU(3)$ [60]. If the Dirac spinor [6] (anti-)quark field ($\bar{q} = -iq^\dagger\gamma^4$) q transforms under the fundamental representation

$$q(x) \to {}^G q(x) = G(x)q(x) \ , \tag{2.39}$$

with corresponding covariant derivative $D_\mu = \partial_\mu - igA_\mu$, the full action is invariant under local gauge transformations. Apart from color and spinor components, the quark field comes in six flavors, dubbed up, down, strange, charm, bottom and top with growing bare mass. These bare quark masses cannot be explained within QCD and the mass matrix M is a consequence of the interaction with the Higgs-field.

In functional approaches, which rely heavily on the gauge-dependent n-point functions, it is additionally necessary to fix the gauge in the Yang-Mills part of the theory. In this thesis, solely Landau gauge is employed, which corresponds to the condition $\partial_\mu A_\mu = 0$. The gauge condition can be implemented with the Faddeev-Popov method, see e.g. [61]. This procedure introduces a scalar anticommuting field in the adjoint representation of the gauge group ($\bar{c}$) c called (anti-)ghost field. The renormalized, gauge-fixed Euclidean action of QCD in four dimensions reads then

$$S = \int_{\mathbb{R}^4} \left\{ Z_3 A_\mu^a \left(\frac{1}{2} \left(-\partial_\sigma \partial_\sigma \delta_{\mu\nu} + \partial_\mu \partial_\nu \right) \right) A_\nu^a \right. \tag{2.40}$$

$$\left. + Z_1 g f^{abc} \left(\partial_\mu A_\nu^a \right) A_\mu^b A_\nu^c + Z_4 \frac{g^2}{4} f^{abc} f^{ade} A_\mu^b A_\nu^c A_\mu^d A_\nu^e \right\}$$

$$- \int_{\mathbb{R}^4} \left\{ \tilde{Z}_3 \bar{c}^a \partial_\mu \partial_\mu c^a - \tilde{Z}_1 g f^{abc} \bar{c}^a \partial_\mu (c^b A_\mu^c) + \bar{q} \left(Z_2 \left(\partial_\mu \gamma_\mu - iZ_M M \right) - Z_{1F} ig\partial_\mu A_\mu \right) q \right\} \ .$$

Unfortunately, the Faddeev-Popov method is only capable of fixing the gauge perturbatively [28,62]. In general the local condition $\partial_\mu A_\mu = 0$ is not unique and it is possible to construct global gauge transformations G_G, such that ${}^{G_G} A_\mu$ also fulfills the gauge condition. The existence of such Gribov copies was first realized in [63]. There it was attempted to fix the gauge completely by restricting the functional integral to the Gribov region Ω_G. This is a subset of the linear space fulfilling the Landau condition with positive Faddeev-Popov operator $M[A] = -\partial_\mu D_\mu$

$$\Omega_G = \left\{ A \, \middle| \, M[A] > 0 \wedge \partial_\mu A_\mu = 0 \right\} \ . \tag{2.41}$$

This operator is obviously positive for vanishing A and therefore by continuity a small neighborhood of $A = 0$ is contained in the Gribov region. Additionally this regions is convex, bounded in every direction and every gauge orbit passes at least once through the Gribov region [64,65]. The boundary of the Gribov region ∂G - often called the first Gribov horizon - is characterized by the existence of (at least) one zero mode in the Gribov operator. This implies that its determinant vanishes on ∂G and the divergence theorem used in the derivation of the DSEs Eq. (2.15) is also valid for the restricted integration. Unfortunately,

---

[6]Throughout this thesis, the chiral representation of the Dirac algebra will be used [6]. The corresponding Euclidean Dirac matrices are defined in App. A.1.

even this is not sufficient to fix the gauge completely [66]. Fixing the gauge completely inside the first Gribov region leads to the definition of the fundamental modular region [67], which minimizes the L_2 norm on the gauge orbits $\{^G A\}$ with respect to G globally. It is an open issue how to implement this restriction in functional approaches and only the restriction to Ω_G is assumed here.

Using Slavnov-Taylor identities [68,69] - they constitute the Ward-Takahashi identities [70,71] of the non-Abelian gauge symmetry - it is possible to derive relations between the renormalization constants in Eq. (2.40) like (see e.g. [1,28])

$$Z_1 = Z_g Z_3^{3/2} \ , \quad Z_{1F} = Z_g Z_2 Z_3^{1/2} \ , \quad \tilde{Z}_1 = Z_g \tilde{Z}_3 Z_3^{1/2} \ , \quad Z_4 = Z_g^2 Z_3^2 \ . \qquad (2.42)$$

In Landau gauge, one additionally has non-renormalization of the ghost-vertex $\tilde{Z}_1 = 1$ [69] which implies $Z_{1F} = Z_2/\tilde{Z}_3$. Furthermore, the Slavnov-Taylor identities can be used to show that even the dressed gluon propagator is transversal to its momentum (see e.g. [28]).

After this discussion of gauge symmetry, further important symmetries of the QCD action shall be investigated next.

Symmetries and their Breaking

Symmetries are one of the fundamental building blocks of physical theories, as demonstrated by the gauge principle. Apart from local symmetries, the action of QCD Eq. (2.37) respects also a number of global symmetries. Before discussing the various symmetries of QCD, it is worthwhile to check how they can be broken.

It might happen that a symmetry is only approximate. As an example one could think of a ferromagnet described by the Heisenberg model with only nearest neighbor spin interactions. If the ferromagnet were isolated in space and time, it would possess a perfect symmetry under rotations. In contrast to this, any real ferromagnet will experience electromagnetic forces from its surroundings, which break the rotational symmetry explicitly.

In quantum field theories one has two additional possibilities of breaking symmetries which are respected by the classical action S. The first of these possibilities is connected to the ground state of the theory. If this ground state would respect a given symmetry, it would transform trivially under the corresponding conserved charges Q which are the generators of the symmetry transformation on the state space. These symmetry transformations would then give rise to a characteristic multiplet structure in the spectrum and the theory is said to be in its Wigner-Weyl realization. Another possibility is that the ground state does not respect a subset of symmetry transformations of the full classical symmetry. Whenever this happens, the symmetry is called spontaneously broken or, equivalently, the theory is said to be in its Nambu-Goldstone realization. One observable consequence of spontaneous symmetry breaking is the absence of the corresponding multiplet structure in the spectrum. Any spontaneously broken symmetry can also be characterized by a non-vanishing order parameter which is defined with the help of some operator Φ as

$$\langle [Q, \Phi] \rangle \neq 0 \ , \qquad (2.43)$$

where Q is the charge corresponding to some spontaneously broken current j_μ [7]. In the follow-

---

[7]To be more precise, the defining integration of the charge needs to be restricted to some finite volume Ω.

ing, $\langle \Phi \rangle$ will be called order parameter, when actually the more precise statement Eq. (2.43) is meant. When a continuous symmetry is spontaneously broken, there exist infinitely many degenerate ground states, which are connected by the broken symmetry transformations. Any of these ground states can be used to construct the state space, which leads to equivalent representations of the theory without overlap [72]. This can be illustrated with the quartic effective potential of a single complex scalar field given by $V(\phi) = -\mu^2|\phi|^2 + \lambda|\phi|^4$ and shown in Fig. 2.4.
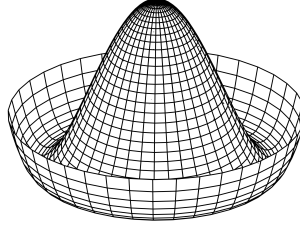
Figure 2.4.: Mexican hat potential (picture from [73]).

This effective potential is invariant under $U(1)$ phase rotations of the complex field ϕ and shows a set of degenerate ground states connected by a phase rotation. Around any minimum one has two possible excitations: one massive radial excitation and one massless excitation in direction of the phase rotation. In general, any spontaneously broken, continuous symmetry implies the existence of such massless modes, which are called Goldstone bosons [9–11]. In case of relativistic quantum field theories, the number of Goldstone bosons is given by the number of broken symmetry generators and they have the quantum numbers of the broken currents. For example, the Heisenberg ferromagnet shows spontaneous magnetization in its ground state, which breaks rotational symmetry. The corresponding Goldstone modes are given by collective spin excitations, which are called magnons [72].

Another possibility of breaking a symmetry in a QFT is by quantum anomalies. Any interacting quantum field theory in four space-time dimensions has to be regularized and renormalized. It can happen that the regularization procedure cannot be performed without breaking some of the classical symmetries. Even after the corresponding cutoff is removed, effects of this symmetry breaking may survive which are due to quantum fluctuations. When this happens, the corresponding symmetry is called anomalously broken [3].

Symmetries of QCD

At vanishing quark masses, the QCD action Eq. (2.37) is invariant under rescaling of space-time, if additionally the fields are rescaled according to their mass dimension

$$x \to x' = e^{-\sigma}x ~, \tag{2.44a}$$

$$A(x) \to A'(x') = e^{\sigma}A(e^{\sigma}x') ~, \tag{2.44b}$$

$$q(x) \to q'(x') = e^{3\sigma/2}q(e^{\sigma}x) ~. \tag{2.44c}$$

If this symmetry were realized, QCD would look the same on all length scales, which is obviously not the case in Nature. This symmetry is explicitly broken by the non-vanishing quark masses. But even at vanishing quark masses one would intuitively expect the symmetry

to be broken by regularization. More precisely, it is broken by the so-called trace anomaly [74] and an order parameter can be given by $\beta(g)/g^3 \langle F^a_{\mu\nu} F^a_{\mu\nu} \rangle$. The trace anomaly is present even in the limit of vanishing quark masses, and implies the ermergence of a characteristic scale, i.e. Λ_{QCD}. This phenomenon of the creation of a scale from a dimensionless coupling is often called dimensional transmutation. Due to asymptotic freedom and perturbative renormalizability of QCD, this scale can be used to specify the theory as it corresponds to its only renormalizable coupling constant g.

One important approximate symmetry of the quark sector of QCD is chiral symmetry. If the quark spinors were massless, the left and right handed components of the spinor $q^T = (q_L\ q_R)$ would decouple. This can be seen from the interchange of left and right handed component in $\bar{q} = -iq^\dagger \gamma^4 = (q_R^\dagger\ q_L^\dagger)$ and

$$D_\mu \gamma_\mu = \begin{pmatrix} 0_{2\times2} & -iD_4 1_{2\times2} - D_i \tau^i \\ -iD_4 1_{2\times2} + D_i \tau^i & 0_{2\times2} \end{pmatrix} , \qquad (2.45)$$

where τ^i are the Pauli matrices defined in App. A.1 and $(0_{2\times2})$ $1_{2\times2}$ is the two by two (zero) unit matrix. Therefore the QCD Lagrangian with N_f massless flavors is invariant under separate unitary rotations of left and right handed spinors in flavor space

$$q_{L,R} \to U_{L,R}\, q_{L,R} , \quad U_{L,R} \in U(N_f)_{L,R} , \qquad (2.46)$$

and the corresponding symmetry group is written as $U(N_f)_L \times U(N_f)_R$. In Nature this symmetry is broken explicitly by the finite quark masses. It can however be treated as an approximate symmetry for all flavors which are light compared $\Lambda_{QCD} \approx 200$ MeV. The heavier flavors, on the other hand, effectively decouple above this scale and are therefore ignored in the remaining discussion [53]. Chiral symmetry is approximately realized for $N_f = 2$, as the bare up and down quark mass is of $\mathcal{O}(1)$ MeV and to a lesser degree also for $N_f = 3$ with the bare strange quark mass $m_s \approx 100$ MeV in the modified MS scheme at $\mu \approx 2$ GeV [8]. If this symmetry were realized in its Wigner-Weyl form one would expect a corresponding multiplet structure in the spectrum. Especially for the nucleons, which are made of up and down quarks, one would expect corresponding almost degenerate (parity) partners which are not found in the spectrum. Additionally, three very light non-strange mesons, the pions are found. From this one concludes that - in the chiral limit and for small enough N_f - one has the spontaneous symmetry breaking pattern

$$U(N_f)_L \times U(N_f)_R \to U(N_f)_V \equiv U(N_f)_{L+R} , \qquad (2.47)$$

where $U(N_f)_{L+R}$ denotes the transformations $U_L = U_R$. The corresponding order parameter is given by the chiral condensate

$$\langle \bar{q}q \rangle = \langle q_R^\dagger q_L + q_L^\dagger q_R \rangle , \qquad (2.48)$$

which is invariant under transformations $U_L = U_R$, but breaks the symmetry under other transformations. The remaining multiplet structure, e.g. the octets, shown in Fig. 2.5 for $N_f = 3$ can then be attributed to this vector symmetry, whereas the light pseudoscalar mesons are the pseudo Goldstone bosons of the broken symmetry.

If one does a careful counting of the number of broken symmetry generators, one finds that

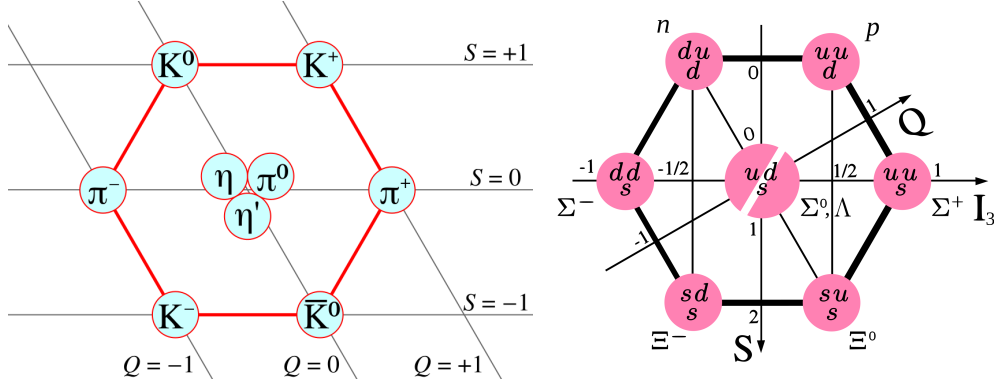Figure 2.5.: Pseudoscalar meson octet (singlet) with pions (π) kaons (K), η, η'- mesons (left panel) and baryon octet (singlet) with neutron (n), proton (p) and hyperons (right panel) (pictures from [73]).

actually there should be four light modes for two flavors. On the other hand, only the three pions are found to be light. Similarly, for $N_f = 3$ one would expect nine light mesons, whereas only three pions, four kaons and the η-meson are light enough to count as pseudo Goldstone modes [75]. In order to understand this, it is useful to rewrite the phase transformations of chiral symmetry in a vector-axialvector representation as

$$U(N_f)_L \times U(N_f)_R \cong U(1)_V / Z_{N_f} \times SU(N_f)_L \times SU(N_f)_R \times U(1)_A / Z_{2N_f} \ . \quad (2.49)$$

The vector transformations correspond to combined left and right phase rotations with $\hat{U}_L = \hat{U}_R \in U(1)/Z_{N_f}$ and the axial transformations to $\hat{U}_L^* = \hat{U}_R \in U(1)/Z_{2N_f}$. The cyclic groups Z_{N_f} have been divided out to get rid of double covering, as is discussed in more detail in App. B.3. The crucial point is that the current corresponding to the $U(1)_A/Z_{2N_f}$ factor group is broken by the axial anomaly [76–78]. It can be shown that the fermionic measure of the path integral cannot be regularized in a way that keeps gauge invariance and the $U(1)_A/Z_{2N_f}$ symmetry at the same time [79]. With this symmetry being anomalously broken, the large mass of the η'-meson - which would otherwise constitute the additional pseudo Goldstone mode - can be explained. It is furthermore possible to relate this anomalous mass to a quantity stemming from pure gauge theory. The Witten-Veneziano relation [80, 81] is given by

$$\frac{m_{\eta'}^2 + m_\eta^2 - 2m_K^2}{6} = \frac{\chi_{YM}}{f_\pi^2} \ , \quad (2.50)$$

where K denotes the kaon, f_π the pion decay constant and χ_{YM} is the topological susceptibility of pure Yang-Mills theory. To understand the relevance of this relation one can investigate QCD with $N_f = 3$ in the chiral limit. The right hand side of the above relation will not be modified by this limit, as it is obtained in the pure gauge theory. On the left hand side, one has due to spontaneous chiral symmetry breaking $m_\eta^2 = m_K^2 = 0$ and furthermore $f_\pi^2 > 0$. The above relation therefore provides a direct link between the anomalous η'-mass and the topological susceptibility χ_{YM}, which can be seen as the corresponding order parameter.

Numerical results for $m_{\eta'}$ in QCD have e.g. been obtained on the lattice [82] and in a DSE based Bethe-Salpeter equation [83].

Additionally, 't Hooft was able to show that integrating topologically non-trivial configurations in the path integral gives a determinant contribution to the fermionic Lagrangian density [84, 85]

$$e^{i\theta_{QCD}} \det \left(q_L q_R^\dagger \right) + e^{-i\theta_{QCD}} \det \left(q_R q_L^\dagger \right) \; , \tag{2.51}$$

where θ_{QCD} is the coefficient of a term proportional $F_{\mu\nu}^a \epsilon_{\mu\nu\rho\sigma} F_{\rho\sigma}^a$. Such a theta term θ_{QCD} would be allowed in the QCD action, as it only violates CP. Experimentally θ_{QCD} has been found to be very small, without any apparent theoretical reason. This unexplained smallness of the theta term is often called the strong CP problem [86, 87]. The 't Hooft determinant Eq. (2.51) breaks the $U(1)_A/Z_{2N_f}$ part of chiral symmetry already in the Lagrangian, as is discussed in more detail in App. B.3.

The gauge symmetry of the QCD action Eq. (2.37) has already been discussed in detail. By Elitzur's theorem it is not possible to spontaneously break local symmetries [88]. On the other hand, it might still happen that after gauge fixing there is some remnant global symmetry, which can be spontaneously broken. In Landau gauge QCD, apart from the global gauge symmetry, there is another remnant of gauge symmetry corresponding to anticommuting gauge transformation, called BRST symmetry [89, 90]. It allows the definition of the nilpotent BRST operator s which generates these transformations on the c-numbered fields. The corresponding nilpotent BRST charge Q_{BRST} can be used to specify the physical space as the cohomology [91]

$$H_{phys} = \overline{\mathrm{ker}Q_{BRST}/\mathrm{im}Q_{BRST}} \; , \tag{2.52}$$

where bar denotes the closure. This construction is necessary, because of the presence of states with negative norm as e.g. the time components of the gauge field. Furthermore, states which are not annihilated by the BRST charge are not gauge-independent. Neither of these states can be physical, the former, because their presence would not allow a probabilistic interpretation and the latter, because predictions cannot depend on the chosen gauge. The above definition of the physical subspace takes care of both issues [92].

As will be discussed in Sec. 2.2, at finite temperature T the infinite time-direction is replaced by the compact interval $[0, 1/T]$. In this case, (fermions) bosons acquire (anti-)periodic boundary conditions

$$\psi(\vec{x}, x_4 + 1/T) = \pm \psi(\vec{x}, x_4) \; . \tag{2.53}$$

These boundary conditions have to be invariant under gauge transformations, which also restricts the boundary conditions of the allowed transformations. Consider a general twisted gauge transformation G with

$$G_h(\vec{x}, x_4 + 1/T) = hG_h(\vec{x}, x_4) \; , \tag{2.54}$$

for some $h \in SU(3)$ [93, 94]. Applying this transformation to the gluon field, its boundary

conditions are modified as

$$^{G_h}A_\mu\left(\vec{x}, x_4 + 1/T\right) = h\left(G_h(x)A_\mu(\vec{x}, x_4 + \frac{1}{T})G_h^\dagger(x) - \frac{i}{g}\left(\partial_\mu G_h(x)\right)G_h^\dagger(x)\right)h^\dagger \quad (2.55)$$
$$= h\,^{G_h}A_\mu(\vec{x}, x_4)\,h^\dagger \ .$$

If h would commute with A_μ, the boundary conditions of the gluon field are not affected by such a twisted gauge transformation. The set of all elements of a group that commute with all other group elements is called the center of a group. The center of $SU(3)$ is isomorphic to the cyclic group Z_3, which can be represented with the phases

$$Z_3 \cong \{1, e^{i2\pi/3}, e^{i4\pi/3}\} \cdot 1_{3\times 3} \ . \quad (2.56)$$

Hence, the pure gauge theory is invariant under the center transformations G_z with $z \in Z_3$. Next it is interesting to investigate, what happens to the boundary conditions of matter in the fundamental representation under G_z

$$^{G_z}\psi_F\left(\vec{x}, x_4 + 1/T\right) = \pm z\,^{G_z}\psi_F(\vec{x}, x_4) \ , \quad (2.57)$$

where the (anti-)periodic boundary conditions of (fermions) bosons have been taken into account. In other words, a center transformation changes the boundary condition of a fundamental field and the transformed field can be written as [95]

$$^{G_z}\psi_F\left(\vec{x}, x_4\right) = {}^{G}\psi_F(\vec{x}, x_4)e^{i\arg(z)Tx_4} \ . \quad (2.58)$$

Therefore, matter in the fundamental representation of the gauge group breaks center symmetry explicitly. On the other hand, matter in the adjoint representation transforms as the gluon field without the derivative term

$$^{G}\psi_A(x) = G(x)\psi_A(x)G^\dagger(x) \ , \quad (2.59)$$

and its boundary conditions are unaffected by center transformations. An order parameter for this center symmetry is given by the Polyakov loop [96,97]

$$L = \text{tr}\left[\mathcal{P}e^{ig\int_0^{1/T} dx_4 A_4(\vec{x}, x_4)}\right] \ , \quad (2.60)$$

where $\mathcal{P}$ denotes path ordering. Under a twisted gauge transformation G_z, the expectation value of the Polyakov loop picks up a phase z due to path ordering and running once around the torus in x^4 direction

$$\langle L \rangle \to z\langle L \rangle \ . \quad (2.61)$$

Therefore a non-vanishing Polyakov loop indicates spontaneous breaking of center symmetry.

Infrared Behavior and Confinement

From experiments it is clear that neither quark nor gluon fields represent physical particle excitations. The only things ever found in experiments are mesons and baryons. A sound

theoretical description of confinement is one of the toughest problems in QCD.

One intuitive picture describes confinement as the emergence of a constant force between an infinitely heavy quark-antiquark pair at large distances. This linearly rising potential can be related to the Wilson loop observable [98]
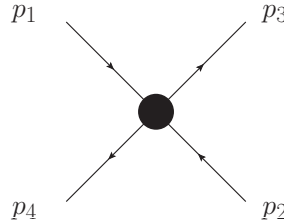
$$W \propto \mathrm{tr} \mathcal{P} \exp \left[ig \oint_{\mathcal{C}} dx^{\mu} A_{\mu}(x) \right] \ . \tag{2.62}$$

If the expectation value of the Wilson loop obeys an area law

$$\langle W \rangle \propto \exp \left(-\sigma \mathrm{Area}(C) \right) \ , \tag{2.63}$$

one can deduce a linearly rising potential [94]. Absence of confinement is then characterized by the dependence of $\langle W \rangle$ on the perimeter of the loop C. In real QCD with finite quark masses, it will be energetically favored at some finite distance to create another quark-antiquark pair, i.e. a second meson. Therefore the string of gluons connecting the quark anti-quark pair breaks at a finite distance. This picture has been nicely confirmed in lattice QCD [99].

In this thesis the question is posed, if and how such a linearly rising potential can be obtained from n-point functions. Due to the exponentiation of the gluon field, the Wilson loop depends on infinitely many n-point functions. A priori there is no compelling reason, why a finite set of n-point functions should already lead to confinement in the sense of a linearly rising potential. On the other hand, one can show that an infrared singular quark interaction can provide such a linearly rising potential. The starting point for this is a quark 4-point function which behaves as

$$\overset{p_1 \to p_3}{\propto} \frac{1}{(p_1 - p_3)^4} \ ,$$

in the limit of vanishing momentum exchange. If it is properly regularized - to make it a well-defined distribution on $\mathbb{R}^4$ - one can take its Fourier transform. In the non-relativistic limit this leads to a heavy quark potential with a term linear in the distance r, i.e. the wanted linearly rising potential [100]. Therefore, confinement can in principle be contained already in a single n-point function.

Actually, a similar $1/k^4$ singularity had been proposed earlier to exist already in the gluon propagator, which would also suffice to yield a linearly rising potential. Careful investigations of the infrared properties of propagators in Landau gauge Yang-Mills theory with DSEs and the FRG have found two possible self-consistent infrared solutions [101–106]. Both solutions can be characterized by a power law behavior at small momenta in the (ghost) gluon propagators proportional $((p^2)^{\kappa_{gh}-1}) \ (p^2)^{\kappa_g - 1}$. In case of the scaling solution, these two exponents are related by $\kappa_g = -2\kappa_{gh} \equiv 2\kappa > 0$. The other consistent solution, often referred to as decoupling or massive solution, corresponds to $\kappa_g = 1$ and $\kappa_{gh} = 0$. Neither solution provides a $1/k^4$ singularity in the gluon propagator.

Apart from this, there are arguments for both infrared solution types. The most important argument for the decoupling solution is that it is the solution usually found in lattice calcu-

lations [107, 108]. It has been pointed out, however, that the quantitative infrared behavior of the propagators depends on the precise gauge fixing procedure [109, 110]. Therefore, this family of solutions might correspond to different ways of lifting the Gribov ambiguity. In this case all solutions would be valid and one could choose solutions, which are especially well suited for the investigation of specific physical phenomena, as e.g. confinement.

There are also compelling arguments for the scaling solution, which are rooted in another confinement criterion: The idea of the Kugo-Ojima confinement scenario is that the physical subspace Eq. (2.52), which is supposed to describe the physical, asymptotic states, does not contain any colored states [91]. In this case, no quarks, gluons and especially no ghosts would appear as asymptotic states. With the BRST charge Q_{BRST} it is then possible to show the existence of quartets of states that do not contribute to the physical S-matrix defined on H_{phys}. One example of such a confined quartet would be given by a ghost, an anti-ghost, a longitudinally polarized gluon and the corresponding gauge-fixing multiplier field (see also [111]). To show confinement by this quartet mechanism, it is necessary to show that the remaining global gauge symmetry is not spontaneously broken and that the cluster decomposition property is violated.

One argument for the scaling solution is now that an unbroken global color symmetry already results in the scaling solution in the Kugo-Ojima confinement scenario [106]. In this scenario a condition for confinement can be given in terms of the ghost propagator $D_{gh}(p^2) \propto G(p^2)/p^2$ as

$$\frac{1}{G(0)} = 0 \ , \tag{2.64}$$

which is not fulfilled by the decoupling solutions.

Also the cluster decomposition property can be used to argue in favor of the scaling solution, but this requires a little detour. It states that for any set of n fields $\{\Phi_i\}$ and some space-like $\lambda \in \mathbb{R}^4$ one has

$$\lim_{\lambda \to \infty} \langle \Phi_1(x_1) \cdots \Phi_i(x_i) \Phi_{i+1}(x_{i+1} + \lambda) \cdots \Phi_n(x_n + \lambda) \rangle \tag{2.65}$$
$$= \lim_{\lambda \to \infty} \langle \Phi_1(x_1) \cdots \Phi_i(x_i) \rangle \langle \Phi_{i+1}(x_{i+1} + \lambda) \cdots \Phi_n(x_n + \lambda) \rangle \ .$$

In other words, this is causality in the sense that measurements at large space-like distances cannot affect each other. It is possible to prove cluster decomposition from the Wightman axioms, which however requires a state space of positive norm [13]. If QCD had this property, it would be possible to separate a colorless product of operators of non-vanishing vacuum expectation values into clusters of colored operators at large space-like distances. These colored operators would then necessarily have non-vanishing vacuum expectation values by Eq. (2.65), which one wants to avoid in a confining theory with only colorless physical states. In QCD, violation of cluster decomposition is not inconsistent as it does not have a state space of positive norm. Furthermore, cluster decomposition implies that in momentum space connected n-point functions do not have δ-like singularities, except for the overall momentum conserving δ-function [2]. A connected four point function can be rewritten as

where different field types have not been discriminated. Assuming no non-trivial cancellation on the right hand side [8] and well behaved quark propagators, a $1/k^4$ singularity in the 1PI 4-point function can be related to such a singularity in the connected 4-point function. It has been stated before that such a singularity has to be regularized also in the infrared, to make it a well-defined distribution on $\mathbb{R}^4$. This can be done in the Epstein-Glaser spirit of identifying its singular support and scaling degree [112]. From this one sees that regularization demands the introduction of one δ-like counter term. On the other hand, the appearance of such a δ-like singularity in the connected 4-point function implies the absence of cluster decomposition.

One important aspect of the scaling solution in the Yang-Mills sector is its possible influence on the infrared behavior of quark n-point functions. It has been found that, given such a scaling solution in the pure gauge theory, there exist again two possibilities for self consistent solutions in the quark sector - one infrared finite and one infrared scaling solution [113]. The scaling solution comes with an infrared singularity in the quark-gluon vertex

$$\overset{p \to q}{\propto} \left((p-q)^2 \right)^{-1/2-\kappa} \ .$$

Plugging this into a skeleton expansion of the quark 4-point function one would get at lowest order

For a soft gluon exchange this results - by adding the exponents of the gluon propagator and the two vertices: $2\kappa - 1 + 2(-\kappa - 1/2) = -2$ - exactly in a $1/k^4$ singularity. A similar set of self-consistent infrared singular solutions has been found in scalar QCD, where the quarks are replaced by fundamentally charged scalars [114]. This is especially interesting, since the number of tensor structures is considerably smaller in the scalar case, which makes numerical investigations easier [115].

Before going on, other approaches to confinement shall be briefly mentioned. In the Gribov-Zwanziger scenario of confinement [63, 116–118], it is possible to derive conditions for the ghost and gluon dressing functions, which are again only consistent with the scaling solution. From positivity of the physical subspace one immediately obtains that n-point functions which correspond to physical states have to fulfill a certain positivity criterion [13] in their Minkowski

---

[8]This type of cancellation will be argued away in Ch. 3 with the help of the color structure of $1/k^4$ divergences in the 4-point function.

formulation. Positivity also relates to the existence of a Källen-Lehmann representation [119, 120], which restricts the allowed values for the wave function renormalization of fields corresponding to physical excitations to values $Z \leq 1$, whereas composite particles correspond to $Z = 0$. In the Euclidean formulation positivity translates into a property termed reflection positivity [16,17]. Unfortunately, such a violation of positivity is at best a necessary condition for confinement, as also unstable excitations are not part of the physical subspace and the corresponding correlators can violate positivity as well. Other possible mechanisms and models for confinement include center vortices [121–126], monopoles and Abelian dominance [127] and the gluon chain model [128, 129]. Additionally it can be shown, that there is no linearly rising potential without linearly rising Coulomb potential [94, 130].

At finite temperature a characterization of (de-)confinement can be given in terms of the free energy of infinitely heavy test quarks. If the free energy of such a static quark were infinite, it would not be possible to create one, i.e. it is confined. On the other hand, a finite free energy could be used to identify deconfinement. The free energy of a single quark F_q is given by

$$e^{-F_q/T} = \frac{Z_q}{Z} \; , \tag{2.66}$$

where Z_q is the partition sum (see Sec. 2.2) in the presence of a static quark. Actually, such a static quark is described by the Polyakov loop Eq. (2.60) [97, 131]. Therefore, one gets the relation

$$e^{-F_q/T} \propto \langle L \rangle \; . \tag{2.67}$$

A vanishing Polyakov loop corresponds to infinite F_q and confinement in this sense. From the previous identification of the Polyakov as an order parameter for center symmetry, the deconfinement phase can be related to spontaneously broken center symmetry. In presence of dynamical quarks - which explicitly break center symmetry - this is only an approximate order parameter. But dynamical quarks also spoil the characterization of confinement in terms of a linearly rising potential due to string breaking. Actually, this discussion is not restricted to quarks and applies to every form of fundamentally charged matter.

To summarize: a simple picture of confinement in terms of n-point functions is still missing. Although there exist very convincing results from lattice calculations, it would be preferable to have a qualitative mechanism for confinement. The associated problems are most certainly linked to the change of degrees of freedom at close to Λ_{QCD}. Above this scale, perturbation theory works, i.e. quarks and gluons at high energies can be treated as approximate asymptotic states, which cannot be the correct picture below the confinement scale. One main questions is, whether a qualitatively correct picture of confined QCD at low energies is possible with a finite number of n-point functions in terms of quarks and gluons. Although QCD is defined solely by the value of the strong coupling at large momenta, it might still be the case that even a qualitatively correct picture of confinement requires information from infinitely many n-point functions. In such a case, describing confinement in terms of n-point functions would probably be even worse than using a Fourier series for representing the Heaviside function (point wise). In Ch. 3 at least the consistency of confinement, as obtained from a finite number of n-point functions in terms of $1/k^4$ singularities, will be investigated.

2.1.3. Effective Descriptions

Taking the change in degrees of freedom around Λ_{QCD} seriously, it is possible to develop effective descriptions in terms of new fields. Such descriptions are usually built on symmetry principles, where chiral symmetry is an important guide line in many cases.

One effective field theory is given by chiral perturbation theory which uses the Goldstone bosons to obtain an effective description [3, 132, 133]. It works very well for two quark flavors and to a lesser degree also for three flavors. Chiral perturbation theory is a very good low energy expansion for QCD. One problem, however, is that at higher energies, this expansion becomes less reliable. This is, because it misses important additional degrees of freedom, especially, when going to energies above 0.5 GeV. Therefore, chiral perturbation theory provides in general no reliable quantitative description of phenomena at temperatures $T \gtrsim 0.1$ GeV.

A simple description of spontaneous chiral symmetry breaking is provided by the Nambu-Jona-Lasinio (NJL) model [134]

$$\mathscr{L}_{NJL} = i\bar{q}\partial_\mu\gamma_\mu q + \frac{\lambda}{2}\left[(\bar{q}q)^2 - (\bar{q}\gamma^5 q)^2\right] \ . \tag{2.68}$$

Due to the presence of a pertubatively non-renormalizable four-quark interaction, this model depends also on the cutoff. Explicit symmetry breaking can be added with a quark mass matrix as in Eq. (2.37). Mesons, which are important for long range phenomena, as well as baryons appear in this model only as bound states. Nevertheless, it finds a large range of applications, especially concerning the QCD phase structure at large densities [135].

Quark-Meson Model

Another effective description of chiral symmetry and its breaking can be given in terms of the quark-meson model. It introduces a complex mesonic field matrix in flavor space, which resembles quark bilinears

$$q_L q_R^\dagger \propto \Sigma = (\sigma^a + i\pi^a)T^a \ , \tag{2.69}$$

where T^a, $a = 1, \ldots, N_f - 1$ are the generators of $SU(N_f)$ (see App. A.2) and $T^0 = 1_{N_f \times N_f}$. The above resemblance immediately implies the transformation law

$$\Sigma \to U_L \Sigma U_R^\dagger \ , \tag{2.70}$$

under chiral symmetry. Via a chirally symmetric Yukawa interaction h, quarks are coupled to this mesonic field to obtain the Lagrangian density of the quark-meson model [136]

$$\mathscr{L}_{qm} = i\bar{q}\partial_\mu\gamma_\mu q + h\left(q_L^\dagger \Sigma q_R + q_R^\dagger \Sigma^\dagger q_L\right) + \text{tr}\left[\partial_\mu\Sigma\partial_\mu\Sigma^\dagger\right] + U(\Sigma) \ . \tag{2.71}$$

Here the potential $U(\Sigma)$, describing self-interactions in the mesonic sector, and a kinetic mesonic term have been introduced. To preserve chiral symmetry, the potential U has to be

a function of the chiral invariants ρ_i defined by

$$\rho_i = \text{tr}\left[\left(\Sigma\Sigma^\dagger\right)^i\right] . \tag{2.72}$$

These are obviously invariant under Eq. (2.70) and only $\rho_1, \ldots, \rho_{N_f}$ are actually independent [136]. If the above Lagrangian is to define a renormalizable theory, only ρ_1 and ρ_2 can be taken into account as $\rho_i = \mathcal{O}(\Sigma^{2i})$. On the other hand, there is no such restriction with the non-perturbative FRG.

The axial anomaly can be implemented by translating the 't Hooft determinant Eq. (2.51) into a mesonic language. Setting $\theta_{QCD} = 0$, the mesonic potential can also depend on

$$\xi = \det\Sigma + \det\Sigma^\dagger , \tag{2.73}$$

which transforms as the original quark determinant under chiral symmetry.

From the transformation law Eq. (2.70), the order parameter of spontaneous chiral symmetry breaking in this model is given by the mesonic field Σ. If its expectation value is proportional the unit matrix

$$\langle\Sigma\rangle = \sigma\,\mathbb{1}_{N_f \times N_f} , \tag{2.74}$$

invariance under Eq. (2.70) leads to the condition $U_L = U_R$, which yields the same symmetry breaking pattern as Eq. (2.47). This condensate induces degenerate constituent quark masses $m_q = h\sigma$ via the Yukawa interaction.

The explicit breaking of chiral symmetry is implemented via a term

$$-\text{tr}\left[C\left(\Sigma + \Sigma^\dagger\right)\right] . \tag{2.75}$$

This leads to a non-vanishing expectation value $\langle\Sigma\rangle$ and as a consequence also to non-vanishing bare quark masses. In the vacuum, the quantum numbers of the ground state dictate the form of C, restricting it to be a diagonal matrix. The diagonal entries in C allow then an adjustment of the different bare quark masses.

Both effective descriptions, the NJL model as well as the quark-meson model, miss explicit gluonic degrees of freedom. In the presented form, they are therefore only applicable to investigations of the chiral transition. This can be improved e.g. by the inclusion of a Polyakov potential [137–148].

Transcending the Model Status via Dynamical Rebosonization

Effective descriptions introduce a model parameter dependence. Recent progresses with the FRG, however, have shown that a dynamical change from QCD degrees of freedom to mesons is possible [49, 149–151]. Investigations within the FRG show that four-quark interactions as in the NJL model are created when the strong coupling exceeds a critical value [152]. In the chiral limit, the onset of spontaneous chiral symmetry breaking is then indicated by a divergence of the corresponding coupling, i.e. a pole in the quark 4-point function at zero momentum. On the other hand, it is possible to replace four-quark interactions via a Hubbard-Stratonovich transformation, which introduces a mesonic auxiliary field [153, 154].

This rebosonization leads to the quark-meson model without kinetic term, i.e. the mesons correspond still to bound states due to their vanishing wave function renormalization $Z = 0$. Another possibility is to employ a dynamical rebosonization by rewriting the four-quark interactions created during the RG flow continuously into renormalizable mesonic interactions [149]. Independent of the details in the mesonic sector at large scales, this provides a continuous transition from QCD degrees of freedom via an intermediate description including bound states of quarks to an effective description in terms of the constituent quarks, condensates and mesons of the quark-meson model [152]. A similar independence of the infrared effective description from the ultraviolet details in the mesonic sector has been reported in [136, 155]. In renormalization group language, this can also be understood in a simple fixed point picture. For a large range of initial values and scales, the flow is governed by a bound-state fixed point of QCD with gluons and quarks. Approaching the critical gauge coupling strength in the infrared lifts this fixed point and pushes the theory into a phase of spontaneous chiral symmetry breaking with mesons which behave as fundamental degrees of freedom, i.e. $Z \neq 0$ [152].

2.2. Thermodynamics and Phases

Before discussing the conjectured phase structure of Quantum Chromodynamics, the most important basics of thermal field theory are briefly summarized to fix the notation [156]. All thermodynamic quantities of a statistical system are characterized by its grand canonical partition function $Z \equiv Z(V, T, \{\mu_i\})$, which is given by the trace over the density matrix

$$\hat{\rho} = \exp\left[\frac{1}{T}(\mathcal{H} - \mu_i \mathcal{N}_i)\right] .$$ (2.76)

Here $\mathcal{H}$ is the Hamiltonian and $\{\mathcal{N}_i\}$ are the number operators for the different conserved quantum numbers with corresponding chemical potentials $\{\mu_i\}$. The expectation value of any observable can be obtained as

$$\langle \mathcal{O} \rangle = \frac{\text{Tr}\, \mathcal{O} \hat{\rho}}{\text{Tr}\, \hat{\rho}} .$$ (2.77)

In the infinite volume limit $V \to \infty$, one can obtain the pressure, particle number and entropy from the grand canonical partition function

$$P = \frac{\partial(T \ln Z)}{\partial V} , \qquad N_i = \frac{\partial(T \ln Z)}{\partial \mu_i} , \qquad S = \frac{\partial(T \ln Z)}{\partial T}.$$ (2.78)

Additionally, the energy is obtained via the Legendre transform

$$E = -PV + TS + \mu_i N_i .$$ (2.79)

In a non-interacting gas, the pressure is actually given by $P = T \ln Z/V$.

Similar to the derivation of the path integral from the canonical formulation of quantum field theory, it is possible to express the trace over Eq. (2.76) as a path integral. The grand

2. Strongly-Interacting Matter

canonical partition function is then given by

$$Z[T, \{\mu_i\}; j] = \int\limits_{\phi(\vec{x},0)=\pm\phi(\vec{x},1/T)} \mathscr{D}\phi \, \exp\left[-S[T, \{\mu_i\}; \phi] + \int\limits_{x\in\mathbb{R}^{d-1}\times[0,1/T]} \phi(x)j(x)\right] . \quad (2.80)$$

Here, path integration has to be restricted to configurations of (anti-)periodic boundary conditions for (fermions) bosons. The exponent $S[T, \{\mu_i\}; \phi]$ is the Euclidean action, where integration in time-direction is restricted to $[0, 1/T]$. Additionally, the negative number operators of any conserved quantum number are contained in S. For quarks q, the number operator is given by

$$\mathcal{N}_q = q^\dagger q \, , \quad (2.81)$$

which corresponds to the conservation of one third of the baryon number. The finite interval in time direction implies that the corresponding momentum space variable is discrete, as the Fourier transform in x_d is replaced by a Fourier series

$$\int \frac{d^{d-1}p}{(2\pi)^{d-1}} \int \frac{dp_d}{2\pi} \longrightarrow T \sum_{\substack{\omega_n(\theta)\\ n\in\mathbb{Z}}} \int \frac{d^{d-1}p}{(2\pi)^{d-1}} \, . \quad (2.82)$$

The Fourier modes

$$\omega_n(\theta) = T(2\pi n + \theta) \, , \qquad n \in \mathbb{Z} \, , \quad (2.83)$$

are called generalized Matsubara frequencies, where $(\theta = \pi)$ $\theta = 0$ ensures (anti-)periodic boundary conditions for (fermions) bosons.

The thermodynamic ground state corresponds to $\phi_{cl}[j = 0]$ and by straightforward generalization of Eq. (2.27) one obtains

$$\Gamma[T, \{\mu_i\}; \phi_{cl} = \phi_{cl}[0]] = -\ln Z[T, \{\mu_i\}; 0] \, . \quad (2.84)$$

Recalling the definition of the effective potential Eq. (2.14) and replacing $V_d \rightarrow V/T$ one obtains in a dilute gas approximation

$$P = -\Omega(T, \{\mu_j\}; \phi_{min}) \, , \quad \frac{N_i}{V} = -\frac{\Omega(T, \{\mu_j\}; \phi_{min})}{\partial\mu_i} \, , \quad \frac{S}{V} = -\frac{\Omega(T, \{\mu_j\}; \phi_{min})}{\partial T}, \quad (2.85)$$

where $\Omega(T, \{\mu_i\}; \bar{\phi})$ is the effective potential (grand canonical potential) at finite temperature and chemical potential and ϕ_{min} its minimum. These relations lead furthermore to the energy density via Eq. (2.79).

Phase Transitions and Critical Phenomena [9]

In a system with a finite number of degrees of freedom, the grand canonical partition function is a finite sum of analytic contributions, and therefore analytic. An infinite number of degrees

---

[9]See e.g. [157, 158] for a more thorough discussion of the topics sketched in this section.

of freedom can be obtained in two ways. Already in a classical system it is possible to take the thermodynamic limit $N, V \to \infty$, while keeping the density constant. Furthermore, a quantum field in the continuum describes already infinitely many degrees of freedom, but here only the thermodynamic limit case will be discussed.

Macroscopic objects are usually described by a huge number of microscopic degrees of freedom, and therefore the thermodynamic limit is a good approximation. This can lead to the emergence of quasi non-analyticities in the grand canonical partition function, which in turn lead to discontinuities and divergences in the derivatives of Z, starting at a given order. It is often possible to find a quantity, called order parameter, which reflects such a discontinuity and in many cases such a discontinuous change is related to a change in the symmetry of the ground state.

The Heisenberg ferromagnet is a good example to illustrate such phase transitions. As noted previously, the ferromagnet is in a state of spontaneous magnetization at vanishing or low temperatures. As the temperature is increased, more and more energy is pumped into the system and the thermal fluctuations reduce the magnetization successively. At some point the fluctuations are strong enough to make the net magnetization M vanish completely and the ground state of the ferromagnet is symmetric again. Exactly at the critical temperature, where the magnetization vanishes for the first time, there is a discontinuity in the derivative of the corresponding order parameter M.

A qualitatively different example is given by the liquid-gas transition of water. Given a constant pressure close to the atmospheric pressure, water is liquid up to some temperature around 100° Celsius. At this temperature, two phases of different density coincide. As more energy is added to the system, the system goes into its gaseous phase. In this case the order parameter is the density, which itself already shows a discontinuity at the phase transition.

Therefore, phase transitions can be classified by the behavior of the order parameter at the phase transition, which is either continuous or discontinuous. A transition of the latter type is called of first order, whereas second-order phase transitions fall in the class with continuous order parameter.

In case of the effective potential $\Omega(T, \{\mu_i\}; \bar{\phi})$, a first-order transition is often indicated by a discontinuous jump of the minimum, which implies discontinuities in the thermodynamical quantities derived from $\Omega(T, \{\mu_i\}; \phi_{min})$. Hence, the minimum can often serve as an order parameter - especially in cases where the phase transition is related to a change in the symmetries of the ground state. For a first-order transition it is often possible to successively decrease the discontinuous jump in the minimum by adjusting $T, \{\mu_i\}$, while staying exactly on the line where the phase transition occurs. Assuming a very simple model for the effective potential in case of a scalar field [10]

$$\Omega(T, \mu; \bar{\phi}) = m^2(T, \mu)\bar{\phi}^2 + \lambda_3(T, \mu)\bar{\phi}^3 + \lambda_4(T, \mu)\bar{\phi}^4 \ , \tag{2.86}$$

a discontinuous jump in the minimum can occur if $\lambda_3 < 0$ and $m^2, \lambda_4 > 0$, as this implies the existence of two local minima. Fixing the temperature as function of the chemical potential $T(\mu)$ such that both minima yield the same value of the effective potential, one can write the

---

[10]Alternatively, the potential $m^2\bar{\phi}^2 + \lambda\bar{\phi}^4 + \lambda_2\bar{\phi}^6$, which respects the symmetry transformation $\bar{\phi} \to -\bar{\phi}$ could have been chosen.

potential as

$$\Omega(T(\mu), \mu; \bar{\phi}) = a(T(\mu), \mu)\bar{\phi}^2(\bar{\phi} - \phi_{min}(T(\mu), \mu))^2 , \qquad (2.87)$$

where the first minimum is at the origin, ϕ_{min} is the second minimum and $a(T, \mu) > 0$. Varying the chemical potential to decrease ϕ_{min} leads to a smaller jump in the minimum. In the limit where both minima coincide, there is no first-order transition anymore. Additionally, the second derivative of the potential at the origin vanishes at this point due to degeneracy of the minimum. Therefore, the second-order transition at this critical endpoint of a line of first-order transitions is characterized by the emergence of a massless excitation. This is also seen in a divergent correlation length, which is a measure of the characteristic length scale for fluctuations in the system. More precisely, it defines the length scale, where the exponential suppression in the connected 2-point function of the critical mode sets in. Going even further, the second-order phase transition turns into a crossover, where no clear phase separation is possible. Such a behavior can for example be observed in the liquid-gas transition of water. At its critical endpoint one can observe scale invariance in the sense of liquid and gas regions that fluctuate on all length scales. Density fluctuations with sizes comparable to the wavelengths of visible light lead to scattering and the liquid-gas mixture becomes milky, which is termed critical opalescence.

If a phase transition is related to some spontaneously broken symmetry, it is usually not necessary to perform such a fine-tuning as the minima are connected by symmetry transformations. In such a case it is sufficient to adjust only one parameter to reach the critical point. In a renormalization group language, second-order phase transitions are governed by fixed points with just one relevant direction, i.e. only the value of one relevant coupling has to be specified. The stability matrix at this fixed point possesses therefore one negative eigenvalue ω_0. The negative inverse $\nu \equiv -1/\omega_0$ of this eigenvalue controls the scaling of the diverging correlation length close to the critical temperature T_c

$$\xi \propto \left(\frac{T - T_c}{T_c}\right)^{-\nu} . \qquad (2.88)$$

Also the susceptibility, specific heat and order parameter show a similar scaling with the temperature corresponding to the exponents $-\gamma$, $-\alpha$ and β respectively.

Additionally, the order parameter Φ scales with an external field h at $T = T_c$ as

$$\Phi \propto h^{1/\delta} . \qquad (2.89)$$

In case of the Heisenberg ferromagnet, this external field would be given by an external magnetic field, which explicitly breaks the rotational symmetry of the theory.

Actually only two of the critical exponents are independent, as they fulfill so-called (hyper)scaling relations. Furthermore, the 2-point function of a theory can show a scaling behavior that differs from the expected canonical scaling due to its dimension. In field theories this deviation from the canonical scaling is controlled by the wave function renormalization and usually quantified by the anomalous dimension η.

From the fact that second-order transitions are controlled by a fixed point with just one relevant direction it seems intuitively clear that the critical behavior cannot depend on the microscopic details of a given system. As in the case of renormalizable theories, any infor-
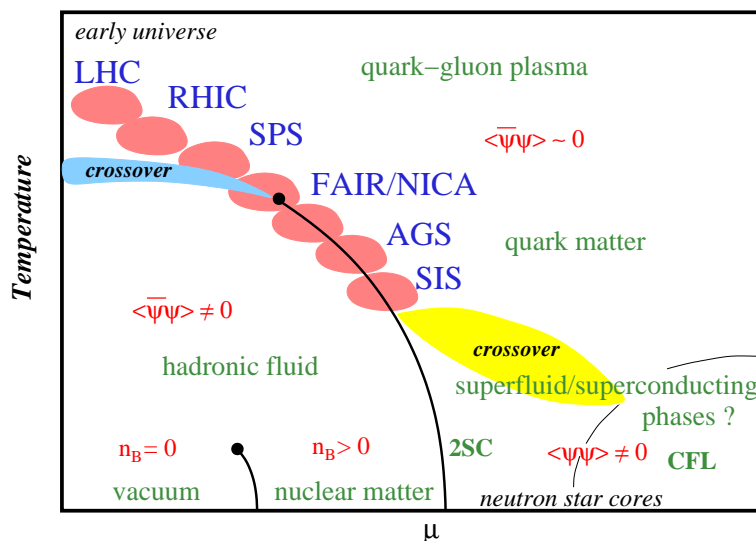
Figure 2.6.: Conjectured phase diagram for Quantum Chromodynamics (picture from [159]).

mation about the short range specifics of the interaction are lost and collective fluctuations take over at the critical point. This dependence on just a number of macroscopic quantities as dimensionality, number of degrees of freedom and symmetries of the system is called universality.

Universality provides a justification for employing simplified models, when one is interested just in universal quantities. It has to be stressed, however, that such a description does not allow quantitatively correct predictions of non-universal quantities such as, e.g. the critical temperature T_c. Finally it should be added that a mean-field treatment of degrees of freedom corresponding to critical fluctuations is in general not capable of reproducing the correct numerical values for the critical exponents. Very good numerical results for critical exponents, on the other hand, are also provided by Monte-Carlo methods (see [158] for a comparison of RG and MC results).

Phases of QCD

A sketch of the expected phase diagram of QCD is shown in Fig. 2.6 in terms of temperature T and chemical potential μ [12,160,161]. Most important for this work is the temperature axis $\mu = 0$, which is also best understood in theoretical terms. First principle lattice calculations show that QCD experiences a rapid crossover from a center symmetric phase of spontaneously broken chiral symmetry at low temperatures to a chirally symmetric phase of spontaneously broken center symmetry - termed quark-gluon plasma. The approximate order parameters are given by the quark condensate for the chiral transition and the Polyakov loop for the center transition.

This means that there are actually two crossovers, which would become phase transitions in different limits for the quark masses. The center-symmetry phase transition is turned into a crossover due to the presence of dynamical quark with small masses. In pure gauge theory, this turns into a first-order transition with transition temperature 277 MeV for gauge group $SU(3)$ [162]. On the other hand, the chiral transition is turned into a crossover by the non-

vanishing quark masses, which explicitly break chiral symmetry. Small quark masses require a lot of computational effort in lattice calculations as they necessitate a realistic implementation of chiral symmetry. This is related to the presence of so-called fermion doublers. One solution to this are Wilson fermions, but they violated chiral symmetry. Other possibilities include staggered, chirally improved, domain-wall and overlap fermions [23, 163], where the latter two options are preferred, but also computationally expensive. Only quite recently has it been possible to implement these better representations of the fermionic part of the QCD action at quark masses close to their physical value [164, 165].

One crucial property of both crossovers is that they occur at approximately the same temperature [166, 167]. Recent estimates of two of the biggest lattice collaborations give a transition temperature around 150 MeV [168, 169]. Within the picture drawn by the dynamical rebosonization approach, chiral symmetry breaking occurs only, if the gauge coupling exceeds a critical strength [170–172]. On the other hand, an explanation why the critical coupling strength is reached exactly at the center-symmetry crossover is still missing (see e.g. [173, 174]). If confinement were controlled by the emergence of a scaling solution in the quark-gluon vertex, this connection could also be explained: As this scaling solution exists only in the chirally broken phase, restoration of chiral symmetry would also imply absence of confinement in terms of a $1/k^4$ singularity as created by the singular quark-gluon vertex [113].

Things become less certain if one leaves the temperature axis. The problem is that the fermionic action is not real anymore as soon as the quark chemical potential deviates from zero. Therefore the Monte-Carlo method Eq. (2.5) used for evaluating the path integral becomes less and less reliable with growing chemical potential, which is called the sign problem. Consequently, most of the knowledge in this region stems from model calculations, where the few things that are certain include the existence of a liquid-gas transition from a nuclear gas at low densities to nuclear matter [175]. Across this transition, the baryon density n_B jumps from zero to the nuclear density. Similar to the liquid-gas transition of water, this transition ends in a critical endpoint.

Many models, including the NJL or the quark-meson model agree on the existence of a chiral first-order transition at low temperatures and quark chemical potentials around $\mu = 300$ MeV [147, 176–179]. This first-order transition would lead to the conclusion that a critical endpoint must lie somewhere in between due to the crossover observed on the temperature axis. Such statements have to be taken with care, as many of these model calculations miss important degrees of freedom such as baryons and diquark contributions, which are expected to become relevant at high chemical potential. Also, the different model approaches do not agree on the location of the critical endpoint. First calculations with diquarks have been performed for a quark-meson model with $SU(2)$ gauge group, where their importance was demonstrated [180, 181]. In $SU(2)$ gauge theory a comparison between model approaches and lattice calculations is furthermore easier, since the fermion determinant is real even at $\mu \neq 0$ and Monte-Carlo methods can be applied easier (see e.g. [182]). The importance of diquarks is related to the expected emergence of a diquark condensate $\langle qq \rangle$ which signals breaking of color symmetry. This is related to the existence color superconducting phases [135, 183], where several mechanisms like 2-flavor color superconductivity (2SC) and color-flavor locking (CFL) have been proposed. These mechanisms compete against each other, where at large chemical potential the CFL phase is favored. The intermediate region is still subject to ongoing research and for example DSE investigations find the CFL phase to be favored [184–186].

Further proposed phases include a confined, but chirally symmetric quarkyonic phase at low temperatures and intermediate chemical potential which has been proposed on the basis of $1/N_c$ arguments [187]. Recent FRG calculations in a Polyakov extended quark-meson model, on the other hand, show that the proper inclusion of matter back reactions can bring the two transitions closer to each other even at larger chemical potentials in $N_c = 3$ [148]. A similar conclusion has been reached in a DSE based approach from the quark propagator [188, 189]. Finally, the cold but very dense region in the phase diagram is expected to be realized in the interior of neutron stars [190].

A number of methods such as imaginary chemical potential [166, 191–193], Taylor expansions or reweighting techniques [194–198] have been proposed to overcome the sign problem in lattice calculations, but none of them work reliably outside $\mu/T \lesssim 1$. Some of these calculations have reported a weakening of the transition with growing chemical potential, which does not support the critical endpoint scenario.

Before going on it should be noted that the second-order transition at the critical endpoint falls in the Z_2 universality class of the Ising model. A correct calculation of critical exponents can for example be provided by the FRG method [199], whereas DSE calculations usually yield mean-field exponents (see [200] for attempts to improve on this via including meson effects). The mean-field exponents in the latter case are connected to the rainbow-ladder approximation together with quark-gluon vertex models. A better knowledge of this quantity would therefore be desired, as additionally a strong vertex model dependence of the chiral as well as the center transition can be observed [201].

Some experiments concerned with dense and hot QCD matter are shown in Fig. 2.6 as blobs at roughly the temperatures and densities they explore. The high temperature region of the phase diagram is covered by Au-Au collisions at the Relativist Heavy Ion Collider (RHIC) of the Brookhaven national lab and Pb-Pb collisions at the Large Hadron Collider (LHC) at the European Organization for Nuclear Research (CERN) in Geneva. Higher densities will be explored at the RHIC as well as the future experiments at the Facility for Antiproton and Ion Research (FAIR) at the GSI Helmholtzzentrum für Schwerionenforschung in Darmstadt, the Nuclotron-based Ion Collider Facility (NICA) at the Joint Institute for Nuclear Research (JINR) in Dubna and the Japan Proton Accelerator Research Complex (J-PARC) at the Tokai site of the Japan Atomic Energy Agency (JAEA). Finally, it should be stressed that the shown phase diagram assumes a system in the thermodynamic limit and in equilibrium.

Axial Anomaly, Quark Mass Dependence and Critical Surface

A recent analysis of experimental data from the PHENIX and STAR collaborations at RHIC has found a weakening of the mass splitting between η'-meson and pions at the temperature of the chiral transition [202]. This has lead to the speculation that the axial anomaly might be lifted at least partially at temperatures slightly above the chiral transition. On the other hand, a full restoration of $U_A(1)$ is expected at very large temperatures [203]. Furthermore, the fate of the Witten-Veneziano relation Eq. (2.50) at non-vanishing temperature is interesting (see e.g. [204]).

Very recently, the lattice QCD community has become more interested in the axial anomaly at finite temperatures. First results have been obtained with computationally less expensive staggered fermions [205, 206] and also results using the more expensive domain wall [164] and overlap fermions [165] are available. These new results indicate that $U(1)_A$ is still broken
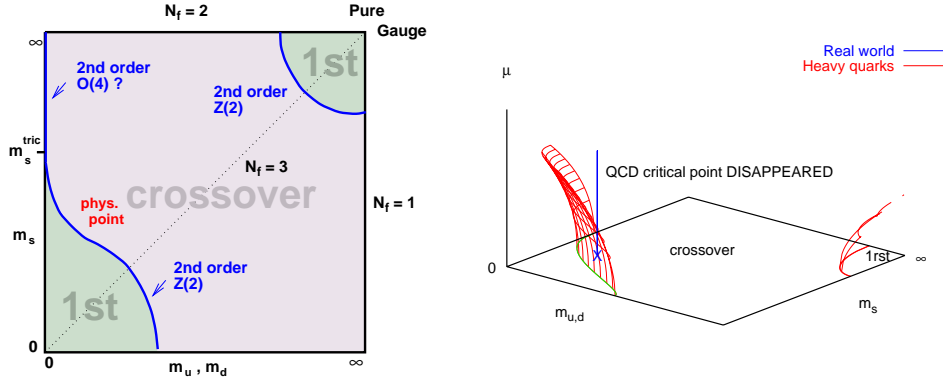
Figure 2.7.: Expected quark mass dependence of the order of the phase transitions as function of light (up, down) and strange quark masses (left panel) and chiral critical surface as obtained in [193].

slightly above the transition temperature. It should be noted, however that the results obtained with chiral fermions are from calculations with $m_\pi \geq 200$ MeV and at small volumes, due to the large numerical effort involved.

Additionally, for large quark chemical potential - where lattice investigations are hampered by the sign problem - it has been argued that $U(1)_A$ violation should also decrease [207–211]. From mean-field studies of effective descriptions it is furthermore expected that anomaly effects can play an important role at intermediate chemical potential [212, 213].

Some crucial results concerning the influence of the axial anomaly on the order of the chiral transition have been obtained in the purely mesonic part of Eq. (2.71). In [214], the infrared stability of the fixed point governing the phase transition has been investigated in an ϵ-expansion. An infrared unstable fixed point has been argued to correspond to a first-order transition induced by fluctuations [215]. Without 't Hooft determinant Eq. (2.73), the transition has been found to be of first order in the chiral limit at $\mu = 0$ for

$$N_f \geq \sqrt{3} \, , \tag{2.90}$$

where the chiral invariant ρ_2 of Eq. (2.72) is responsible for the instability in the fixed point [216]. It has furthermore been argued in [214] that for $N_f = 2$ the mass-like 't Hooft determinant can transform the transition to second order, if the corresponding coupling is approximately temperature independent. In case of $N_f = 3$ no influence of the 't Hooft determinant on the fist order phase transition is expected as the determinant is of $\mathcal{O}(\Sigma^3)$ [214]. The Columbia plot in the left panel of Fig. 2.7 shows the expected quark-mass dependence of the phase transitions of QCD at $\mu = 0$ without restoration of $U(1)_A$ at the chiral transition. At large quark masses (upper right corner) the limit of a pure gauge theory is approached, which shows a first-order transition. This first-order region is separated from the crossover region, which includes the physical mass point, by a line of second-order transitions in the Z_2 universality class [217, 218]. A similar scenario applies to the first-order transition in the three flavor chiral limit (lower left corner), which is also separated by a line of second order transitions from the crossover region. This chiral critical line has been found to be in the Z_2 universality class of the Ising model as well [219]. The situation in the light chiral limit with

$m_{u,d} = 0$ (left edge) is less clear, but from universality arguments it is expected that the Z_2 second-order line merges with the light chiral limit axis at some finite value of the strange quark mass m_s. A line of second-order transitions connecting to the light chiral limit (upper left corner), corresponding to the $O(4)$ universality class, might be the consequence.

Finally, if the Columbia plot is extended by a third axis of chemical potential, the line of second-order transitions separating crossover region from chiral limit turns into a surface of second-order transitions. In lattice calculations, this chiral critical surface has been found to bend away from the physical mass point of QCD at small chemical potential [193]. This is a hint for the absence of the critical endpoint in the phase diagram. On the other hand, there remains the option that the surface bends back towards the physical mass point at higher chemical potentials, which are not accessible with lattice methods. This section is closed with the observation that mean-field calculations in quark-meson models are not capable of reproducing all these features as they miss the crucial mesonic fluctuations and often also vacuum fluctuations of the quark sector (see e.g. [213]).

3. Consequences of an Infrared Singular Four Quark Interaction

In Sec. 2.1.2 a $1/k^4$ singularity in the quark 4-point function has been discussed as a possible source of confinement in terms of a linearly rising potential [100]. This singularity would also violate cluster decomposition, as required by the Kugo-Ojima confinement criterion [91]. Furthermore, it has been argued that such an infrared behavior could be induced by a self-consistent infrared singular solution for the quark-gluon vertex [113].

With this motivation such a $1/k^4$ singularity is assumed as a working hypothesis in the following [220]. Using the Dyson-Schwinger equations Eq. (2.16), the consistency of such a singularity is investigated and possible consequences for other n-point functions are explored with a focus on color structures. The spinorial structures are neglected in this first study with the argument that fundamentally charged scalar matter also has a confined phase [221, 222]. The derivation of the DSEs for higher n-point functions ranges from tedious to impossible by hand. Therefore, the programs DoDSE [223] and DoFun [224] will be used extensively in this chapter. The gauge group is taken as $SU(N)$ with generators and basis elements as defined in App. A.2 and App. A.3.1.

The Dyson-Schwinger equation for the quark 4-point function is given by
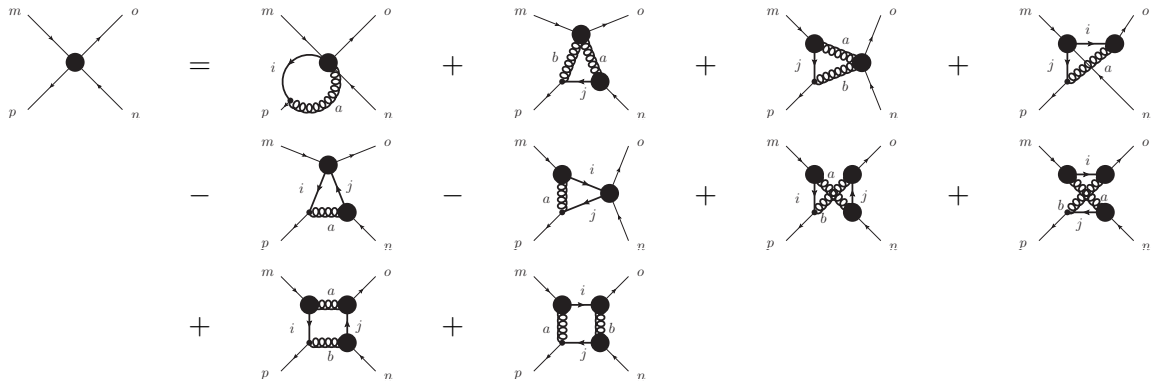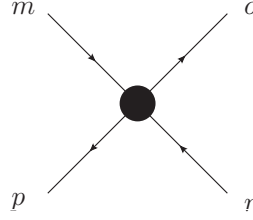
Figure 3.1.: DSE for the quark 4-point function.

where generalized indices - including continuous as well as discrete variables - are used. In addition to the graphical rules introduced below Fig. 2.1, bare vertices are indicated by small black dots.
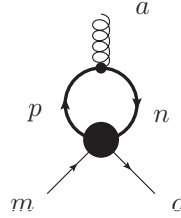
To understand possible problems associated with the proposed singularity, assume that the quark 4-point function $\Gamma(p_m, p_n, p_o, p_p)$ behaves as

3. Consequences of an Infrared Singular Four Quark Interaction
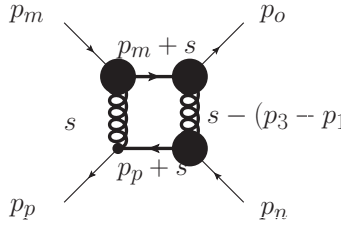
$$\overset{p_m \to p_o}{\propto} \frac{1}{(p_m - p_o)^4} \, , \qquad (3.1)$$

in the limit of vanishing momentum exchange between quark and antiquark. In the DSE for the 4-point function alone, this causes no immediate contradictions. However, this singularity can also influence other n-point functions via the corresponding equations. The induced singularities might in turn lead to trouble, if put back in DSE of the quark 4-point function again. For example, the quark-gluon vertex, which also appears in the above DSE, would inherit the singularity from one of the diagrams in its DSE

$$\overset{p_m \to p_o}{\propto} \frac{1}{(p_m - p_o)^4} \, , \qquad (3.2)$$

as the singular behavior is independent of the loop integration. This divergence in the soft-gluon limit is stronger then the self-consistent singularity of the scaling solution for the verteix with exponent $\propto (k^2)^{-1/2-\kappa}$. Putting this singular quark-gluon vertex in the box diagram, infrared power counting [225] leads to a singular contribution

$$\overset{p_m \to p_o}{\propto} \left[(p_m - p_o)^2\right]^{2+2(\kappa_g-1)+3(-2)} = \left[(p_m - p_o)^2\right]^{2\kappa_g-6} \, . \quad (3.3)$$

in the limit of soft gluon exchange, where only the momenta are shown for brevity. In the exponent the first term, 2, comes from the loop integration over s, the second term, $2(\kappa_g-1)$, from the infrared scaling of the two gluon propagators and the third term, $3(-2)$, from the quark-gluon vertices at soft gluon momenta. The inequality $\kappa_g < 2$ holds independent of the type of infrared solution and the above diagram leads to a stronger singularity than assumed in the beginning in the quark 4-point function.
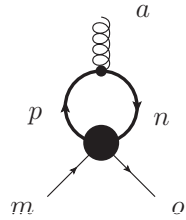
Therefore the only possibility for having $1/k^4$ consistently is without a contribution to the quark-gluon vertex via Eq. (3.2). Algebraic cancellations in the color structure are then a natural suspect, which is the subject in the remainder of this section. Consequently, the following investigation is equally valid for any kind of fundamentally charged matter, independent of its spin. Nevertheless, the term quark will be used instead of matter.

3.1. Quark 4-Point Function

According to [226] and the discussion in App. A.3.1, the momentum space quark 4-point function of fundamentally charged quarks can be expanded in two color structures

$$\frac{\Gamma_{mnop}(p_m, p_n, p_o, p_p)}{\tilde{\delta}^{(4)}(p_o + p_p - p_m - p_n)} = F_1(p_m, p_n, p_o)\delta_{mo}\delta_{np} + F_2(p_m, p_n, p_o)\delta_{mp}\delta_{no} , \qquad (3.4)$$
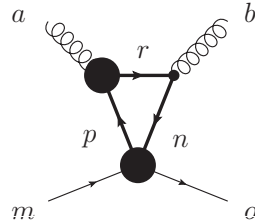
if only those structures compatible with (color) charge conservation are considered. From the previous discussion it is necessary to identify tensor structures that do not contribute to the quark-gluon vertex Eq. (3.2). To simplify the investigation, Feynman graphs represent only the color structure of n-point functions in the remainder of this chapter. The contribution to the quark-gluon vertex is

$$: \qquad T^a_{pn}\left(F_1\delta_{mo}\delta_{np} + F_2\delta_{mp}\delta_{no}\right) = F_2 T^a_{mo} . \qquad (3.5)$$

Therefore, a $1/(p_m - p_o)^4$ singularity in $\Gamma_{mnop}(p_m, p_n, p_o, p_p)$ is only admissible in F_1 without contradiction.

From symmetry arguments one expects a similar singularity in F_2 in the limit $p_n \to p_o$, but this can also be obtained from the DSEs directly. The derivation requires a detour via the equation for the quark-gluon 4-point function, where in one formulation there is a singular contribution from the diagram

$$: \qquad \delta_{mo}\delta_{np}T^a_{pr}T^b_{rn} = \frac{1}{2}\delta_{mo}\delta^{ab} , \qquad (3.6)$$
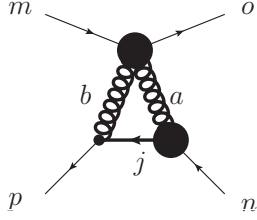
behaving as $1/(p_m - p_o)^4$ in the limit of degenerate quark momenta $p_m \to p_o$. Therefore, the singularity in the quark 4-point function implies a similar infrared behavior in its quark-gluon counterpart

$$\Gamma^{ab}_{mo}(p_m, p_o, p_a) = G_1(p_m, p_o, p_a)T^a_{mi}T^b_{io} + G_2(p_m, p_o, p_a)T^b_{mi}T^a_{io} + G_3(p_m, p_o, p_a)\delta^{ab}_{mo} , \quad (3.7a)$$
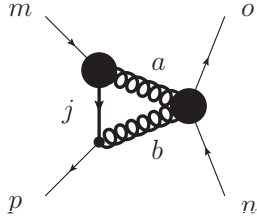
$$G_3(p_m, p_o, p_a) \to \frac{1}{(p_m - p_o)^4} \quad \text{for} \quad p_m \to p_o . \qquad (3.7b)$$

It is interesting to investigate the consistency of this new singularity in the DSE for the quark 4-point function. There are two relevant diagrams

3. Consequences of an Infrared Singular Four Quark Interaction

$$T_{nj}^a T_{jp}^b \delta^{ab} \delta_{mo} = \frac{N^2-1}{2N} \delta_{mo}\delta_{np} , \qquad (3.8)$$

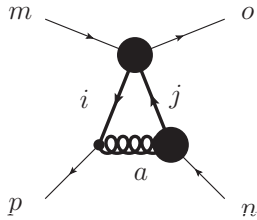$$T_{mj}^a T_{jp}^b \delta^{ab} \delta_{no} = \frac{N^2-1}{2N} \delta_{mp}\delta_{no} . \qquad (3.9)$$

This shows that - as expected from symmetry arguments - there are actually two infrared singularities

$$F_1(p_m, p_n, p_o) \to \frac{1}{(p_m - p_o)^4} \quad \text{for} \quad p_m \to p_o , \qquad (3.10\text{a})$$

$$F_2(p_m, p_n, p_o) \to \frac{1}{(p_n - p_o)^4} \quad \text{for} \quad p_n \to p_o , \qquad (3.10\text{b})$$

in the quark 4-point function Eq. (3.4). It is important to note that the second singularity does not pose a threat to consistency in Eq. (3.2). This is, because the singularity depends on the integrated loop momentum and is therefore mitigated by the integration.
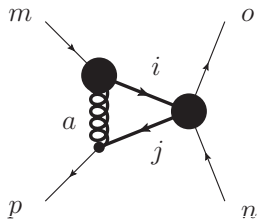
It remains to show that the two singularities Eq. (3.10) do not lead to inconsistencies in the DSE for the quark 4-point function. The relevant diagrams are

$$T_{nj}^a \left(F_2 \delta_{jo}\delta_{mi} + F_1 \delta_{mo}\delta_{ji}\right) T_{ip}^a \qquad (3.11)$$
$$= \left(\frac{1}{2}\delta_{np}\delta_{ij} - \frac{1}{2N}\delta_{nj}\delta_{ip}\right)\left(F_2\delta_{jo}\delta_{mi} + F_1\delta_{mo}\delta_{ji}\right)$$
$$= \left(\frac{F_2}{2} + F_1\frac{N^2-1}{2N}\right)\delta_{mo}\delta_{np} - \frac{F_2}{2N}\delta_{mp}\delta_{no} ,$$

$$T_{mi}^a \left(F_1 \delta_{io}\delta_{nj} + F_2 \delta_{ij}\delta_{no}\right) T_{jp}^a \qquad (3.12)$$
$$= \left(\frac{1}{2}\delta_{mp}\delta_{ji} - \frac{1}{2N}\delta_{mi}\delta_{jp}\right)\left(F_1\delta_{io}\delta_{nj} + F_2\delta_{ij}\delta_{no}\right)$$
$$= \left(\frac{F_1}{2} + F_2\frac{N^2-1}{2N}\right)\delta_{mp}\delta_{no} - \frac{F_1}{2N}\delta_{mo}\delta_{np} ,$$
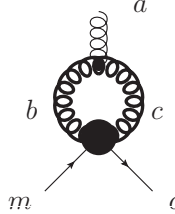
where the singularity is in F_1 in the upper diagram and in F_2 in the lower diagram for $p_m \to p_o$ and $p_n \to p_o$ respectively. In either case the singular parts just contribute to consistent color structures $\delta_{mo}\delta_{np}$ and $\delta_{mp}\delta_{no}$ in the first and second diagram respectively.
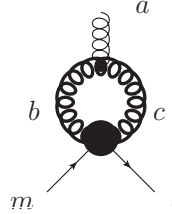
Consistency in Quark-Gluon Vertex

Before going on it should be checked that also the new singularity in the quark-gluon 4-point function is not forwarded to the quark-gluon vertex. Two graphs might lead to problems, where the first cancels similarly as before via the trace over the (adjoint) generator
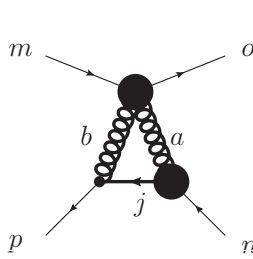

$$: \quad f^{abc}\delta^{bc}\delta_{mo} = 0 \; . \tag{3.13}$$

It is interesting to note that also a quark-gluon 4-point function proportional to $\{T^a, T^b\}_{mn}$ cancels algebraically

$$f^{abc}\{T^b, T^c\}_{mo} = -i\{T^b, [T^a, T^b]\}_{mo} \tag{3.14}$$

$$= (-i)\left(T^bT^aT^b - T^bT^bT^a + T^aT^bT^b - T^bT^aT^b\right)_{mo}$$

$$= (-i)\left(T^aT^bT^b - T^bT^bT^a\right)_{mo} = 0 \; .$$

In the last line it has been used that T^aT^a is proportional the unit matrix. It is possible to rule out this additional $1/k^4$ singularity by using the diagram Eq. (3.8). To see this, note that

$$T^a_{nj}T^b_{jp}\{T^a, T^b\}_{mo} = T^a_{nj}T^b_{jp}\left(T^a_{ml}T^b_{lo} + T^b_{ml}T^a_{lo}\right) \tag{3.15}$$

$$= \left(\frac{1}{2}\delta_{nl}\delta_{mj} - \frac{1}{2N}\delta_{nj}\delta_{ml}\right)\left(\frac{1}{2}\delta_{jo}\delta_{lp} - \frac{1}{2N}\delta_{jp}\delta_{lo}\right)$$

$$+ \left(\frac{1}{2}\delta_{no}\delta_{jl} - \frac{1}{2N}\delta_{nj}\delta_{lo}\right)\left(\frac{1}{2}\delta_{jl}\delta_{mp} - \frac{1}{2N}\delta_{jp}\delta_{ml}\right)$$

$$= \delta_{mo}\delta_{np}\left(\frac{1}{4}\right) + \delta_{mp}\delta_{no}\left(\frac{N^2 - 4}{4N}\right) \; .$$
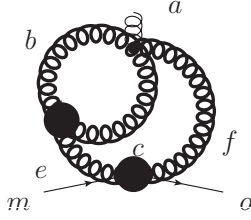
which would lead to singular contribution also in forbidden tensor structures of the quark 4-point function. In the case of $N = 2$, on the other hand, the commutator is just

$$\{T^a, T^b\}_{mn} \propto \delta^{ab}\delta_{mn} \; , \tag{3.16}$$

as the structure constants d^{abc} all vanish for $N = 2$.

The second diagram that might cause trouble in the quark-gluon vertex DSE also annihilates the tensor structure $\delta^{ab}\delta_{mo}$

$$(c_1 f^{bce} + c_2 d^{bce}) \left(f^{iab} f^{icf} + f^{iac} f^{ibf} + f^{iaf} f^{ibc} \right) \delta^{ef} \qquad (3.17)$$

$$= (c_1 f^{bce} + c_2 d^{bce}) \left(f^{iab} f^{ice} + f^{iac} f^{ibe} + f^{iae} f^{ibc} \right)$$

$$= c_1 \left(f^{iab} N \delta^{bi} + f^{iac} (-N) \delta^{ic} + f^{iae} N \delta^{ie} \right) + c_2 \cdot 0 = 0 .$$

This shows consistency of the combined singularities Eq. (3.10) and Eq. (3.7) in the quark and quark-gluon 4-point functions at least in the subset of DSEs investigated so far.

Contributions to the $1/k^4$ singularity in the quark 4-point function can have two qualitatively different sources. First, they can be of the loop independent form encountered in the previous cases, as e.g. the $1/k^4$ singularity of the quark 4-point function immediately induces a similar singularity in the quark-gluon 4-point function. Another source of singular contributions are the loop integrations. In either case it is possible to make restrictions on the tensor structures which are allowed to contribute by investigating the diagrams in Fig. 3.1 one by one. The corresponding results and calculations are lengthy and can be found in App. B.1.

To summarize, it has been shown in this section that the only way of having a $1/k^4$ infrared singularity in the quark 4-point function Eq. (3.4) without inconsistencies is in a non-trivial tensor-structure Eq. (3.10). Furthermore this singularity is necessarily accompanied by a similar singularity in the quark-gluon 4-point function Eq. (3.7). Graphically this can be represented as shown in Figs. 3.2 and 3.3
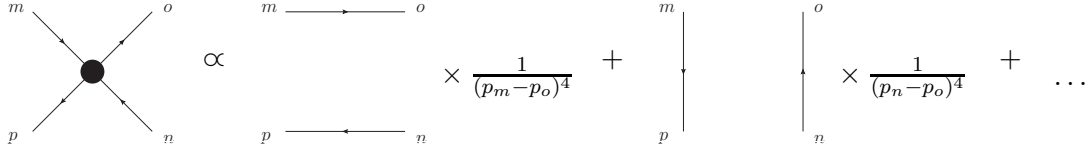

Figure 3.2.: Diagrammatic representation of the $1/k^4$ singularity in the quark 4-point function.
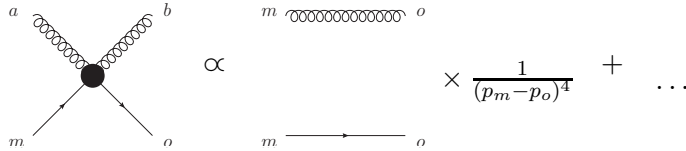

Figure 3.3.: Diagrammatic representation of the $1/k^4$ singularity in the quark-gluon 4-point function.

where the ellipses represent contributions less singular than $1/k^4$.

If, however, the quark-gluon 4-point function were the source of the singularity, Casimir scaling [227] would be a consequence of the Eqs. (3.8) and (3.9). It will be seen in the next chapter, that this diagram also give the correct Casimir invariant in case of the adjoint repre-

sentation. Furthermore, it is shown in App. B.1 that all allowed loop momentum independent sources of the singularity in Fig. 3.1 are proportional to the quadratic Casimir operator.

3.2. General n-Point Functions

Before jumping blindly into tedious calculations of tensor structure in general n-point functions it is useful to perform some general calculations. Furthermore, a simple rule for identifying the color structure of singular contributions will be derived.

4-Point Functions

The diagrams that led to a forwarding of the $1/k^4$ divergence from the quark to the quark-gluon 4-point function are contained in the general class of diagrams shown in Fig. 3.4.
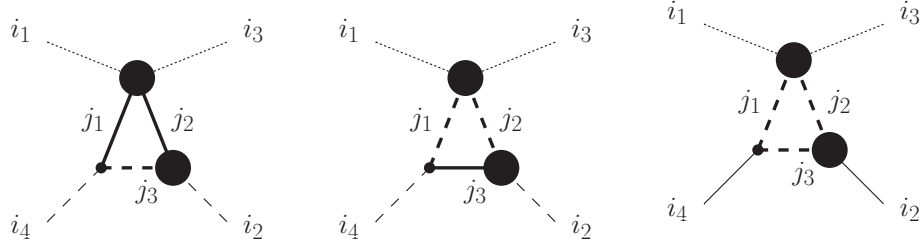
Figure 3.4.: General diagrams of 4-point functions contributing to 4-point functions.

Here, solid, dashed and dotted lines represent different fields. Although, restrictions could also be derived from the conservation of other quantum numbers, color charge conservation is sufficient to restrict the types of field lines. There are two types of lines corresponding to the representation of the color group, i.e. fundamental lines and adjoint lines. Color conservation implies that 3-point functions must involve at least one adjoint line. This implies that the solid lines in any of the above diagrams can only correspond to the adjoint representation. One general statement is that in any of the diagrams shown in Fig. 3.4 a color structure

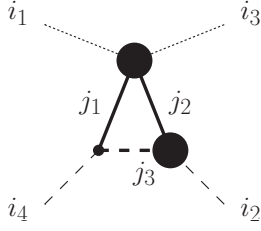$$\Gamma^{(4)}_{i_1 i_3 j_1 j_2} : \qquad \delta_{i_1 i_3} \delta_{j_1 j_2} , \qquad (3.18)$$

in the four point function contributes solely to the color structure

$$\Gamma^{(4)}_{i_1 i_3 i_2 i_4} : \qquad \delta_{i_1 i_3} \delta_{i_2 i_4} . \qquad (3.19)$$

This statement is true for any combination of fundamental and adjoint lines. This can be checked explicitly for all cases allowed by (color) charge conservation.

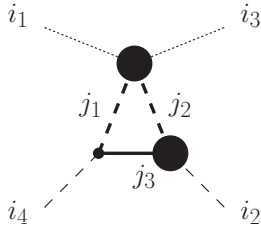In the first diagram of Fig. 3.4 the dashed line is either fundamental or adjoint giving

$$\delta_{i_1 i_3}\delta_{j_1 j_2}T^{j_2}_{i_2 j_3}T^{j_1}_{j_3 i_4} = \frac{N^2-1}{2N}\delta_{i_1 i_3}\delta_{i_2 i_4} \ , \tag{3.20}$$

$$\delta_{i_1 i_3}\delta_{j_1 j_2}\left(-c_1 f^{j_2 i_2 j_3} - c_2 d^{j_2 i_2 j_3}\right)f^{j_1 j_3 i_4} = c_1 N\delta_{i_1 i_3}\delta_{i_2 i_4} \ ,$$
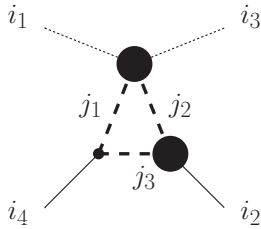
respectively, where total (anti-)symmetry of the structure constants (f^{ijk}) d^{ijk} has been used. The quark-gluon 4-point function would contribute to the quark 4-point function via a diagram of this type. Therefore, depending on the type of representation for the quarks, this diagram would induce exactly the correct factors for Casimir scaling.

In the second diagram of Fig. 3.4 the case of fundamental dashed line has not been treated already with the above diagram

$$\delta_{i_1 i_3}\delta_{j_1 j_2}T^{j_3}_{i_2 j_2}T^{j_3}_{j_1 i_4} = \frac{N^2-1}{2N}\delta_{i_1 i_3}\delta_{i_2 i_4} \ . \tag{3.21}$$

Finally, the third diagram of Fig. 3.4 with fundamental dashed line gives

$$\delta_{i_1 i_3}\delta_{j_1 j_2}T^{i_2}_{j_2 j_3}T^{i_4}_{j_3 j_1} = \frac{1}{2}\delta_{i_1 i_3}\delta_{i_2 i_4} \ , \tag{3.22}$$

confirming that color structures like Eq. (3.18) contribute only to Eq. (3.19) via diagrams of the form Fig. 3.4.

Contributions to 3-Point Functions

From the discussion at the beginning of this chapter it is interesting to calculate the contribution of the tensor structure Eq. (3.18) to 3-point functions. In general one encounters diagrams of the form shown in Fig. 3.5.
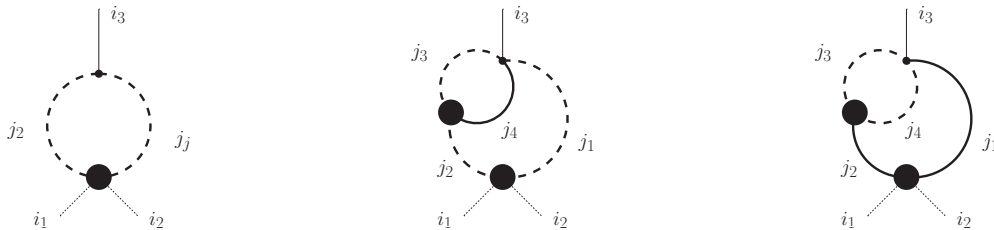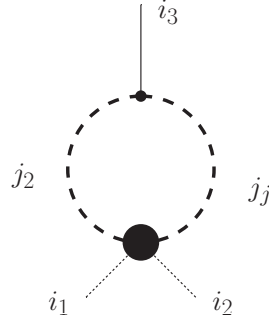

Figure 3.5.: General diagrams of 4-point functions contributing 3-point functions.
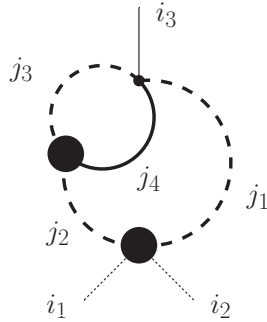
Again, charge conservation can be invoked to see that solid lines have to be adjoint and only the dashed lines are allowed to be fundamental.

The tensor structure of Eq. (3.18) gives a vanishing contribution in the first diagram of Fig. 3.5 as the fundamental as well as the adjoint generators are traceless
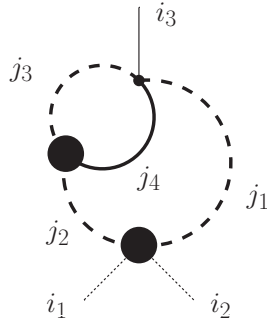

$$\delta_{i_1 i_2} \delta_{j_1 j_2} T^{i_3}_{j_2 j_1} = 0 \,,$$
$$\delta_{i_1 i_2} \delta_{j_1 j_2} f^{i_3 j_2 j_1} = 0 \,. \tag{3.23}$$

For the second diagram of Fig. 3.5 the case with fundamental dashed line gives the contribution

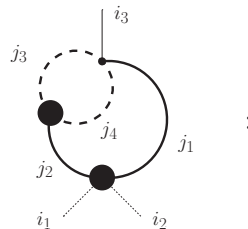$$\delta_{i_1 i_2} \delta_{j_1 j_2} T^{j_4}_{j_2 j_3} \left(T^{j_4}_{j_3 l} T^{i_3}_{l j_1} + T^{i_3}_{j_3 l} T^{j_4}_{l j_1} \right) \tag{3.24}$$
$$= \delta_{i_1 i_2} \left(T^{i_3}_{l j_1} \frac{N^2 - 1}{2N} \delta_{j_1 l} + T^{i_3}_{j_3 l} \frac{N^2 - 1}{2N} \delta_{l j_3} \right) = 0 \,.$$

With adjoint dashed lines one obtains

$$(c_1 f^{j_3 j_4 j_2} + c_2 d^{j_3 j_4 j_2}) \times$$
$$\left(f^{i i_3 j_3} f^{i j_4 j_1} + f^{i i_3 j_4} f^{i j_3 j_1} + f^{i i_3 j_1} f^{i j_3 j_4} \right) \delta^{j_2 j_1}$$
$$= (c_1 f^{j_3 j_4 j_2} + c_2 d^{j_3 j_4 j_2}) \times$$
$$\left(f^{i i_3 j_3} f^{i j_4 j_2} + f^{i i_3 j_4} f^{i j_3 j_2} + f^{i i_3 j_2} f^{i j_3 j_4} \right)$$
$$= c_1 \left(f^{i i_3 j_3} N \delta^{j_3 i} + f^{i i_3 j_4} (-N) \delta^{i j_4} + f^{i i_3 j_2} N \delta^{i j_2} \right)$$
$$= 0 \,. \tag{3.25}$$

Finally the third figure of Fig. 3.5 with fundamental dashed line gives

$$\delta_{i_1 i_2} \delta_{j_1 j_2} T^{j_2}_{j_4 j_3} \left(T^{j_1}_{j_3 l} T^{i_3}_{l j_4} + T^{i_3}_{j_3 l} T^{j_1}_{l j_4} \right) \tag{3.26}$$
$$= \delta_{i_1 i_2} \left(T^{i_3}_{l j_4} \frac{N^2 - 1}{2N} \delta_{j_4 l} + T^{i_3}_{j_3 l} \frac{N^2 - 1}{2N} \delta_{l j_3} \right) = 0 \,.$$

Therefore the tensor structure Eq. (3.18) does not contribute to any 3-point function via diagrams of type Fig. 3.5.
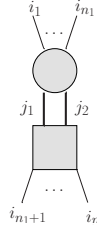
Factorization of Tensor Structures

In addition to the explicit calculation of loop momentum independent $1/k^4$ singular contributions in 4-point functions it is useful to develop a strategy of identifying singular terms in general n-point function.

Given some graph with external legs $i_1, \ldots, i_n$, suppose that a n_1-point function $\Gamma_{i_1 \cdots i_{n_1} j_1 j_2}$ is attached to the remaining part of the graph with its two legs $j_1 j_2$ only. Let furthermore be $R_{j_1 j_2 i_{n_1+1} \cdots i_n}$ the color structure of the remainder of the graph. Then any tensor structures of the form $G_{i_1 \cdots i_{n_1}} \delta_{j_1 j_2}$ in $\Gamma_{i_1 \cdots i_{n_1} j_1 j_2}$ contributes only to the tensor product

$$G_{i_1 \cdots i_{n_1}} R_{jj i_{n_1+1} \cdots i_n} \ . \tag{3.27}$$

This graph can also be represented pictorially as

where the circular blob represents $\Gamma_{i_1 \cdots i_{n_1} j_1 j_2}$ and the square the remainder. Any tensor structure in $\Gamma_{i_1 \cdots i_{n_1} j_1 j_2}$ proportional to $\delta_{j_1 j_2}$ leads to the factorization
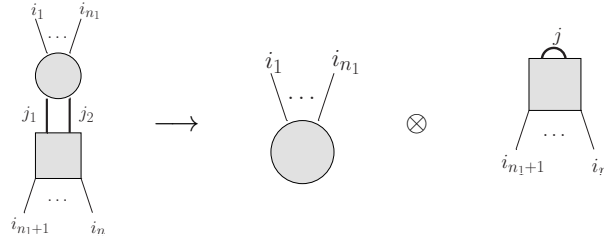
Figure 3.6.: Factorization of color structures.

where the circle represents $G_{i_1 \cdots i_{n_1}}$ and the square $R_{j_1 j_2 i_{n_1+1} \cdots i_n}$.

As an application of this observation one can prove again, but with less effort, that the tensor structure Eq. (3.18) in the 4-point function of any of the diagrams shown in Fig. 3.4 contributes only to Eq. (3.19). Note first that $\delta_{i_1 i_3} \delta_{j_1 j_2}$ is of the form $G_{i_1 i_3} \delta_{j_1 j_2}$ leading to the factorization

Figure 3.7.: Factorization of contribution to 4-point function.

The second factor is a self-energy term of some propagator, i.e. it contributes only to the color structure $\delta_{i_2 i_4}$. Therefore, the the tensor structure $\delta_{i_1 i_3} \delta_{j_1 j_2}$ in the 4-poi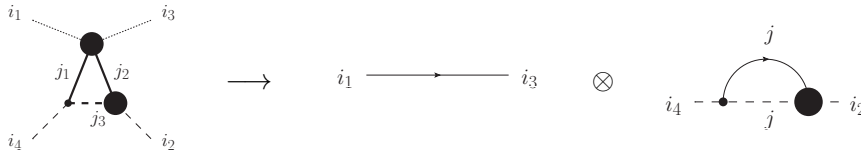nt function contributes just to $\delta_{i_1 i_3} \delta_{i_2 i_4}$ via the above factorization, which is the previously derived rule. Obviously this method [1] yields also the correct algebraic factors if one performs the remaining calculations. However, the main reason for introducing this diagrammatic method is that one wants to avoid such tedious calculations. From this example it should be clear that the product tensor structures in Eq. (3.27) or Fig. 3.6 can only be tensor structures that appear in the corresponding n_1- and $(n - n_1)$-point functions.

3.2.1. Infrared Singularities in General 4-Point Functions

Equipped with these tools, it is easy to investigate the consequences of the $1/k^4$ singularity for other 4-point functions of the theory. In Sec. 3.1 it has already been found that such a singularity can only be of the type shown in Fig. 3.2 which implies a divergence as in Fig. 3.3 in the quark-gluon 4-point function. The divergence in the quark-gluon 4-point function stems from the diagram Eq. (3.1). To get similar singular contributions to other 4-point functions it is necessary to identify the corresponding diagrams in their DSE. Actually, all the necessary calculations have already been performed. In general there will be a plethora of diagrams contributing to any of the 4-point functions. For example, the DSE for the gluon 4-point function as calculated with DoFun contains 79 diagrams. Therefore only diagrams of the type shown in Fig. 3.4 are collected and used for the following analysis.

For the quark-gluon 4-point function there exist different DSEs corresponding to the order of differentiating with respect to the fields. Here the version obtained by differentiating the DSE for the gluon propagator with respect to the quark field is used. There are three relevant diagrams
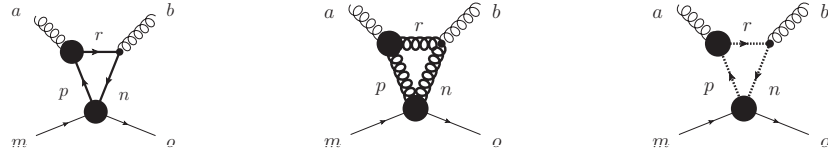
Figure 3.8.: Contribution of 4-point functions to the quark-gluon 4-point function.

In any of these diagrams a tensor structure $\delta_{mo} \delta_{pn}$ will only contribute to $\delta_{mo} \delta^{ab}$. Additionally, there are the diagrams
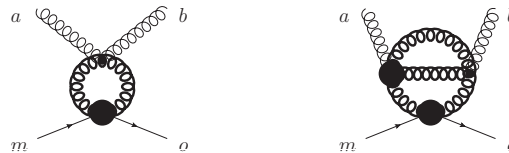
Figure 3.9.: Contribution of 4-point functions to the quark-gluon 4-point function.

Using the factorization induced by a tensor structure $\delta_{mo} \delta^{pn}$ in the quark-gluon 4-point function one sees that any of the above diagram factorizes to δ_{mo} times the tadpole or sunset

---

[1] A similar diagrammatic method has been introduced e.g. in [228].

graph to the gluon propagator DSE.

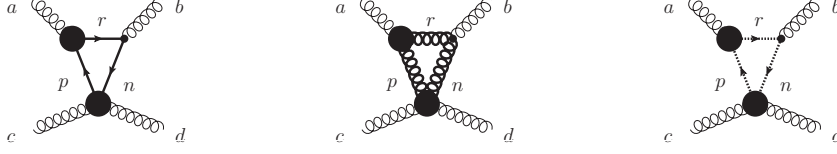In the DSE for the gluon 4-point function the diagrams

Figure 3.10.: Contribution of 4-point functions to the gluon 4-point function.

as well as graphs that can be treated as the previous graphs in Fig. 3.9 appear.

In the DSE for the ghost-gluon 4-point function obtained from the ghost propagator DSE one gets
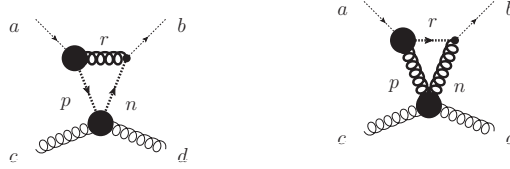
Figure 3.11.: Contribution of 4-point functions to the ghost-gluon 4-point function.

Finally, the DSE for the quark-ghost 4-point function obtained from the quark propagator yields
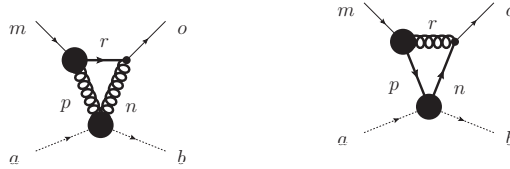
Figure 3.12.: Contribution of 4-point functions to the quark-ghost 4-point function.

From all these graphs and the general calculations performed previously it is clear that as soon as one 4-point function $\Gamma_{i_1 i_2 i_3 i_4}$ has a $1/k^4$ infrared singularity in the tensor structure $\delta_{i_1 i_3} \delta_{i_2 i_4}$, it is immediately forwarded to the corresponding tensor structures in all other 4-point functions. As has been shown previously, none of the three point functions are affected by these singularities due to algebraic cancellations and in turn also the propagators are protected.

One consequence is that if only one species of fundamentally charged matter has an infrared singularity of the $1/k^4$ type in its 4-point function, than all other matter gets it as well.

3.2.2. Highter n-Point Functions

In fact, the singularities thus found are not restricted to 4-point functions. Exemplary for higher correlation functions, the DSE for the 5-point function with one gluon and four quark legs is investigated. Among others, the diagrams shown in Fig. 3.13 contribute.
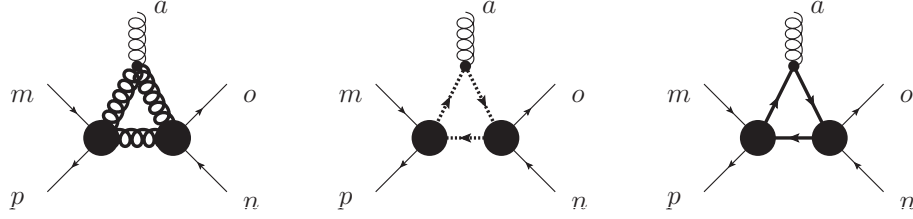
Figure 3.13.: Contribution of 4-point functions to the quark-1-gluon 5-point function.

Using the factorization of tensor structures
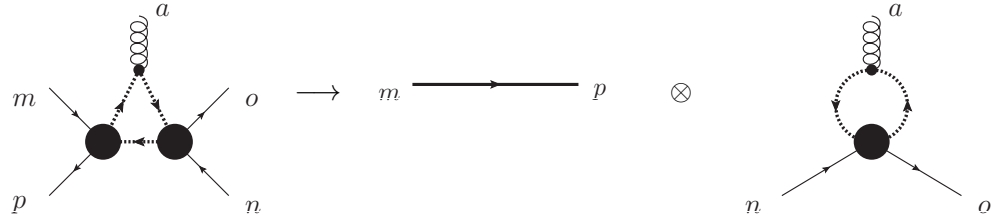
Figure 3.14.: Factorization in quark-1-gluon 5-point function.

one gets a singular contribution to the tensor structure $\delta_{mp}T_{no}^a$ in the limit $p_m \to p_p$. Similarly a $1/k^4$ singularity is induced in $\delta_{no}T_{mp}^a$ for $p_n \to p_o$. It has been checked already in Eq. (B.9) that this kind of singularity is consistent with the quark 4-point function. Note furthermore that a cataclysmic $1/k^8$ singularity in the simultaneous limit $p_m \to p_p$ and $p_n \to p_o$ is prevented due to an algebraic cancellation in the second factor of Fig. 3.14.

Similarly the DSE for the 5-point function with three gluon and two quark legs gets $1/k^4$ singular contributions via the diagrams shown in Fig. 3.15.
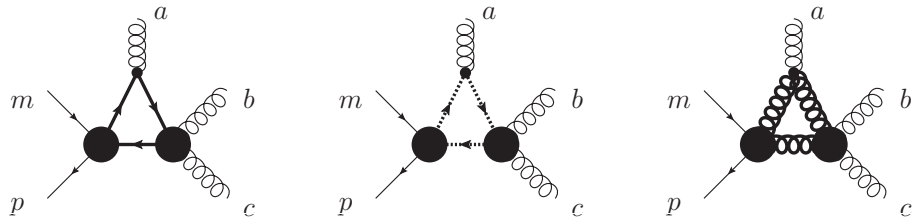
Figure 3.15.: How 4-point functions can contribute to the quark-3-gluon 5-point function.

Using factorization once more one gets singular contributions to the tensor structures proportional $\delta_{mp}f^{abc}$ for $p_m \to p_p$ and $T_{mp}^a\delta^{bc}$ for $p_b \to p_c$. Additionally, there are similar diagrams leading to corresponding singularities demanded by symmetry in the gluon legs.

3. Consequences of an Infrared Singular Four Quark Interaction

General Structure of Singularities

From these examples a general picture of the singular tensor structures emerges, which is summarized as follows. Given some n-point function, it is possible to separate the n-legs into $r > 1$ clusters with $2 \leq n_1, \ldots, n_r$ members. If the exchanged momentum k_j between any of these clusters j and the remaining clusters goes to zero, one gets a singular contributions $1/k_j^4$. Furthermore this singularity appears only in specific color structures. Let the most general color structure of the corresponding n_j-point function be $G^{1,\ldots,n_j}$. Similarly let $R^{1,\ldots,n-n_j}$ be the most general color structure representing the remaining clusters. Then the $1/k_j^4$ singularity of the full n-point function is restricted to the tensor structure

$$G^{1,\ldots,n_j} \otimes R^{1,\ldots,n-n_j} . \tag{3.28}$$

To substantiate this claim, is is instructive to investigate e.g. some graphs contributing to the quark 6-point function
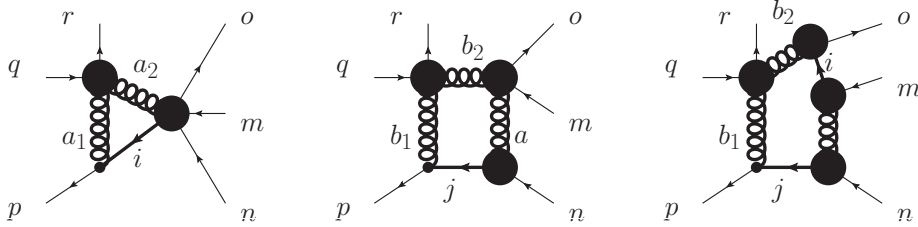
Figure 3.16.: How 4-point functions can contribute to the quark 6-point function.

Assuming in all three cases the limit $p_q \to p_r$, the singular color structures factorize as
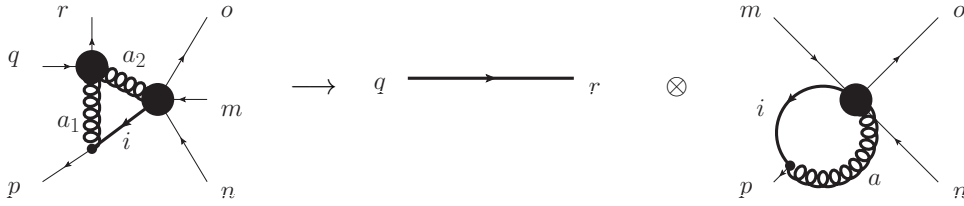
Figure 3.17.: Factorization in quark 6-point function.
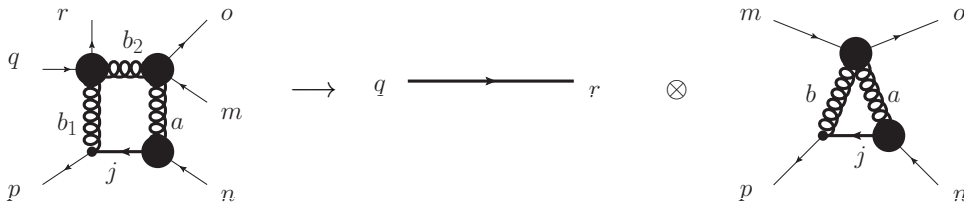
Figure 3.18.: Similar as Fig. 3.17.
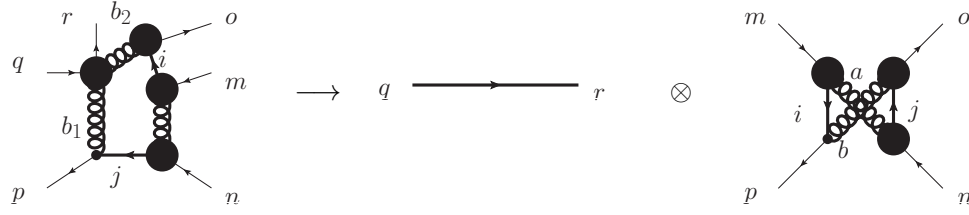
Figure 3.19.: Similar as Fig. 3.17.

As any of the second factors on the right hand side are present in the DSE for the quark 4-point function factorization is confirmed for these cases.

Summary

The consequences of a $1/k^4$ singularity in the quark 4-point function have been investigated, where only the color structures have been taken into account. The singularity has been found consistent if it appears in a special color structure that cannot be reproduced by the exchange of one gluon. This singularity is immediately forwarded to the corresponding connected 4-point function. Proper regularization of the $1/k^4$ singularity in the latter results in a δ-like contribution which implies the violation of cluster decomposition. Additionally, similar singularities are induced in all n-point functions with $n \geq 4$, whereas the 3-point functions and propagators are protected. Singularities appear, whenever the exchanged momentum between colored subsets of legs of a n-point function becomes small.

It is interesting that already one 4-point function, corresponding to a, potentially very heavy, fundamental field, could forward such a singularity to other matter. Although this is no contradiction to the decoupling theorem, which holds only in the absence of singularities, it is still intriguing. If, however, a confining $1/k^4$ singularity is induced in the quark 4-point function, a simple explanation of Casimir scaling can be given.

4. Center Transition from Matter Propagators

In this chapter, the center phase transition is investigated from fundamentally charged matter propagators [229, 230]. A definition of confinement in Yang-Mills theory in terms of the free energy F_q of static fundamental color charges has been introduced Sec. 2.1.2. The free energy for static fundamental charges is related to the expectation value of the Polyakov loop via

$$e^{-F_q/T} = \left\langle \text{Tr} \left[\mathcal{P} e^{ig \int_0^{1/T} dx^4 A_4(\vec{x}, x^4)} \right] \right\rangle .$$ (4.1)

Additionally, the Polyakov loop serves as an order parameter for spontaneous breaking of center symmetry. Therefore, the confinement of static fundamental charges can be characterized by a vanishing Polyakov loop which is translated into a ground state respecting center symmetry. The phase of spontaneously broken center symmetry, on the other hand, corresponds to a deconfined phase in this picture.

The actual calculation of the Polyakov loop requires the evaluation of path ordered expectation values, which - in contrast to lattice calculations - are hard to access with functional methods. Within the latter approach it is therefore useful to define order parameters that can be accessed easier. One such order parameter is given by the dressed Polyakov loop Σ_1, which consists of the set of closed loops with winding number one around the temporal direction [231, 232]. Due to the explicit breaking of center symmetry by the presence quarks, this is just an approximate order parameter in QCD. The advantage of this quantity is that it can also be obtained from the quark condensate with general $\exp(i\theta)$-valued boundary conditions via

$$\Sigma_1 = \int_0^{2\pi} \frac{d\theta}{2\pi} e^{-i\theta} \langle \bar{q}q \rangle_\theta .$$ (4.2)

This dual quark condensate has been successfully used to extract the center transition at finite temperature from the solution to the quark propagator DSE [162, 188, 233, 234]. Although one might be tempted to interpret Eq. (4.2) as a link between confinement and spontaneous chiral symmetry breaking, this is not the case [95].

In general, any quantity that transforms under center symmetry with $z \in Z_3$ as

$$\Sigma_1 \to z\Sigma_1 ,$$ (4.3)

can serve as an order parameter for the deconfinement transition [95, 235, 236]. Furthermore, not only quarks, but any fundamentally charged matter, as fundamentally charged scalars, is expected to be confined. It is clear that in case of scalars, there is no quark condensate and as a consequence Eq. (4.2) cannot serve as an order parameter. When investigating fundamentally charged scalars it is therefore necessary to find other order parameters.

Another motivation for the investigation of scalar QCD is the simpler tensor structure in the

higher n-point functions. In spinor QCD the quark-gluon vertex plays an essential role in spontaneous chiral symmetry breaking and possibly also in the confinement mechanism, as has been discussed already in Sec. 2.1.2. Equally important is the expected non-trivial behavior of the vertex at non-vanishing temperatures. In contrast to this, it is very hard to solve the DSE for the quark-gluon vertex due to the large number of tensor structures [113, 237, 238], which increases even further at non-vanishing temperatures. In contrast to this, there are only two tensor structures necessary for the scalar-gluon vertex (in the vacuum), which has been the subject of a master thesis [115]. Therefore, scalar QCD can provide a testing ground for investigations of the vertex DSE at finite temperature. Unfortunately, this simple tensor structure comes at the price of additional vertices in the renormalized Euclidean action of Scalar QCD in Landau gauge [114]

$$S = \int d^4x \left\{ Z_3 A_\mu^a \left(\frac{1}{2} \left(-\partial^2 \delta_{\mu\nu} + \partial_\mu \partial_\nu \right) \right) A_\nu^a + Z_1 g f^{abc} \left(\partial_\mu A_\nu^a \right) A_\mu^b A_\nu^c \right.$$

$$\left. + Z_4 \frac{g^2}{4} f^{abc} f^{ade} A_\mu^b A_\nu^c A_\mu^d A_\nu^e - \tilde{Z}_3 \bar{c}^a \partial^2 c^a - \tilde{Z}_1 g f^{abc} \bar{c}^a \partial_\mu (c^b A_\mu^c) + \phi^* \hat{Z}_3 \left(-\partial^2 + Z_m m_0^2 \right) \phi \right.$$

$$\left. + i g \hat{Z}_1 \phi^* \left(2 A_\mu (\partial_\mu \phi) + (\partial_\mu A_\mu) \phi \right) + \hat{Z}_4 \frac{\lambda}{4} (\phi^* \phi)^2 + \frac{\hat{Z}_{4,2}}{2} g^2 \phi^* \{A_\mu, A_\mu\} \phi \right\} . \tag{4.4}$$

When compared to the QCD action Eq. (2.40), only the charged scalar (anti)field (ϕ^*) ϕ is new and the corresponding mass and quartic coupling is given by m_0 and λ respectively. Renormalization constants have been introduced for all primitively divergent vertices in Eq. (4.4) [114], where $\hat{Z}_4$ and $\hat{Z}_{4,2}$ have no analogues in spinor QCD. Similar as in QCD, not all of the renormalization constants are independent, which can be shown by using Slavnov-Taylor identities [1] and one gets for example the relation, $Z_3/Z_1 = \tilde{Z}_3/\tilde{Z}_1$. In Landau gauge the non-renormalization of the ghost-gluon vertex $\tilde{Z}_1 = 1$ can be used again, which implies $\hat{Z}_1 = \hat{Z}_3/\tilde{Z}_3$ [69]. Additionally, if the theory were in the Higgs phase a non-vanishing scalar condensate would occur [221, 222]. This possibility will be neglected in the following investigation as the focus is put on confinement aspects.

4.1. The Scalar Propagator Dyson-Schwinger Equation

The Dyson-Schwinger equation for the scalar propagator as obtained with DoDSE/DoFun [223, 224] is shown in Fig. 4.1.
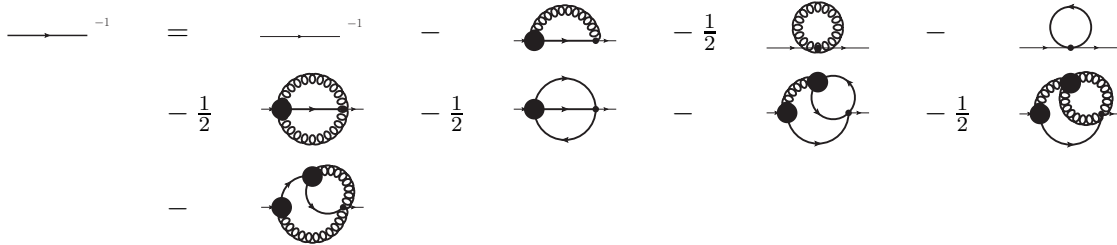

Figure 4.1.: DSE for the fundamentally charged scalar propagator.

In addition to the graphical rules introduced below Fig. 2.1, bare vertices are indicated by

small black dots. All, but the first two diagrams would be absent without the bare scalar-gluon and scalar 4-point functions. Furthermore, the tadpole diagrams - given by the third and fourth contribution - are actually independent of the external momentum. Therefore, these two diagrams contribute just a constant, which can be compensated by adjusting $\hat{Z}_m m_0^2$ via some renormalization condition. The one loop approximation of the DSE for the scalar propagator is then of the same form as the full quark propagator DSE and given by
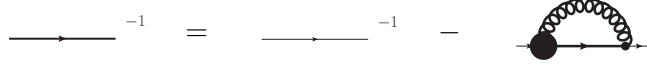
Figure 4.2.: DSE for the fundamentally charged scalar propagator in one loop approximation.

This truncated equation is used in the following analysis, where inserting explicit expressions yields

$$D_{S,ab}^{-1}(p) = \hat{Z}_3 \left(p^2 + \hat{Z}_m m_0^2\right) \delta_{ab} - \int \frac{d^4 q}{(2\pi)^4} \Gamma_{0,\mu,ac}^e(p,q) D_{\mu\nu}^{ef}(p-q) D_{S,cd}(q) \Gamma_{\nu,db}^f(q,p) \ . \ (4.5)$$

Here momentum conservation

$$D_{S,ab}(p,q) = D_{S,ab}(p)(2\pi)^4 \delta^{(4)}(p-q) \ , \tag{4.6a}$$

$$D_{\mu\nu}^{ab}(p,q) = D_{\mu\nu}^{ab}(p)(2\pi)^4 \delta^{(4)}(p-q) \ , \tag{4.6b}$$

$$\Gamma_{\mu,bc}^a(p,q,k) = \Gamma_{\mu,bc}^a(p,q)(2\pi)^4 \delta^{(4)}(p+k-q) \ , \tag{4.6c}$$

has been used. The scalar-gluon vertex can be simplified further by separating its color tensor structure

$$\Gamma_{\mu,bc}^a(p,q) = g T_{bc}^a \Gamma_\mu(p,q) \ , \tag{4.7}$$

where for the bare vertex one has $\Gamma_{0,\mu}(p,q) = \hat{Z}_1 (p+q)_\mu$. Using color conservation in the propagators and $\text{tr}[T^a T^a] = (N_c^2 - 1)/2$ results in

$$D_S^{-1}(p) = \hat{Z}_3 \left(p^2 + \hat{Z}_m m_0^2\right) - \hat{Z}_1 g^2 C_F \int \frac{d^4 q}{(2\pi)^4} (p+q)_\mu D_{\mu\nu}(p-q) D_S(q) \Gamma_\nu(q,p) \ , \ (4.8)$$

with the quadratic Casimir operator $C_F = (N^2 - 1)/(2N)$.

4.1.1. Vacuum

The propagators can be simplified further by employing Euclidean invariance, which requires any scalar function of one momentum p to be a function of the invariant p^2. In Landau gauge it can be shown that the gluon propagator is transversal to its momentum [28]. Introducing the dressing functions Z_S and Z and the transversal projector

$$P_{\mu\nu}(p) = \left(\delta_{\mu\nu} - p_\mu p_\nu / p^2\right) \ , \tag{4.9}$$

4. Center Transition from Matter Propagators

it is possible to express the propagators as

$$D_S(p^2) = \frac{Z_S(p^2)}{p^2} \ , \tag{4.10a}$$

$$D_{\mu\nu}(p) = P_{\mu\nu}(p)\frac{Z(p^2)}{p^2} \ . \tag{4.10b}$$

Similarly, any scalar function of two momenta p, q can actually depend only on the invariants $p^2, q^2, z \equiv \hat{p} \cdot \hat{q}$ with $\hat{p} = p/\|p\|$. Furthermore, Slavnov-Taylor identities restrict the allowed tensor structures for the scalar-gluon vertex, yielding the expansion [237]

$$\Gamma_\mu(p, q) = A(p^2, q^2, z)(p + q)_\mu + B(p^2, q^2, z)\left(p_\mu\left[q_\nu(q - p)_\nu\right] - q_\mu\left[p_\nu(q - p)_\nu\right]\right) \ . \tag{4.11}$$

To express Eq. (4.8) in terms of dressing functions it is useful to note that (see App. B.2)

$$(p + q)_\mu P_{\mu\nu}(p - q)\Gamma_\nu(q, p) = 2\left(2\frac{A(q^2, p^2, z)}{(p - q)^2} + B(q^2, p^2, z)\right)p^2q^2\left(1 - z^2\right) \ , \tag{4.12}$$

showing that the integral in Eq. (4.8) depends only on $\|q\|$ and the relative angle $\cos\phi = z$, between the internal and external momentum q and p respectively. This motivates the introduction of hyperspherical coordinates

$$d^4q = q^3 \sin^2\phi \sin\phi_1 \, dq \, d\phi \, d\phi_1 \, d\phi_2 \ , \tag{4.13}$$
$$(q, \phi, \phi_1, \phi_2) \in [0, \infty) \times [0, \pi] \times [0, \pi] \times [0, 2\pi] \ ,$$

which allow to perform the trivial integration

$$\int\limits_0^\pi d\phi_1 \, \sin\phi_1 \int\limits_0^{2\pi} d\phi_2 = 4\pi \ , \tag{4.14}$$

The integral of some $f(q^2, \cos\phi)$ in four dimension can be rewritten as

$$\int\limits_0^\infty dq \, q^3 \int\limits_0^\pi d\phi \, \sin^2\phi f(q^2, \cos\phi) = \int\limits_0^\infty dy \, \frac{y}{2} \int\limits_{-1}^1 dz \, \sqrt{1 - z^2} f(y, z) \ . \tag{4.15}$$

Using the previous steps in the DSE for the scalar propagator Eq. (4.8) and dividing by p^2 gives the equation for the dressing function

$$Z_S^{-1}(x) = \hat{Z}_3\left(1 + \hat{Z}_m\frac{m_0^2}{x}\right) + \hat{Z}_1\Sigma(x) \ , \tag{4.16}$$

$$\Sigma(x) = -\frac{8}{3}\frac{\alpha(\mu)}{\pi^2}\int\limits_0^\infty dy \, yZ_S(y)\mathcal{K}(x, y) \ ,$$

$$\mathcal{K}(x,y) = \int\limits_{-1}^{1} dz \left(1 - z^2\right)^{3/2} \frac{Z(k^2)}{k^2} \left\{ \frac{A(y,x,z)}{k^2} + \frac{B(y,x,z)}{2} \right\} \ ,$$

where $x = p^2$ is the external scalar momentum, $y = q^2$ the loop momentum and $k^2 = x + y - 2\sqrt{xy}z$ the gluon momentum. Additionally, the coupling strength $\alpha(\mu) = g^2(\mu)/(4\pi)$ evaluated at the renormalization scale μ has been introduced.

Before this equation can be solved, it is necessary to provide expressions for the gluon propagator as well as the scalar-gluon vertex. Note that in case of the vertex, just one effective dressing function is necessary, as only the sum $A/k^2 + B/2$ is relevant. Furthermore, the above equation has to be regularized in the ultraviolet and a renormalization scheme for fixing the renormalization constants $\hat{Z}_3$, $\hat{Z}_m$ and $\hat{Z}_1$ has to be specified.

Before going on, it is interesting to determine the behavior of the self-energy $\Sigma(x)$ at small external momenta x. Singularities can be caused by the integration of momenta $y \approx x$ due to the $1/k^2$ terms. If x becomes small, danger comes from small y which implies that $k^2 = x + y - 2\sqrt{xy}z$ is necessarily small. In this case $Z(k^2)/k^2$ becomes either constant or vanishes, depending on the type of solution in the Yang-Mills sector. Therefore one has to check the behavior of

$$\int\limits_{0}^{\epsilon} dy\, y Z_S(y) \int\limits_{-1}^{1} dz \frac{\left(1 - z^2\right)^{3/2}}{x + y - 2\sqrt{xy}z} \ , \tag{4.17}$$

for some $\epsilon > x$. Using that $Z_S(y)$ either vanishes or becomes constants at $y = 0$, one can easily check that this is finite in the limit $x \to 0$.

Physically this means that the self-energy does not contribute directly to the value of the propagator at vanishing momentum or, in other words, to the screening mass.

This will be useful when specifying the renormalization scheme.

Gluon Propagator and Vertex Function

In previous works, gluon propagators from lattice calculations have been successfully applied in DSE calculations of the dual chiral condensate [162, 234]. The same lattice results for the gluon propagator are used in this investigation, but in principle also other results, e.g. from functional methods, could have been used (see e.g. [239–241]). It is important to notice that they are obtained from calculations in the pure gauge theory, i.e. back reactions of matter loops on the gluon are not taken into account. In spinor QCD parts of these effects have been included, e.g. in [188], leading to more realistic transition temperatures. For the calculations performed here, matter back reactions are expected to be small, due to the large mass terms that will be taken for the scalar field. The fit for the gluon dressing function provided in [162] is given by

$$Z(x) = \frac{x\Lambda^2}{(x + \Lambda^2)^2} \left\{ \left(\frac{c}{x + a\Lambda^2}\right)^b + \frac{x}{\Lambda^2} \left(\frac{\beta_0 \alpha(\mu) \ln\left[x/\Lambda^2 + 1\right]}{4\pi}\right)^\gamma \right\} \ , \tag{4.18}$$

with the parameters $a = 0.595$, $b = 1.355$, $c = 11.5$ GeV^2 and anomalous dimension $\gamma = -13/22$. The renormalization scale of the Yang-Mills part is fixed by $\alpha(\mu) = 0.3$, with

$\beta_0 = 11N_c/3$ and $\Lambda = 1.4$ GeV.

Similar to [242], the vertex dressing is assumed to factorize into an Abelian and a non-Abelian part. As discussed previously, only one dressing function has to be specified, where here A is taken. In case of the Abelian gauge theory, Slavnov-Taylor identities have been used in [237] to obtain the corresponding dressing function

$$A_A(x, y, z) = \frac{D_S^{-1}(x) - D_S^{-1}(y)}{x - y} \; . \tag{4.19}$$

In accordance with previous investigations of spinor QCD [162, 234, 242], the fact that the non-Abelian running coupling - given by the product of g^2 with gluon dressing function and the square of the ghost dressing function - is independent of the renormalization scale μ is used here. In general this is true on all scales [242]. For the construction of an effective vertex model, it can at least be used in the perturbative regime, where the ghost dressing function runs as

$$G(x) \propto \left(\frac{\beta_0 \alpha(\mu) \ln\left[x/\Lambda^2 + 1\right]}{4\pi} \right)^{\delta} , \tag{4.20}$$

for large momenta $p^2 = x$ with anomalous dimension $\delta = -9/44$. Similar as in [162, 234] this leads to the vertex model [162, 234]

$$A(x, y, z) = \tilde{Z}_3 \frac{D_S^{-1}(x) - D_S^{-1}(y)}{x - y} d_1 \times \tag{4.21}$$

$$\left\{ \left(\frac{\Lambda^2}{\Lambda^2 + k^2} \right) + \frac{k^2}{\Lambda^2 + k^2} \left(\frac{\beta_0 \alpha(\mu) \ln\left[\frac{k^2}{\Lambda^2} + 1\right]}{4\pi} \right)^{2\delta} \right\} ,$$

where the gluon momentum $k^2 = x + y - 2\sqrt{xy}z$ has been used again. The factor $\tilde{Z}_3$ allows to use the Slavnov-Taylor identity $\hat{Z}_1 \tilde{Z}_3 = \hat{Z}_3$ to get rid of $\hat{Z}_1$ in the self-energy in Eq. (4.16). Additionally a model parameter $d_1 = 0.53$ has been added, which will be varied later to investigate the vertex model dependence of the center-symmetry phase transition.

Regularization and Renormalization

With the Ansätze Eq. (4.18) and Eq. (4.21), the equation for the dressing function of the scalar propagator takes the form

$$(Z_S(x)\hat{Z}_3)^{-1} = 1 + \hat{Z}_m \frac{m_0^2}{x} + \Sigma(x) \; . \tag{4.22}$$

To make this expression well-defined, a sharp cutoff Λ_c is introduced in the self-energy, restricting the loop integration to $y \leq \Lambda_c^2$. This introduces an unphysical cutoff dependence in the equation, which requires the introduction of renormalization conditions for $\hat{Z}_3$ and $\hat{Z}_m$ at some scale μ^2. Therefore the renormalization constants depend in general on the scale μ^2 as well as the cutoff Λ_c^2

$$\hat{Z}_3 = \hat{Z}_3(\mu^2, \Lambda_c^2) \ , \tag{4.23a}$$

$$\hat{Z}_m = \hat{Z}_m(\mu^2, \Lambda_c^2) \ , \tag{4.23b}$$

whereas the solution Z_S depends just on μ^2

$$Z_S(x) = Z_S(x, \mu^2) \ . \tag{4.24}$$

It has been noted previously that $\Sigma(x)$ does not contribute to $1/x$ and one can use the μ^2-independent renormalization condition of setting the value of $\hat{Z}_m m_0^2 \equiv m^2$. Apart from the wave function renormalization factor, this resembles the squared screening mass of the propagator

$$\lim_{x \to 0} \frac{x}{Z_S(x, \mu^2)} = \hat{Z}_3(\mu^2, \Lambda_c^2) m^2(\Lambda_c^2) \ . \tag{4.25}$$

Here m^2 has to depend on the cutoff Λ_c^2 to make the propagator cutoff independent. As second renormalization condition, the value of the propagator at μ^2 in the perturbative regime is specified, where the value of the propagator is set to $1/\mu^2$. After a short calculation this yields

$$\hat{Z}_3(\mu^2, \Lambda_c^2) = \frac{\mu^2}{\mu^2(1 + \Sigma(\mu^2)) + m^2(\Lambda_c^2)} \ . \tag{4.26}$$

With this prescription the DSE is multiplicatively renormalizable in the perturbative regime, i.e. $\hat{Z}_3(\mu^2, \Lambda_c^2) Z_S(x, \mu^2)$ is independent of μ^2 as long as μ^2 is considerable larger than Λ^2 in Eq. (4.18) and Eq. (4.21). To see this, note first that $\hat{Z}_m m_0^2$ is μ^2 independent by definition. Then the only μ^2-dependence in the right hand side of Eq. (4.22) can be in $\Sigma(x)$. In the self-energy, $\alpha(\mu)$ times the gluon dressing function Eq. (4.18) times the part in braces in Eq. (4.21) describes the perturbative running coupling, which is independent of μ^2 in the given scheme [243]. At large μ^2, the only μ^2 dependence in the integrand of Eq. (4.16) can then be in the product

$$Z_S(y, \mu^2) \left[D_S(x, \mu^2)^{-1} - D_S(y, \mu^2)^{-1} \right] \tag{4.27}$$

$$= \hat{Z}_3(\mu^2, \Lambda_c^2) Z_S(y, \mu^2) \left[\frac{x}{\hat{Z}_3(\mu^2, \Lambda_c^2) Z_S(x, \mu^2)} - \frac{y}{\hat{Z}_3(\mu^2, \Lambda_c^2) Z_S(y, \mu^2)} \right] \ .$$

This shows that in the perturbative regime, the only μ^2 dependence in $\Sigma(x)$ is via $\hat{Z}_3 Z_S$, which in turn implies that $\hat{Z}_3 Z_S$ is actually the solution of a μ^2 independent equation (4.22). Therefore the product $\hat{Z}_3 Z_S$ cannot depend on μ^2.

With the given prescription one is now in a position to investigate the dependence of the solution $Z_S(x, \mu^2)$ on the cutoff Λ_c^2. Cutoff independence is hidden in the used renormalization prescription, as the trivial running of a m^2 with Λ_c^2 has to be taken into account. To see, how $m^2(\Lambda_c^2)$ depends on on the cutoff one can use that the value of the propagator at $x = 0$ given by

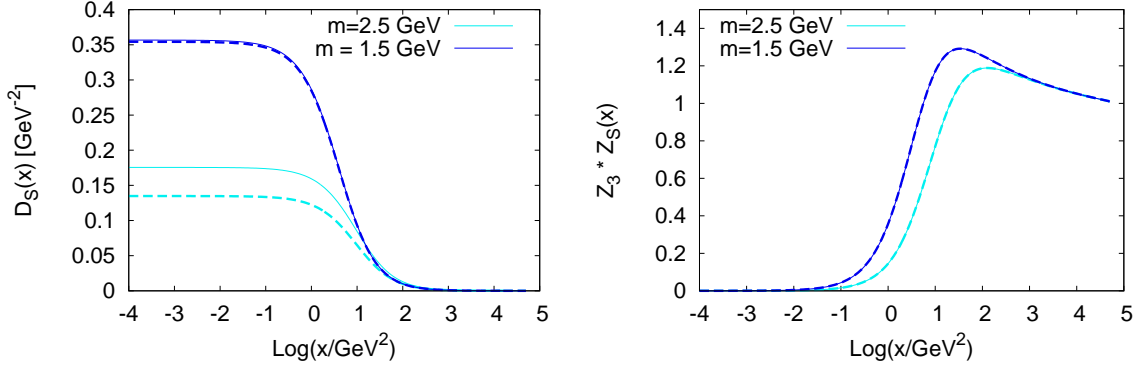$$D_S^{-1}(0, \mu^2) = \hat{Z}_3(\mu^2, \Lambda_c) m^2(\Lambda_c^2) \ , \tag{4.28}$$

Figure 4.3.: Solution of the one-loop DSE Fig. 4.2 for the scalar propagator Eq. (4.16) for different masses m^2 and renormalization points μ^2. The solid line corresponds to $\mu = 4$ GeV and the dashed line to $\mu = 10$ GeV. The sharp cutoff has been taken to be $\Lambda_c^2 = 5 \cdot 10^4$ GeV^2.

must not depend on Λ_c^2. With this relation one can replace the previous prescription by an equivalent one that is inherently cutoff independent at the cost of loosing inherent multiplicative renormalizability. In this second prescription, the Λ_c^2-independent, but μ^2-dependent quantities $D_S^{-1}(0, \mu^2)$ and $D_S^{-1}(\mu^2, \mu^2)$ are fixed, resulting in

$$\hat{Z}_3(\mu^2, \Lambda_c^2) = \frac{D_S^{-1}\left(\mu^2, \mu^2\right) - D_S^{-1}\left(0, \mu^2\right)}{\mu^2(1 + \Sigma(\mu^2))} \ . \tag{4.29}$$

But even here cutoff independence is not obvious and will therefore be checked numerically in the results section.

Numerical Results

Results for the propagator and its dressing function for different masses m^2 and renormalization points with the prescription Eq. (4.26) are shown in Fig. 4.3. Details of the numerical implementation can be found in App. C.1. The theoretically predicted multiplicative renormalizability - in the sense of μ^2 independence of $\hat{Z}_3 Z_s$ - is confirmed by these results. In contrast to this, $D_S(0, \mu^2)^{-1}$ depends on the renormalization scale, as anticipated.

Checking cutoff independence requires a little work. First, the value of the propagator at vanishing momentum is calculated in the scheme defined by Eq. (4.26). Knowing this cutoff independent value, allows to use Eq. (4.29), which takes the correct Λ_c^2-dependence of $m^2(\Lambda_c^2)$ into account. Changing the cutoff to $\bar{\Lambda}_c^2$ yields then the new $\hat{Z}_3(\mu^2, \bar{\Lambda}_c^2)$, which can be used to calculate $m^2(\bar{\Lambda}_c^2)$ from Eq. (4.28). Using this in Eq. (4.26) again, independence of the propagator from the cutoff can finally be confirmed. Results for these steps are shown in Fig. 4.4. First Eq. (4.16) has been solved, using $\mu = 10$ GeV with $m(\Lambda_c^2) = 1.5$ GeV and $\Lambda_c^2 = 5 \cdot 10^4$ GeV^2 with Eq. (4.26) to obtain $D(0, \mu^2)$ (cyan solid line). To check that the second prescription is really equivalent, this value has been used in Eq. (4.29) (magenta dashed line). Then the cutoff has been changed to $\bar{\Lambda}_c^2 = 5 \cdot 10^6$ GeV^2 with Eq. (4.29) (blue long dashed line). Finally, to confirm independence of the cutoff, the value for $m(\bar{\Lambda}_c^2)$ as
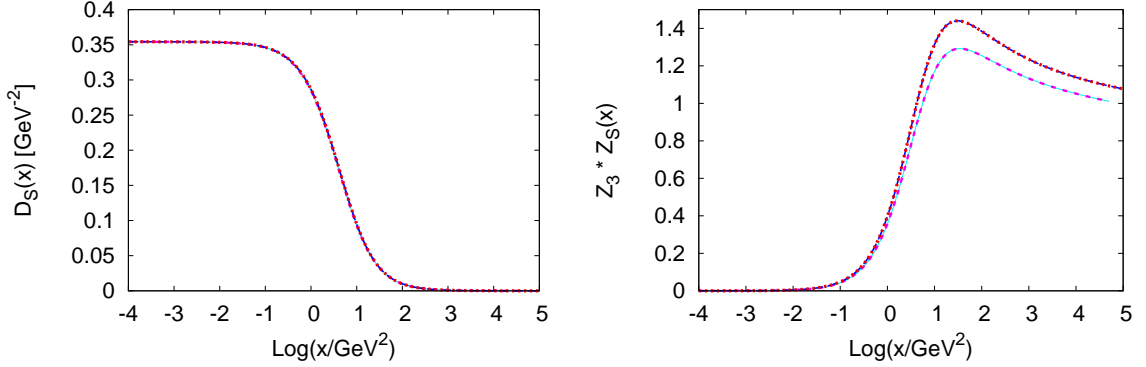
Figure 4.4.: Solutions of the truncated DSE for the scalar propagator Eq. (4.16) at $\mu = 10$ GeV with $m = 1.5$ GeV for different cutoffs Λ_c^2. The cyan solid and the magenta dashed lines correspond to $\Lambda_c^2 = 5 \cdot 10^4$ GeV^2 with Eq. (4.26) and Eq. (4.29) respectively. The red dotted and the blue long dashed line correspond to $\bar{\Lambda}_c^2 = 5 \cdot 10^6$ GeV^2 with Eq. (4.26) and Eq. (4.29) respectively.

obtained from this calculation has been used in Eq. (4.26) (red dotted line). As expected, only the propagator is independent of the cutoff.

Negativity of the self-energy term together with the renormalization prescription Eq. (4.26) implies in some cases a renormalization constant $\hat{Z}_3 > 1$. Therefore one is lead to the conclusion that the state created by the scalar field cannot be one of positive norm, i.e. in the asymptotic state space, as it has no Kaellen-Lehmann representation. This is not changed by the inclusion of tadpoles, as they only lead to a shift in the bare mass. Whether this is modified by the inclusion of two-loop terms, containing the two-scalar-two-gluon interaction, would be very interesting. Furthermore, with the employed methods, solutions can only be found for large values for the mass of the scalar field. This could be an artifact of the truncation, where several sources are possible. One could use a self-consistent solution for the vertex as in [115, 244] or include two-loop diagrams. Another important contribution at smaller masses can come from matter loops which can also change the temperature of the deconfinement transition as in spinor QCD [188].

4.1.2. Non-Vanishing Temperatures

As a next step towards getting information about the center-symmetry transition from the scalar propagator, the DSE Eq. (4.8) is formulated and solved at non-vanishing temperatures in equilibrium. For this, the Matsubara formalism, as introduced in Sec. 2.2, is employed. Already here, general $U(1)$ valued boundary conditions

$$\psi(\vec{x}, x^4 + 1/T) = e^{i\theta} \psi(\vec{x}, x^4) , \quad \theta \in [0, 2\pi) , \tag{4.30}$$

as will be necessary for the calculation of order parameters for the center symmetry transition are implemented via the Matsubara frequencies

4. Center Transition from Matter Propagators

$$\omega_n(\theta) = T(2\pi n + \theta) \ , \tag{4.31a}$$

$$e^{i\omega_n(\theta)(x^4 + 1/T)} = e^{i\theta} e^{i\omega_n(\theta)x^4} \ . \tag{4.31b}$$

In the following, the dependence on θ will not be shown explicitly for better readability.

Thus, the finite temperature DSE is obtained from Eq. (4.8) by replacing

$$\int \frac{dq_4}{2\pi} \longrightarrow T \sum_{\substack{\omega_n \\ n \in \mathbb{Z}}} \ , \quad (\vec{q}, q_4) \longrightarrow (\vec{q}, \omega_n) \ , \quad (\vec{p}, p_4) \longrightarrow (\vec{p}, \omega_m) \ . \tag{4.32}$$

In particular this implies that the propagators become functions of $(\vec{p}, \omega_m)$. For the scalar propagator one dressing function is again sufficient and one can use the remaining $O(3)$ invariance to write

$$D_S(\vec{p}^2, \omega_m) = \frac{Z_S(\vec{p}^2, \omega_m)}{\omega_m^2 + \vec{p}^2} \ . \tag{4.33}$$

In case of the gauge field propagator, the fact that the heat bath breaks Lorentz symmetry has to be taken into account. Due to the vector nature of the particle, two dressing functions - corresponding to components longitudinal and transversal to the heat bath - are necessary. With these, the gluon propagator can then be written as

$$D_{\mu\nu}(\vec{p}, \omega_m) = \frac{Z_L(\vec{p}^2, \omega_m)}{\omega_m^2 + \vec{p}^2} P_{L,\mu\nu}(\vec{p}, \omega_m) + \frac{Z_T(\vec{p}^2, \omega_m)}{\omega_m^2 + \vec{p}^2} P_{T,\mu\nu}(\vec{p}, \omega_m) \ , \tag{4.34}$$

with transversal and longitudinal dressing functions Z_T, Z_L and projectors

$$P_{T,\mu\nu}(\vec{p}, \omega_m) = \delta_{i\mu}\delta_{j\nu} \left(\delta_{ij} - p_i p_j / \vec{p}^2 \right) \ , \tag{4.35a}$$

$$P_{L,\mu\nu}(\vec{p}, \omega_m) = P_{\mu\nu}(\vec{p}, \omega_m) - P_{T,\mu\nu}(\vec{p}, \omega_m) \ , \tag{4.35b}$$

and the transversal projector $P_{\mu\nu}$ of Eq. (4.9).

Also at finite temperature, the pure Yang-Mills lattice data of [162] is taken for the gluon propagator dressing functions. The form of the fit function is the same as in the vacuum Eq. (4.18) for the longitudinal as well as the transversal dressing function. Temperature dependence is then included in the fit parameters a, b, which are different for Z_T and Z_L.

The scalar-gluon vertex Eq. (4.11) would in general acquire additional tensor structures due to breaking of Lorentz invariance, see e.g. [115]. Here only the dressing function of the bare vacuum tensor structure $(p + q)_\mu$ is taken into account, which depends on $\vec{p}^2, \omega_m, \vec{q}^2, \omega_n, z$, where $z \equiv \hat{p} \cdot \hat{q}$ with $\hat{p} = \vec{p}/\|p\|$. The non-Abelian factor of the dressing function is taken to be the same as in the vacuum Eq. (4.21) with replaced argument $k^2 = (p - q)^2 = \vec{p}^2 + \omega_m^2 - \vec{q}^2 - \omega_n^2 - 2\|\vec{p}\|\|\vec{q}\|z$. It should be noted that temperature effects are usually restricted to $k^2 \leq (2\pi T)^2$ [156]. Therefore the behaviour at large momenta, which served as a partial motivation in the construction of the non-Abelian part of the vertex is not spoiled. A straightforward generalization of the Abelian part of the vertex to non-vanishing temperature leads to problems. To see this, note that it is possible to have a vanishing denominator

in

$$\frac{D_S^{-1}(\vec{p}^2, \omega_m) - D_S^{-1}(\vec{q}^2, \omega_n)}{\vec{p}^2 + \omega_m^2 - \vec{q}^2 - \omega_n^2} \ , \tag{4.36}$$

even for $(\vec{p}, \omega_m) \neq (\vec{q}, \omega_n)$, whereas the numerator does not necessarily vanish in this case. To avoid such singularities, the simpler choice

$$A_A(\vec{p}^2 + \omega_m^2, \vec{q}^2 + \omega_n^2) = \frac{D_S^{-1}(\vec{p}^2 + \omega_m^2) - D_S^{-1}(\vec{q}^2 + \omega_n^2)}{\vec{p}^2 + \omega_m^2 - \vec{q}^2 - \omega_n^2} \ , \tag{4.37}$$

with the solution of the vacuum DSE $D_S(x)$ is used.

To obtain the DSE for the dressing function Z_S it is useful to perform the contractions of Lorentz indices in Eq. (4.8) separately for the occurring projectors Eq. (4.35)

$$(p+q)^\mu P_{T,\mu\nu}(\vec{p}-\vec{q}, \omega_{m-n})(q+p)^\nu = 4 \frac{\vec{p}^2 \vec{q}^2 - (\vec{p} \cdot \vec{q})^2}{(\vec{p} - \vec{q})^2} \ , \tag{4.38a}$$

$$(p+q)^\mu P_{\mu\nu}(p-q)(q+p)^\nu = 4 \frac{\left(\omega_m^2 + \vec{p}^2\right)\left(\omega_n^2 + \vec{q}^2\right) - \left(\omega_m \omega_n + \vec{p} \cdot \vec{q}\right)^2}{\left(\omega_m - \omega_n\right)^2 + \left(\vec{p} - \vec{q}\right)^2} \ , \tag{4.38b}$$

where the corresponding calculations are performed in App. B.2.

Only one of the angular integrations in Eq. (4.8) can be performed trivially and by a change of variables $y = q^2$, $z = \cos\phi$ one gets with spherical coordinates in three dimensions

$$\int\limits_0^\infty dq\, q^2 \int\limits_0^\pi d\phi\, \sin\phi \int\limits_0^{2\pi} d\phi_1\, f(q^2, \cos\phi) = \pi \int\limits_0^\infty dy\, \sqrt{y} \int\limits_{-1}^1 dz\, f(y, z) \ . \tag{4.39}$$

Replacing $x = \vec{p}^2$ and dividing Eq. (4.8) by $x + \omega_m^2$ one obtains, by collecting all contributions

$$\frac{1}{Z_S(x, \omega_m)} = \hat{Z}_3 \left(1 + \hat{Z}_m \frac{m^2}{\omega_m^2 + x} + \Sigma(x, \omega_m)\right) \ , \tag{4.40}$$

$$\Sigma(x, \omega_m) = -\frac{2}{6\pi} \alpha(\mu) T \sum_{n \in \mathbb{Z}} \int\limits_0^\infty dy\, \sqrt{y} \frac{Z_S(y, \omega_n)}{\omega_n^2 + y} \mathcal{A}(x, \omega_m, y, \omega_n) \ .$$

Here, the integration kernel is given by

$$\mathcal{A}(x, \omega_m, y, \omega_n) = \frac{4}{\omega_m^2 + x} \int\limits_{-1}^1 dz\, A(x + \omega_m^2, y + \omega_n^2, z) \times \tag{4.41}$$

$$\left\{ \frac{Z_L\left(k^2\right)}{k^2} \frac{\left(\omega_m^2 + x\right)\left(\omega_n^2 + y\right) - \left(\omega_m \omega_n + z\sqrt{xy}\right)^2}{k^2} + \frac{Z_T\left(k^2\right) - Z_L\left(k^2\right)}{k^2} \frac{xy\left(1 - z^2\right)}{\vec{k}^2} \right\} \ ,$$

where $\vec{k}^2 = x + y - 2\sqrt{xy}z$ and $k^2 = (\omega_m - \omega_n)^2 + \vec{k}^2$ is the gluon momentum.

Again regularization is necessary where a $O(4)$ symmetric sharp cutoff with $\omega_n^2 + x \leq \Lambda_c^2$ with the vacuum cutoff Λ_c is used. When going to finite temperature $T \neq 0$ no additional
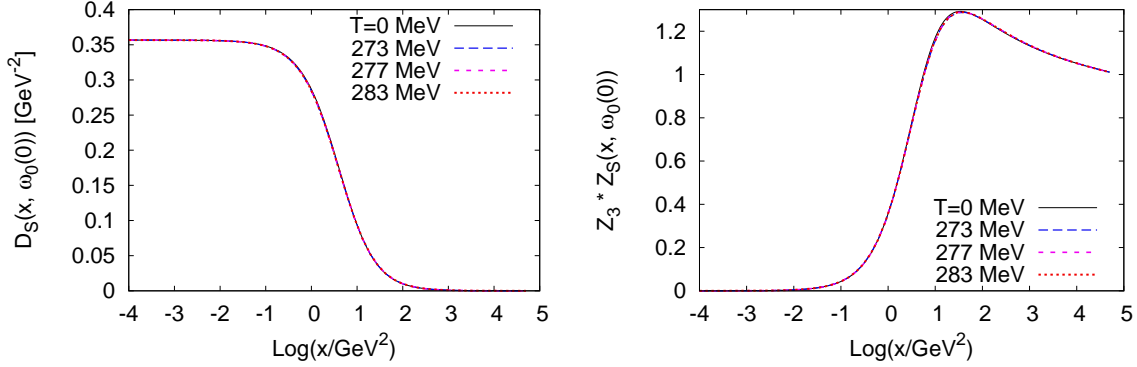
Figure 4.5.: Solution of the truncated DSE for the scalar propagator Eq. (4.40) as function of $\vec{p}^2 = x$ at fixed Matsubara frequency $\omega_0(0)$. The propagator (left panel) and dressing function (right) panel are plotted for different temperatures with periodic boundary conditions for renormalization scale $\mu = 4$ GeV and mass $m = 1.5$ GeV.
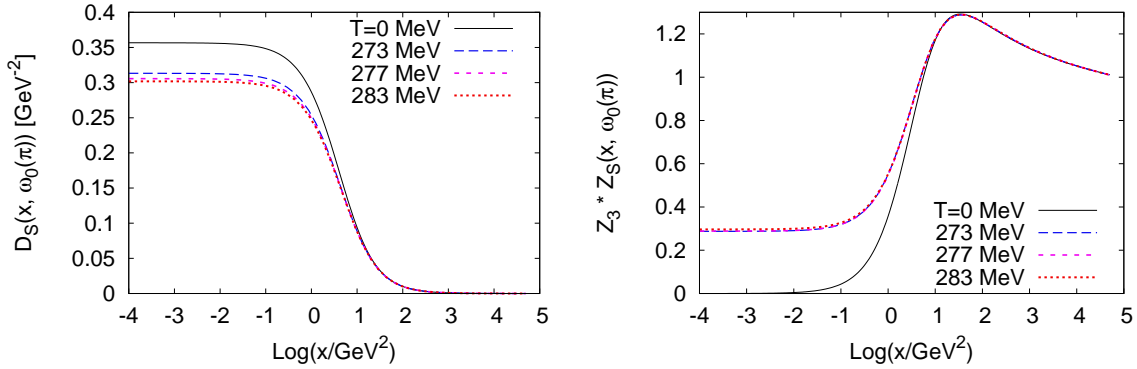
Figure 4.6.: As Fig. 4.40 Solution of the truncated DSE for the scalar propagator Eq. (4.40) with anti-periodic boundary conditions and $\omega_0(\pi)$.

renormalization constants are necessary [156]. As has been stated already, the behavior of a given theory is probed only up to momenta of order $2\pi T$. For sufficiently large renormalization scale μ^2, the renormalization constants can therefore be taken from the vacuum calculation.

Numerical results

In Fig. 4.5 solutions of Eq. (4.40) are shown for periodic boundary conditions, i.e. $\theta = 0$. Again, details concerning the numerical implementation can be found in App. C.1. The results for different temperatures close to the center transition show no visible change across the transition temperature. This is not unexpected, as the mass of the scalar field is very large and the thermal fluctuations are not strong enough to cause a large change in the propagator. Motivated by the stronger temperature dependence observed in the quark propagator close to

the transition in [234], results obtained with anti-periodic boundary conditions are shown in Fig. 4.6. There is a trivial temperature dependence due to the lowest Matsubara frequency, i.e. the propagator at vanishing temperature becomes trivially smaller. Apart from this, it seems rather hopeless to see any obvious effect of the phase transition from the propagator directly, motivating a search for proper order parameters.

4.2. Probing the Center Symmetry Transition

In the last section it has become clear that due to the large mass of the scalar field it is not possible to see any sign of the center phase transition directly from the corresponding propagator. Therefore it is necessary to construct order parameters for center symmetry which will be done along the lines of [95, 162, 231–236].

4.2.1. Order Parameters

The dual chiral condensate as implemented in [234] can serve as a guiding principle in the construction of order parameters. It is given by the first Fourier coefficient of the chiral condensate $\langle \bar{q}q \rangle_\theta$ as a function of the phase angle θ

$$\Sigma_1 = \int_0^{2\pi} \frac{d\theta}{2\pi} e^{-i\theta} \langle \bar{q}q \rangle_\theta \ .$$

It is important to distinguish different cases of defining the θ-dependence in the chiral condensate. In lattice QCD, as in [231, 232, 235, 236] one usually evaluates the expectation value of the θ-dependent chiral condensate in QCD with antiperiodic boundary. In contrast to this, continuum calculations often change the boundary conditions of the quarks in the theory, which is then termed QCD$_\theta$. Generalized boundary conditions in QCD$_\theta$ correspond actually to imaginary chemical potential and dual order parameters for center symmetry vanish only if QCD$_\theta$ is symmetric for all θ in presence of a fixed background [95].

A center transformation changes the boundary condition of the quark field which yields the properties

$$\langle \bar{q}q \rangle_\theta = \langle \bar{q}q \rangle_{\theta+2\pi}, \qquad \theta \in [0, 2\pi) \ , \tag{4.42a}$$

$$z \langle \bar{q}q \rangle_\theta = \langle \bar{q}q \rangle_{\theta+\arg(z)}, \qquad z \in \left\{ 0, e^{i2\pi/3}, e^{i4\pi/3} \right\} \ . \tag{4.42b}$$

Actually, any quantity Σ_θ that fulfills Eq. (4.42) can be used to construct order parameters. It is easy to show that the first Fourier coefficient of Σ_θ

$$\Sigma_S = \int_0^{2\pi} \frac{d\theta}{2\pi} e^{-i\theta} \Sigma_\theta \ , \tag{4.43}$$

transforms as the Polyakov loop under center symmetry

$$\Sigma_S \rightarrow \int_0^{2\pi} \frac{d\theta}{2\pi} e^{-i\theta} \Sigma_{\theta + \arg(z)} \tag{4.44}$$

$$= \int_{\arg(z)}^{2\pi + \arg(z)} \frac{d\theta}{2\pi} e^{-i(\theta - \arg(z))} \Sigma_\theta \ ,$$

$$= z \int_0^{2\pi} \frac{d\theta}{2\pi} e^{-i\theta} \Sigma_\theta$$

$$= z\Sigma_S \ .$$

Here Eq. (4.42b) has been used in the first line, a trivial change of variables has been performed in the second line and the periodicity Eq. (4.42a) has been used in the last line.

From the above considerations one can see that one way of defining an order parameter is to find some quantity Σ_θ with the properties Eq. (4.42). Here such a quantity shall be constructed from the matter propagator of scalar QCD_θ

$$D_{S,\theta}(x) \equiv D_{S,\theta}(x, y = 0) = \langle \phi_\theta(x) \phi_\theta^*(y = 0) \rangle \ , \tag{4.45}$$

where translational invariance has been used. As has been discussed in Sec. 2.1.2, any field in the fundamental representation changes its boundary conditions under center transformations. The boundary conditions in the x^4 variable of the scalar propagator $D_{S,\theta}(\vec{x}, x^4)$ are therefore changed in a similar way under center symmetry

$$z D_{S,\theta}(\vec{x}, x^4) = D_{S,\theta + \arg(z)}(\vec{x}, x^4) \ . \tag{4.46}$$

To find a Σ_θ that can easily be calculated in momentum space it is useful to use invariance of the L_2 inner product under unitary transformations. Recalling that Fourier transform/expansion defines a unitary transformation, it is natural to define Σ_θ in terms of such a L_2 inner product. Here, the momentum $\vec{p}$ is set to zero in the definition of

$$\langle D_{S,\theta}(\vec{p}^2 = 0, \cdot), D_{S,\theta}(\vec{p}^2 = 0, \cdot) \rangle_{L_2(0,1/T)} \equiv \int_0^{1/T} dx^4 \, D_{S,\theta}^2(\vec{p}^2 = 0, x^4) \tag{4.47}$$

$$= T \sum_{\substack{\omega_n(\theta) \\ n \in \mathbb{Z}}} D_{S,\theta}^2(\vec{p}^2 = 0, \omega_n(\theta)) \ .$$

This quantity has the advantage that it can easily be evaluated from the propagator in momentum space as only the Matsubara frequencies are summed. Additionally, it is well-defined and no further regularization is necessary. Eq. (4.47) has already the properties Eq. (4.42). Periodicity Eq. (4.42a) can be seen trivial, as the boundary conditions are periodic

in 2π

$$D_{S,\theta+2\pi} = D_{S,\theta} \ . \tag{4.48}$$

A center-symmetry transformation changes only the boundary condition in the propagator and therefore

$$z\langle D_{S,\theta}(0,\cdot), D_{S,\theta}(0,\cdot)\rangle_{L_2(0,1/T)} = \langle D_{S,\theta+\arg(z)}(0,\cdot), D_{S,\theta+\arg(z)}(0,\cdot)\rangle_{L_2(0,1/T)} \ , \tag{4.49}$$

as in Eq. (4.42b). Using Eq. (4.43) with

$$\Sigma_\theta = T \sum_{\substack{\omega_n(\theta) \\ n\in\mathbb{Z}}} D_{S,\theta}^2(0,\omega_n(\theta)) \ , \tag{4.50}$$

yields then an order parameter for center symmetry in case of fundamentally charged scalar QCD.

The above reasoning can also be used in QCD with quarks to find new order parameters. One possibility is given by

$$\Sigma_{q,\theta} = T \sum_{\omega_n(\theta)} \frac{1}{4i} \left(\text{tr}\ S_\theta(\vec{0},\omega_n(\theta)) \right)^2 \ , \tag{4.51}$$

where the trace is over Dirac indices only. Here, the quark propagator

$$S_\theta(p) = -i\frac{\gamma^4 \omega_n(\theta)C(p) + \gamma^i p^i A(p) - B(p)}{(\omega_n(\theta)C(p))^2 + (\vec{p}A(p))^2 + B^2(p)} \ , \tag{4.52}$$

$$\frac{1}{4i}\text{tr}\left[S_\theta(\vec{0},\omega_n(\theta)) \right] = \frac{B(\vec{0},\omega_n(\theta))}{\left(\omega_n(\theta)C(\vec{0},\omega_n(\theta))\right)^2 + B^2(\vec{0},\omega_n(\theta))} \ ,$$

with dressing functions A, B, C has been introduced. Using $\Sigma_{q,\theta}$ in Eq. (4.43) serves than as an alternative to the dual chiral condensate. In contrast to the latter, it is well-defined even away from the chiral limit.

Note that the derivation of the order parameter for the center symmetry transition was possible without any reference to the (dressed) Polyakov loop as is used, e.g. when showing that the dual chiral condensate transforms like the Polyakov loop in [231]. Only the transformation properties of fundamental matter under center symmetry are used when showing the properties Eq. (4.42). Nevertheless, it would be interesting whether the new order parameter can be related to some set of Polyakov loops with winding number one. Furthermore the continuum limit of the new order parameter is well-defined as the integral is taken over x^4 with volume $1/T$ and only the finite part of the propagator is taken into account, which avoids an unwanted infinite volume contribution $\propto \delta^{(3)}(\vec{0})$. Another possibility of taking a well-defined continuum limit in the order parameter was introduced in [236], which relies on the evaluation of the full trace of the squared Dirac operator.
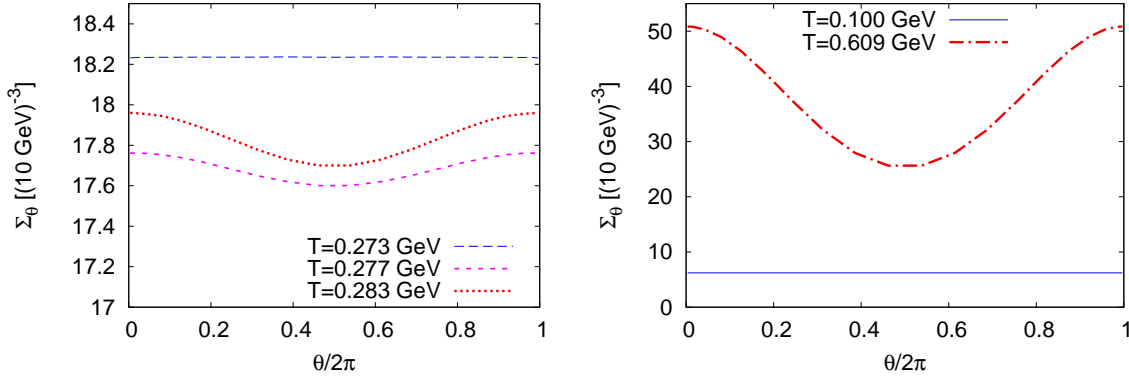
Figure 4.7.: Σ_θ as defined in Eq. (4.50) as function of the boundary conditions for different temperatures with $\mu = 4$ GeV and $m = 1.5$ GeV.

4.2.2. Numerical Results

Before investigating the center transition from the scalar propagator via evaluating Σ_S it is interesting to look at Σ_θ as a function of θ for different temperatures. Recalling the definition of Σ_S in Eq. (4.43) it is clear that whenever Σ_θ is constant, the defining integral of Σ_S will vanish. Additionally, a mirror-symmetric Σ_θ around $\theta = \pi$, i.e. $\Sigma_{\pi-\theta} = \Sigma_{\pi+\theta}$ for $\theta \in [0, \pi]$, implies a real Σ_S. This is due to the antisymmetric imaginary part of the remaining factor in the integral. Results for Σ_θ are shown in Fig. 4.7. Apparently, Σ_θ is constant for temperatures below the critical temperature of $T_c = 0.277$ GeV in the pure gauge theory, indicating a vanishing order parameter. Above the transition temperature Σ_θ is not constant anymore but it is still mirror-symmetric around $\theta = \pi$ and therefore the order parameter is expected to be a real number. The suppressed values of Σ_θ around $\theta = \pi$, where the cosine is negative furthermore indicate that Σ_S will take positives values above the transition temperature. At periodic boundary conditions $\theta \in \{0, 2\pi\}$, Σ_0 rises quickly with temperature above T_c as compared to anti-periodic boundary conditions $\theta = \pi$. In general the behavior of Σ_θ is qualitatively comparable to the behavior of the chiral condensate at general boundary conditions in spinor QCD [162, 232, 235].

From this discussion of Σ_θ it is no surprise that the order parameter shown in Fig. 4.8 behaves as expected. Below the transition temperature is is (almost) zero, whereas it takes non-vanishing values above $T_c = 0.277$ GeV. Although the transition is known to be of first order, this is hard to see from the results shown here, as lattice results for the gluon propagator are only available for a finite number of temperatures. Furthermore, the small deviations from a vanishing value of the order parameter below the transition temperature can partially be attributed to numerical uncertainties in the lattice results for the gluon propagator. However, this is not the only possible source of such deviations. As discussed previously, the scalar-gluon vertex is expected to play an important role at the transition. To check its influence, the model parameter d_1 of Eq. (4.21) is varied and the corresponding results for the order parameter are shown in the left panel of Fig. 4.9. The quality of the transition depends strongly on the vertex. Therefore, the scalar theory can be used as a testing ground for calculations of the quark-gluon vertex at finite temperature.
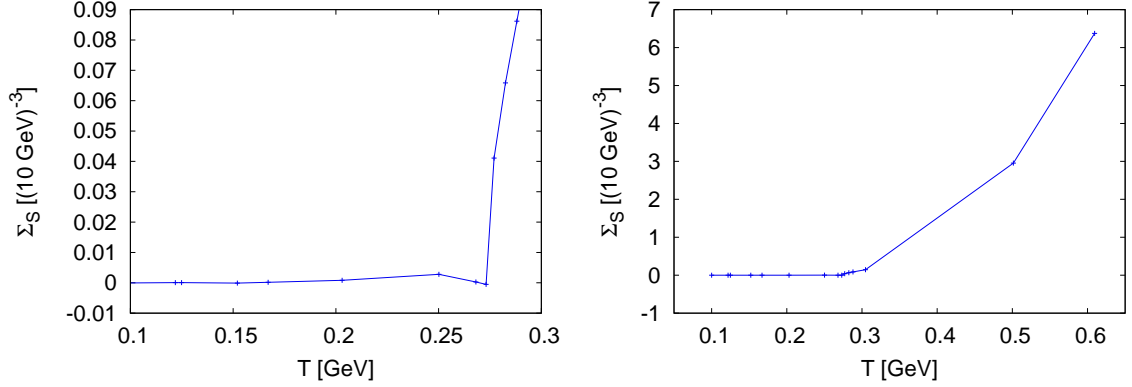
Figure 4.8.: Order parameter Σ_S as defined in Eq. (4.43) as function of the temperature with $\mu = 4$ GeV and $m = 1.5$ GeV.
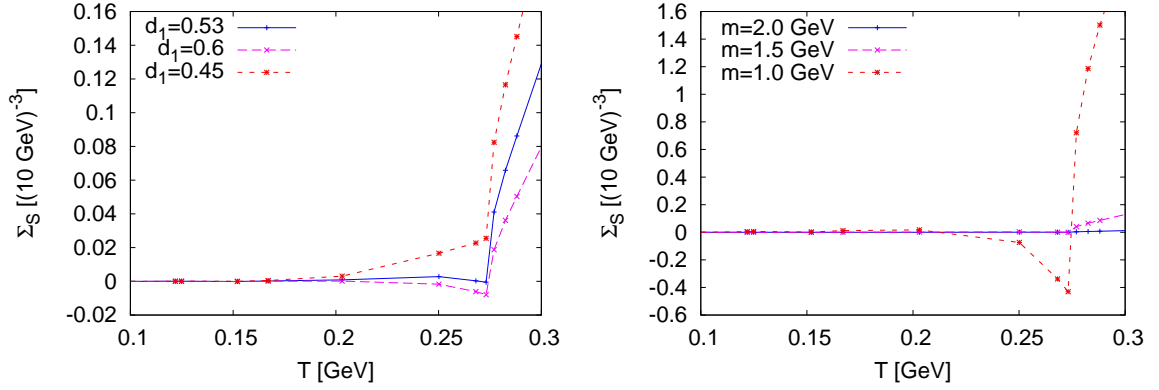
Figure 4.9.: Order parameter Σ_S as defined in Eq. (4.43) as function of the temperature for different masses and vertices with $\mu = 4$ GeV.

Additionally, results for different masses are shown in the right panel of Fig. 4.9. For smaller masses the numerical values of the order parameter above the transition become larger. This can be explained by the fact that the scalar field becomes more susceptible to thermal fluctuations with smaller masses. Furthermore, the quality of the transition seems to worsen, which can be seen as another indication for the importance of the vertex, but is possibly also due to truncation effects and missing matter back reactions.

Finally, it is confirmed that $\Sigma_{q,\theta}$ from Eq. (4.51) leads via

$$\Sigma_q = \int\limits_0^{2\pi} \frac{d\theta}{2\pi} e^{-i\theta} \Sigma_{q,\theta} \; , \tag{4.53}$$

to an order parameter in spinor QCD. A comparison of this new order parameter with the dual chiral condensate [233] and the dual scalar dressing function [234] is shown in Fig. 4.10. Here, the same model interaction and numerical setup as in [162] have been used. The

Figure 4.10.: Left diagram: The quark dressing function B, the quark condensate $\langle \bar{q}q \rangle$ and $\Sigma_{q,\phi}$ as functions 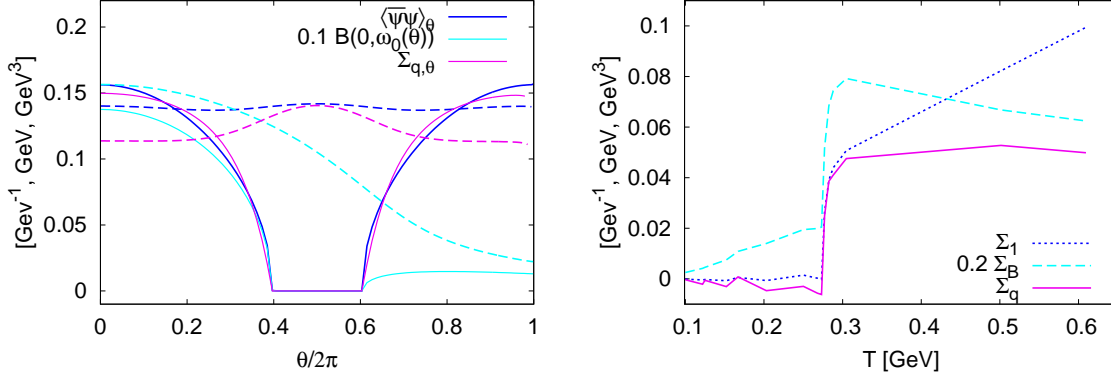of the boundary conditions for different temperatures (dashed lines correspond to a temperature of $T = 0.273$ GeV, solid lines to $T = 0.283$ GeV). Right diagram: The order parameter Σ_q as obtained from the quark propagator using $\Sigma_{q,\phi}$ as defined in Eq. (4.51) as well as Σ_1 and Σ_B as functions of the temperature in the chiral limit (The author is grateful to Markus Hopfer for providing the numerical data for this graph [229, 230]).

quark condensate $\langle \bar{q}q \rangle_\theta$, the quark dressing function $B_\theta(\vec{0}, \omega_0(\theta))$, as well as $\Sigma_{q,\theta}$ as defined in Eq. (4.51) are plotted as a function of the boundary angle θ for different temperatures. In contrast to the chiral condensate and $\Sigma_{q,\theta}$, the quark dressing function $B_\theta(\vec{0}, \omega_0(\theta))$ does not fulfill the properties Eq. (4.42). The former two behave qualitatively similar - also to Σ_θ as obtained from the scalar propagator. One difference to Σ_θ is that $\langle \bar{q}q \rangle_\theta$ as well as $\Sigma_{q,\theta}$ vanish at temperatures above the transition on a sharp plateau around the anti-periodic boundary conditions $\theta = \pi$. This is, because the shown results have been obtained in the chiral limit and the chiral transition happens at the same temperature as the center transition. Above the chiral transition the condensate $\langle \bar{q}q \rangle_\pi$ vanishes due to the restoration of chiral symmetry. Also, $\Sigma_{q,\theta}$ is directly proportional to the scalar dressing function B of the quark propagator Eq. (4.52), which vanishes as soon as chiral symmetry is restored. Away from the chiral limit the behavior of $\langle \bar{q}q \rangle_\pi$ and $\Sigma_{q,\theta}$ is expected to be closer to the behavior of Σ_θ of scalar QCD, which is seen at least for $\langle \bar{q}q \rangle_\theta$ in lattice calculations [232].

Furthermore, the dual order parameters Σ_1, Σ_B and Σ_q are plotted as a functions of temperature in Fig. 4.10. Note that Σ_B deviates from zero considerably already below the transition temperature, whereas Σ_1 and Σ_q stay close to zero. Similar to the case of scalar QCD, the behavior of the order parameters close to the transition temperature depends strongly on the model chosen for the quark-gluon vertex [201]. The behavior above the transition temperature depends on the chosen order parameter which can be understood by their different dimensionality.

Summary

Confinement of fundamentally charged matter has been investigated in terms of center symmetry. Truncated versions of the Dyson-Schwinger equation for matter propagators have been solved at zero and finite temperature.

Along the lines of previous investigations it was possible to construct an order parameter for the center transition from the matter propagator of fundamentally charged scalar Quantum Chromodynamics. The crucial point in the construction of this order parameter is the inclusion of information from all Matsubara modes. For very heavy masses of $\mathcal{O}(1)$ GeV of the scalar field, where it is not possible to see any effects of the phase transition in the propagator itself, this order parameter still shows a clear sign of the phase transition.

Additionally a new order parameter for center symmetry in QCD was found, which compares well with the previously introduced dual chiral condensate. In contrast to the latter the new order parameter needs no regularization in case of non-vanishing bare quark masses.

5. Chiral Transition with Quarks and Mesons

In this chapter, an effective description in terms of quarks and mesons Eq. (2.71) will be used in the Wetterich equation. The goal is to investigate the relevance and fate of $U(1)_A$ violating interactions close to the chiral transition. In principle this would require calculations with QCD degrees of freedom. However, the discussion of Sec. 2.1.3 shows that close to the chiral transition, a description in terms of effective degrees of freedom can also be justified. Also, from universality arguments an implementation of the correct symmetries and the relevant degrees of freedom can yield a qualitatively correct description of phenomena associated with phase transitions. With this motivation, in Sec. 5.2 the full temperature and scale dependence of a 't Hooft determinant term will be included in the flow of the mesonic potential of the two flavor quark-meson model [245]. The $2+1$ flavor formulation is treated in Sec. 5.3, where the effect of a temperature independent 't Hooft term is investigated in the light chiral limit of $m_{u,d} = 0$ [246].

It has been stated already in Sec. 2.1.2 that a careful investigation of the global structure of the symmetry group is necessary, when going from the left-right (L, R) representation to the (axial-)vector (V, A) representation. The global structure is of no importance in the L, R representation, but the V, A representation is usually preferred, when investigating the axial anomaly. Here, only the relevant results are presented briefly, whereas the corresponding calculations are performed in App. B.3. The representation of chiral symmetry without double covering is given by

$$U(N_f)_L \times U(N_f)_R = U(1)_L/Z_{N_f} \times SU(N_f)_L \times SU(N_f)_R \times U(1)_R/Z_{N_f} \tag{5.1a}$$

$$= U(1)_V/Z_{N_f} \times SU(N_f)_L \times SU(N_f)_R \times U(1)_A/Z_{2N_f} \ . \tag{5.1b}$$

The left and right handed quark spinors transform under the latter two representations as

$$q_{L,R} \to \hat{U}_{L,R} \tilde{U}_{L,R} q_{L,R} \ , \quad \hat{U}_{L,R} \in U(1)_{L,R}/Z_{N_f} \ , \quad \tilde{U}_{L,R} \in SU(N_f)_{L,R} \ , \tag{5.2}$$

and

$$q_L \to \hat{U}_V \hat{U}_A^\dagger \tilde{U}_L q_L \ , \quad \hat{U}_V \in U(1)_V/Z_{N_f} \ , \quad \hat{U}_A \in U(1)_A/Z_{2N_f} \ , \quad \tilde{U}_L \in SU(N_f)_L \ , \tag{5.3a}$$

$$q_R \to \hat{U}_V \hat{U}_A \tilde{U}_R q_R \ , \quad \hat{U}_V \in U(1)_V/Z_{N_f} \ , \quad \hat{U}_A \in U(1)_A/Z_{2N_f} \ , \quad \tilde{U}_R \in SU(N_f)_L \ . \tag{5.3b}$$

The transformation laws for the mesonic field of the quark-meson model can be obtained from this via the identification relation $\Sigma \propto q_L q_R^\dagger$.

From Eq. (5.1b) one can deduce that the 't Hooft determinant Eq. (2.51) breaks the full symmetry to $U(1)_V/Z_{N_f} \times SU(N_f)_L \times SU(N_f)_R$. As is discussed in more detail in App. B.3, this is actually true for any odd power of the determinant. Even powers of the determinant, on the other hand, respect an additional $Z_2 \subset U(1)_A/Z_{2N_f}$. In the two flavor quark-meson model, this Z_2 symmetry plays an important role related to the temperature dependence of the axial anomaly close to the chiral transition.

5.1. Mesonic Effective Potential

Symmetries of the ground state and phase transitions can be investigated with the mesonic effective potential. In the next two sections, two methods of calculating the effective potential in the quark-meson model will be discussed. The simplest possibility is to treat the mesonic field as a constant mean-field. Qualitatively this neglects important contributions by mesonic fluctuations, which are especially important in the vicinity of phase transitions. Therefore, when investigating the phase transitions of a theory an improvement can be achieved by including mesonic fluctuations. These will be included with the Wetterich equation in a leading order derivative expansion.

5.1.1. The Bosonic Mean-Field

The purpose of this section is the calculation of the grand canonical potential of the quark-meson model in the approximation of a constant mesonic mean-field $\Sigma(x) \to \bar{\Sigma}$. In this case, the fermionic integration is Gaussian and can be performed analytically. The mean-field action of the quark-meson model is given by

$$S[T, \{\mu_i\}; \bar{q}, q, \bar{\Sigma}] = \int\limits_{\mathbb{R}^3 \times [0, 1/T]} \left\{ i\bar{q}\gamma_\mu \partial_\mu q - q^\dagger \mu_q q + h\left(q_L^\dagger \bar{\Sigma} q_R + q_R^\dagger \bar{\Sigma}^\dagger q_L\right) + U(\bar{\Sigma}) \right\} , \quad (5.4)$$

where $\mu_q = \text{diag}(\mu_1, \dots, \mu_{N_f})$ is the quark chemical potential matrix in flavor space. The grand canonical partition function Eq. (2.80) can be evaluated by performing the Gaussian integration in

$$Z(T, \{\mu_i\}; \bar{\Sigma}) = \int \mathcal{D}\bar{q}\mathcal{D}q \, \mathrm{e}^{-S[T, \{\mu_i\}; \bar{q}, q, \bar{\Sigma}]} . \quad (5.5)$$

After a straightforward calculation (see e.g. [247, 248]), this leads to the effective potential

$$\tilde{\Omega}(T, \{\mu_i\}; \bar{\Sigma}) = \tilde{\Omega}_{\bar{q}q}(T, \{\mu_i\}; \bar{\Sigma}) + \tilde{\Omega}_{\bar{q}q}(T, -\{\mu_i\}; \bar{\Sigma}) + U(\bar{\Sigma}) , \quad (5.6)$$

$$\tilde{\Omega}_{\bar{q}q}(T, \{\mu_i\}; \bar{\Sigma}) = -\frac{2NT}{(2\pi)^2} \sum_{i=1}^{N_f} \int\limits_{y \in [0, \infty]} \sqrt{y} \, \log\left[1 + \mathrm{e}^{-\left(\sqrt{y + m_{q,i}^2(\bar{\Sigma})} + \mu_i\right)/T}\right] ,$$

where $m_{q,i}^2(\bar{\Sigma})$ are the eigenvalues of $h^2\bar{\Sigma}\bar{\Sigma}^\dagger$ and N is the number of colors. In the above expression a divergent contribution related to the fermionic vacuum self-energy has been dropped. It has been shown that neglecting this contribution can change the phase transition qualitatively and leads, e.g., to the false prediction of a first-order transition in the chiral limit of the $O(4)$ quark-meson model [249–251]. Nevertheless the vacuum term will be ignored here in the mean-field calculation, which is often referred to as the no-sea approximation. It is easier to include this term in the FRG by dropping the mesonic loop.

Details on the numerical calculation of the mean-field potential are discussed in App. C.2.1. The mesonic potential $U(\bar{\Sigma})$ is independent of the temperature and fixed such that the mesonic spectrum, obtained by diagonalizing its Hessian $\nabla_{\bar{\Sigma}}^2 U$, matches experiment. The number of parameters obviously depends on N_f and the number of chiral invariants taken into account. The fermionic spectrum is then obtained from the value of $\bar{\Sigma}$ at the minimum

of the potential and the constituent quark masses are used to fix the strength of the Yukawa interaction h. The explicit set of parameters will be given in the corresponding cases. The results at $T, \mu \neq 0$ are predictions within this simple approximation.

5.1.2. Including Bosonic Fluctuations with the Wetterich Equation

The flow equation Eq. (2.32) is used in the leading order derviative expansion. This means that the full flow is truncated to

$$\Gamma_k = \int\limits_{x \in \mathbb{R}^3 \times [0,1/T]} \left\{ i\bar{q}\partial_\mu\gamma_\mu q - q^\dagger \mu_q q + h \left(q_L^\dagger \Sigma q_R + q_R^\dagger \Sigma^\dagger q_L \right) + \text{tr}\left[\partial_\mu \Sigma \partial_\mu \Sigma^\dagger \right] + U_k(\Sigma) \right\} , \quad (5.7)$$

where $\mu_q = \text{diag}(\mu_1, \dots, \mu_{N_f})$ is again the quark chemical potential matrix in flavor space. Since only the mesonic field may take non-vanishing expectation values, the trace in the Wetterich equation splits into a bosonic and fermionic loop

$$\partial_k \Gamma_k = \frac{1}{2}\text{Tr}\left\{ \left(\Gamma_k^{(0,0,2)} + R_{B,k} \right)^{-1} \partial_k R_{B,k} \right\} - \text{Tr}\left\{ \left(\Gamma_k^{(1,1,0)} + R_{F,k} \right)^{-1} \partial_k R_{F,k} \right\} . \quad (5.8)$$

with corresponding regulators R_B and R_F. For the fermionic field, the ordering of derivatives is important, where the conventions are defined in App. A.3. It is possible to find unitary transformations U_B and U_F that diagonalize $\Gamma_k^{(0,0,2)}$ and $\Gamma_k^{(1,1,0)}$ in flavor space. Assuming a flavor blind regulator, these transformations allow to evaluate the flavor space part of the trace in the Wetterich equation trivially. Therefore, the flow equation for the mesonic effective potential splits further into

$$\partial_k U_k(T, \{\mu_i\}; \Sigma) = \frac{k^3}{2} \left[\sum_{i=1}^{2N_f^2} l_B \left(\frac{m_{b,i}^2}{k^2}; T \right) - 4N \sum_{i=1}^{N_f} l_F \left(\frac{m_{f,i}^2}{k^2}; T, \mu_i \right) \right] . \quad (5.9)$$

Here, the squared (pseudo-)masses are given by the field- and k-dependent eigenvalues, $m_{b,i}^2$, of the Hessian of U_k in case of bosons and by the eigenvalues, $m_{f,i}^2$, of the fermionic mass matrix $h^2\Sigma\Sigma^\dagger$ in case of the fermions. Note that the physical masses are obtained by evaluating these eigenvalues at the minimum of the effective potential. The exact form of the threshold functions $l_{B,F}$ depends on choice for the regulators $R_{B,F}$ and are the same as in case of just one flavor. Here the three dimensional optimized regulator [55, 56]

$$R_{B,k}(\omega_n, \vec{p}) = (k^2 - \vec{p}^2)\theta\left(1 - \frac{\vec{p}^2}{k^2} \right) 1_{N_f \times N_f} , \quad (5.10a)$$

$$R_{F,k}(\nu_n, \vec{p}) = -i\gamma_i p_i \left(\sqrt{\frac{k^2}{\vec{p}^2}} - 1 \right) \theta\left(1 - \frac{\vec{p}^2}{k^2} \right) , \quad (5.10b)$$

is used, where θ denotes the Heaviside step function. The corresponding dimensionless threshold functions are given by [252]

$$l_B(x;T) = \frac{1}{6\pi^2} \frac{\coth\left(\frac{\sqrt{k^2(1+x)}}{2T}\right)}{\sqrt{1+x}} \; , \tag{5.11a}$$

$$l_F(x;T,\mu) = \frac{1}{6\pi^2} \frac{\tanh\left(\frac{\sqrt{k^2(1+x)}+\mu}{2T}\right) + \tanh\left(\frac{\sqrt{k^2(1+x)}-\mu}{2T}\right)}{2\sqrt{1+x}} \; . \tag{5.11b}$$

The two terms in the fermionic threshold function with different sign in the chemical potential correspond to particle and antiparticle.

In this approximation, the task is reduced to solving a highly non-linear partial differential equation for the mesonic effective potential U_k. Symmetries restrict the effective potential to be a function of the chiral invariants Eq. (2.72) and the 't Hooft determinant Eq. (2.73). A linear explicit breaking term Eq. (2.75) cannot affect the flow as only second derivatives appear. An explanation of the general numerical implementation is given in App. C.2.2. The flow at $T = \mu = 0$ is used to fix the parameters. Apart from the Yukawa coupling h and the explicit breaking terms, the initial effective potential U_Λ has to be specified. Only renormalizable interactions are taken into account at Λ to fit the physical mesonic spectrum at $k = 0$. The results at $T \neq 0$ and $\mu_i \neq 0$ are then predictions within this approximation.

5.2. Flow of $U(1)_A$ Violating Couplings

The goal of this section is an investigation of the temperature dependence of 't Hooft determinant couplings in the mesonic effective potential of the two flavor quark-meson model [245]. The most general mesonic potential, respecting all symmetries except for $U(1)_A$ is given by

$$U(\Sigma) = \tilde{U}(\rho_1, \rho_2, \xi) \; . \tag{5.12}$$

The invariants ρ_1, ρ_2 and the determinant ξ are defined in Eqs. (2.72) and (2.73) with the mesonic field

$$\Sigma = (\sigma^a + i\pi^a)\tau^a/2 \; . \tag{5.13}$$

Here, $\tau^0 = 1_{2\times2}$ and τ^a are the Pauli matrices with $a \in \{1,2,3\}$ defined in App. A.1. The mesonic field consists of four scalars $J^P = 0^+$ and pseudoscalars $J^P = 0^-$. The scalar fields σ^a correspond for the index $a = 0$ to the σ-meson ($f_0(500)$) and the remaining indices $a = 1, 2, 3$ denote the isotriplet $\vec{a}$-bosons. The pseudoscalars π^a represent the η'-meson ($a = 0$) and the three pions $\vec{\pi}$ ($a = 1, 2, 3$). Note that the η'-meson with two flavors lacks the strange contributions that are important in the physical η'. If isospin symmetry is unbroken, i.e., $m_u = m_d$ the masses of all isotriplet particles are degenerate. The most general explicit symmetry breaking term consistent with the quantum numbers of the vacuum

$$U(\Sigma) \rightarrow U(\Sigma) - \text{tr}\left[C(\Sigma + \Sigma^\dagger)\right] \; , \tag{5.14}$$

$$C = \text{diag}\left(\frac{c_0 + c_3}{2}, \frac{c_0 - c_3}{2}\right) \; ,$$

is added to the potential. This gives a different bare mass to up and down quarks, where isospin splitting is controlled by c_3

The O(4) version of the quark-meson model is obtained by keeping only ρ_1 in the potential, setting $c_3 = 0$ and sending the coupling of ξ to $-\infty$, while keeping the σ- and $\vec{\pi}$-masses constant [136]. In this case, the η' and $\vec{a}$-particles decouple from the dynamics due to their diverging masses [253]. Previous works have included a ρ_2-dependence in the potential and found that the order of the finite-temperature phase transition in the chiral limit is changed from second to first order [214, 216, 254].

In order to explore the influence of the axial anomaly on the chiral phase transition, the mesonic potential U is truncated such that it depends only on $\rho \equiv \rho_1$ and ξ. Replacing all fields by their vacuum expectation values yields only two non-vanishing condensates, σ^0 and σ^3. In this truncation the meson potential Eq. (5.12) and (5.14) is replaced by

$$U(\sigma^0, \sigma^3) = \tilde{U}(\rho, \xi) - c_0\sigma^0 - c_3\sigma^3 . \tag{5.15}$$

In the initial potential U_Λ as well as the mean-field treatment only renormalizable couplings are relevant, i.e. the potential can be parametrized as

$$\tilde{U}(\rho, \xi) = a_{10}(\rho - \rho_0) + a_{01}(\xi - \xi_0) \tag{5.16}$$
$$+ \frac{a_{20}}{2}(\rho - \rho_0)^2 + \frac{a_{02}}{2}(\xi - \xi_0)^2 + a_{11}(\rho - \rho_0)(\xi - \xi_0) ,$$

with some expansion point (ρ_0, ξ_0). The chiral invariants in terms of the two condensates are

$$\rho = \frac{(\sigma^0)^2 + (\sigma^3)^2}{2} , \quad \xi = \frac{(\sigma^0)^2 - (\sigma^3)^2}{2} , \tag{5.17}$$

where more details can be found in App. B.4.1.

5.2.1. Masses, Ground State and Goldstone Modes

With the restriction to $\sigma^0, \sigma^3 \neq 0$, the field matrix $\Sigma = \Sigma^\dagger$ is diagonal and the quark masses are given by

$$m_d = h\frac{\langle \sigma^0 + \sigma^3 \rangle}{2} , \tag{5.18a}$$

$$m_u = h\frac{\langle \sigma^0 - \sigma^3 \rangle}{2} . \tag{5.18b}$$

Therefore the expectation value of σ^3 is a measure of isospin symmetry violation, which is expected to come predominantly from the electromagnetic interaction.

The squares of the scalar, $J^P = 0^+$, and the pseudoscalar, $J^P = 0^-$, meson masses are given by the eigenvalues of the Hessian of the mesonic potential with respect to the scalar and pseudoscalar fields, $\varphi_{s,a} = \sigma^a$ and $\varphi_{p,a} = \pi^a$, $(a = 0, \ldots, 3)$

$$m_{i,ab}^2 \equiv \nabla^2 U_{i,ab} = \left.\frac{\partial^2 U(\Sigma)}{\partial \varphi_{i,a} \partial \varphi_{i,b}}\right|_{\text{min}} ; \quad i = s, p , \tag{5.19}$$

evaluated at the minimum of the potential. Expressions for the Hessian are given in the fol-

lowing, where only the contribution from the mesonic part of the effective potential is shown. In the mean-field treatment there is an additional contribution to the effective potential from the quarks which also modifies the Hessian. As this can be obtained via simple differentiation and the resulting expressions are lengthy they will not be shown here. The mesonic Hessian is of the form

$$\nabla^2 U = \begin{pmatrix} m_s^2 & 0 \\ 0 & m_p^2 \end{pmatrix} , \tag{5.20}$$

and its only non-vanishing entries are given by

$$m_\sigma^2/m_{a_0}^2 : m_{s,00}^2 = \tilde{U}_\rho + \tilde{U}_\xi + (\sigma^0)^2 \left(\tilde{U}_{\rho\rho} + 2\tilde{U}_{\rho\xi} + \tilde{U}_{\xi\xi} \right) , \tag{5.21a}$$

$$m_{s,03}^2 = \sigma^0 \sigma^3 (\tilde{U}_{\rho\rho} - \tilde{U}_{\xi\xi}) , \tag{5.21b}$$

$$m_{s,33}^2 = \tilde{U}_\rho - \tilde{U}_\xi + (\sigma^3)^2 \left(\tilde{U}_{\rho\rho} - 2\tilde{U}_{\rho\xi} + \tilde{U}_{\xi\xi} \right) , \tag{5.21c}$$

$$m_{a_{1,2}}^2 : m_{s,11}^2 = m_{s,22}^2 = \tilde{U}_\rho - \tilde{U}_\xi , \tag{5.21d}$$

$$m_{\eta'}^2 : m_{p,00}^2 = \tilde{U}_\rho - \tilde{U}_\xi , \tag{5.22a}$$

$$m_{\vec{\pi}}^2 : m_{p,11}^2 = m_{p,22}^2 = m_{p,33}^2 = \tilde{U}_\rho + \tilde{U}_\xi . \tag{5.22b}$$

These have already been ordered in contributions to the physical particles where only the σ^0 and σ^3 entries mix to yield the σ and a_0 mesons. If the expansion point (ρ_0, ξ_0) in Eq. (5.16) is the minimum of the potential, one has the simple relationships $U_\rho = a_{10}$, $U_\xi = a_{01}$, $U_{\rho\rho} = a_{20}$, etc. The mass splitting between η' and $\vec{\pi}$ is given by

$$m_{\eta'}^2 - m_\pi^2 = -2\tilde{U}_\xi . \tag{5.23}$$

or $-2a_{01}$ if (ρ_0, ξ_0) is the minimum of the effective potential.

For vanishing isospin splitting $\sigma^3 = 0$, all pions are degenerate and also η' is degenerate with $\vec{a}$. The degeneracy in the pions survives isospin splitting, which is due to the fact that couplings proportional to ρ_2 have been neglected. To see the difference, one can additionally take the only renormalizable coupling proportional ρ_2 into account

$$\tilde{U}(\rho, \xi) \to \tilde{U}(\rho, \xi) + a_{\rho_2}(\rho_2 - \rho_{2,0}) , \tag{5.24}$$

where $(\rho_0, \rho_{2,0}, \xi_0)$ is the minimum of the potential. The meson masses are then modified to

$$m_\sigma^2/m_{a_0}^2 : m_{s,00}^2 \to \tilde{U}_\rho + \tilde{U}_\xi + (\sigma^0)^2 \left(\tilde{U}_{\rho\rho} + 2\tilde{U}_{\rho\xi} + \tilde{U}_{\xi\xi} \right) + (\sigma^3)^2 a_{\rho_2} , \tag{5.25a}$$

$$m_{s,03}^2 \to \sigma^0 \sigma^3 (\tilde{U}_{\rho\rho} - \tilde{U}_{\xi\xi}) + 2\sigma^0 \sigma^3 a_{\rho_2} , \tag{5.25b}$$

$$m_{s,33}^2 \to \tilde{U}_\rho - \tilde{U}_\xi + (\sigma^3)^2 \left(\tilde{U}_{\rho\rho} - 2\tilde{U}_{\rho\xi} + \tilde{U}_{\xi\xi} \right) + (\sigma^0)^2 a_{\rho_2} , \tag{5.25c}$$

$$m_{a_{1,2}}^2 : m_{s,11}^2 = m_{s,22}^2 \to \tilde{U}_\rho - \tilde{U}_\xi + (\sigma^0)^2 a_{\rho_2} , \tag{5.25d}$$

$$m_{\eta'}^2/m_{\pi^0}^2 : m_{p,00}^2 \to \tilde{U}_\rho - \tilde{U}_\xi \;, \tag{5.26a}$$

$$m_{p,03}^2 \to \sigma^0 \sigma^3 a_{\rho_2} \;, \tag{5.26b}$$

$$m_{p,33}^2 \to \tilde{U}_\rho + \tilde{U}_\xi \;, \tag{5.26c}$$

$$m_{\pi^\pm}^2 : m_{p,11}^2 = m_{p,22}^2 \to \tilde{U}_\rho + \tilde{U}_\xi + (\sigma^3)^2 a_{\rho_2} \;, \tag{5.26d}$$

which gives the expected splitting in case of $\sigma^3 \neq 0$.

Ground State

The most general ground state is given by

$$\langle \Sigma \rangle = \frac{1}{2} \begin{pmatrix} \langle \sigma^0 \rangle + \langle \sigma^3 \rangle & 0 \\ 0 & \langle \sigma^0 \rangle - \langle \sigma^3 \rangle \end{pmatrix} \;. \tag{5.27}$$

Depending on the values of $\langle \sigma^{0,3} \rangle$ this is invariant under different subsymmetries of Eq. (5.1). Assuming full chiral symmetry in the Lagrangian, the non-trival cases are

(a) chiral symmetry breaking case ($\sigma^0 \neq 0$, $\sigma^3 = 0$): $\qquad U(1)_V/Z_2 \times SU(2)_{L+R}$,

(b) isospin breaking case ($0 \neq |\sigma^0| \neq |\sigma^3| \neq 0$): $\qquad U(1)_{V,d} \times U(1)_{V,u}$,

(c) degenerate isospin breaking case ($|\sigma^0| = |\sigma^3| \neq 0$): $\quad U(1)_{V,d} \times U(1)_{V,u} \times U(1)_{A,u}/Z_2$.

From the transformation law

$$\Sigma \to (\hat{U}_A^\dagger)^2 \tilde{U}_L \Sigma \tilde{U}_R^\dagger \;, \tag{5.28}$$

invariance of Eq. (5.27) under $U_V(1)/Z_2$ is always guaranteed.

In case (a), $\langle \Sigma \rangle$ is proportional to the unit matrix, resulting in the condition $U_L U_R^\dagger = 1$ for $U_{L,R} \in SU(2)_{L,R}$ which is denoted by $SU(2)_{L+R}$. Additionally, for $U_A \in U(1)_V/Z_4$ one gets the condition $(U_A^\dagger)^2 = 1$, which has only the trivial solution.

In case (b), $\langle \Sigma \rangle$ has two nonvanishing and different diagonal entries, which break $SU(2)_{L+R}$ further down to $U(1)$ consisting of opposite phase rotations of the two matrix entries. Therefore, the remaining symmetry in case (b) is $U(1)_V/Z_2 \times U(1) \cong U(1)_{V,u} \times U(1)_{V,d}$ where u, d denote independent vector phase rotations of the two flavors.

The last case (c) corresponds to the situation where one of the two condensates in $\langle \Sigma \rangle$ vanishes. As a consequence, one quark, e.g. the up quark if $\langle \sigma^0 \rangle = \langle \sigma^3 \rangle$, is massless. Therefore, axial rotations affecting only this massless flavor yield an additional symmetry $U(1)_{A,u}/Z_2$ as compared to case (b).

Depending on the original symmetry of the Lagrangian, only a subgroup of the above symmetries is actually realized. A summary of the symmetries of the ground state depending on powers of the determinant ξ present in the Lagrangian is given in Tab. 5.1, where the results of App. B.3 have been used. Only case (c) is affected by the determinant, where the factor $U(1)_{A,u}/Z_2$ is broken completely by odd powers of the determinant. A Z_2 symmetry remains, however, in the presence of even powers of ξ.

5. Chiral Transition with Quarks and Mesons

	ξ^0	ξ^{2n}	ξ^{2n+1}
(a)	$U(2)_{L+R}$	$U(2)_{L+R}$	$U(2)_{L+R}$
(b)	$U(1)_{V,d} \times U(1)_{V,u}$	$U(1)_{V,d} \times U(1)_{V,u}$	$U(1)_{V,d} \times U(1)_{V,u}$
(c)	$U(1)_{V,d} \times U(1)_{V,u} \times U(1)_{A,u}/Z_2$	$U(1)_{V,d} \times U(1)_{V,u}$	$U(1)_{V,d} \times U(1)_{V,u} \times Z_2$

Table 5.1.: Symmetries of the ground-state depending on powers of the 't Hooft determinant couplings ξ and $\langle\Sigma\rangle$ (or Lagrangian depending on c_0 and c_3) for the cases (a)-(c) discussed in the main text, with $n \in \mathbb{Z}$.

Actually, the cases (a)-(c) can also be applied to the explicit breaking terms $c_0, c_3 \neq 0$. Replacing $\sigma^{0,3} \to c_{0,3}$ in the cases (a)-(c) one can read off the symmetries of the Lagrangian with explicit symmetry breaking from Tab. 5.1.

Goldstone Modes

As discussed in Sec. 5.2.1, there exist three different Nambu-Goldstone realizations with symmetry breaking pattern corresponding to the cases (a)-(c). These ground states can also be analyzed in terms of quark masses and Goldstone mesons. The quark masses are given by Eq. (5.18) and the meson masses by Eqs. (5.21) and (5.22). Using the effective potential Eq. (5.16) with (ρ_0, ξ_0) as its minimum, the conditions $\partial_{\sigma^{0,3}} U(\Sigma) = 0$ yield

$$m_{\vec{\pi}}^2 = a_{10} + a_{01} = \frac{c_0}{\langle\sigma^0\rangle} \ , \tag{5.29a}$$

$$m_{\eta',a_{1,2}}^2 = a_{10} - a_{01} = \frac{c_3}{\langle\sigma^3\rangle} \ , \tag{5.29b}$$

at the minimum. Obviously, these relations are well-defined only if $\langle\sigma^0\rangle \neq 0$ and $\langle\sigma^3\rangle \neq 0$. Before going on it should be noted that, if a coupling a_{ρ_2} is present, these relations are changed to

$$a_{10} + a_{01} + a_{\rho_2}\langle\sigma^3\rangle^2 = \frac{c_0}{\langle\sigma^0\rangle} \ , \tag{5.30a}$$

$$a_{10} - a_{01} + a_{\rho_2}\langle\sigma^0\rangle^2 = \frac{c_3}{\langle\sigma^3\rangle} \ . \tag{5.30b}$$

The Wigner-Weyl realization can only occur in the chiral limit $c_0 \sim c_3 \to 0$ and from $\langle\sigma^{0,3}\rangle = 0$ one can deduce that the quarks are massless, whereas nothing can be said about the mesonic spectrum without further calculations.

The case (a) of spontaneous breaking of chiral symmetry to $U(1)_V/Z_2 \times SU(2)_{R+L}$ as it is believed to (approximately) happen in Nature with $f_\pi = \langle\sigma^0\rangle = 93.75$ MeV and $\langle\sigma^3\rangle = 0$ can only be realized in the isospin symmetric case $c_3 = 0$. In the chiral limit $c_0 \to 0$ with $\langle\sigma^0\rangle \neq 0$, two degenerate massive quarks and three massless pions are the consequence. If additionally $U(1)_A/Z_4$ is a symmetry of the Lagrangian one has $a_{01} = 0$ and therefore the η'-particle is the fourth Goldstone mode corresponding to spontaneous breakdown of $U(1)_A/Z_4$. Additionally, the $\vec{a}$-particles are massless. To see that this is only a remnant of ignoring ρ_2, Eq. (5.30) together with the masses Eqs. (5.25) and (5.26) can be employed. As $\langle\sigma^3\rangle = 0$ all pions are massless and $m_{\eta'}^2 = a_{10} - a_{01}$ differs from the degenerate $m_{\vec{a}}^2$ by $\langle\sigma^0\rangle^2 a_{\rho_2}$. Therefore

only $\eta', \vec{\pi}$ become massless if $a_{01} = 0$, whereas the $\vec{a}$ and σ remain massive.

Case (b) with $0 \neq |\langle\sigma^0\rangle| \neq |\langle\sigma^3\rangle| \neq 0$ can happen for any explicit symmetry breaking c_0, c_3. In the chiral limit $c_0, c_3 \to 0$ this corresponds to spontaneous breaking of chiral as well as isospin symmetry with two quarks of different mass. Eq. (5.29) implies six massless modes in such a case. Additionally, if $U(1)_A/Z_4$ were a symmetry of the Lagrangian, a seventh massless mode would be obtained as a mixed state of σ^0, σ^3. This can be seen by calculating the determinant of the corresponding matrix, which vanishes as $a_{11} = a_{02} = 0$. Either way, too many massless modes are obtained, which are lifted again by including a_{ρ_2}. Via Eqs. (5.25) and (5.26), the condition Eq. (5.30) results immediately in $m_{\pi^\pm}^2 = m_{a_{1,2}}^2 = 0$. Additionally, the matrix defining π^0 and π^3 can be seen to have vanishing determinant by using Eq. (5.30) to express the diagonal entries in terms of a_{ρ_2} giving the fifth necessary massless mode. If $U(1)_A/Z_4$ were a symmetry, Eq. (5.30) can only be true for $\langle\sigma^0\rangle \neq \langle\sigma^3\rangle$ if $a_{\rho_2} = 0$, i.e. also the second mixed state of η', π^0 would be massless. Additionally, one mixed state of σ^0, σ^3 is accidentally massless, which is only lifted by including higher non-renormalizable terms in ρ_2.

The special case (c) with $|\langle\sigma^0\rangle| = |\langle\sigma^3\rangle| \neq 0$ corresponds to one massive and one massless quark. In the chiral limit Eq. (5.29) implies six massless modes, which become seven if additionally $U(1)_A/Z_4$ were a symmetry as the determinant of the mass matrix corresponding to σ^0, σ^3 would also vanish. If a_{ρ_2} is added Eq. (5.30) makes $\pi^\pm$ and $a_{1,2}$ massless. Additionally, one of the π^0, π^3 mixing states is massless by the same reasoning as in the previous case. If additionally $U(1)_A/Z_4$ were respected, no additional massless modes arise, as this symmetry is not spontaneously broken.

Interplay of Explicit, Spontaneous and $U(1)_A$ Breaking

Before going on, it is interesting to investigate the interplay of the axial anomaly and spontaneous chiral symmetry breaking, with Eq. (5.29) and Eq. (5.30).

In case of $a_{\rho_2} = 0$, one has from Eq. (5.29)

$$\neg \left(\langle\sigma^0\rangle \neq 0 \wedge \langle\sigma^3\rangle \neq 0 \wedge a_{01} \neq 0 \wedge \frac{c_0}{\langle\sigma^0\rangle} = \frac{c_3}{\langle\sigma^3\rangle} \right) , \tag{5.31}$$

where $\neg$ denotes the negation, i.e. not all statements in the parentheses can be true at the same time. At first sight, this does not seem to be of much help, but it is worthwhile to investigate the consequences.

In a realistic description, $\langle\sigma^0\rangle$ differs considerably from zero due to spontaneous chiral symmetry breaking. In the chiral limit, the last condition is automatically fulfilled and one arrives at the condition that either $a_{01} = 0$ or $\langle\sigma^3\rangle = 0$.

Away from the chiral limit one has from Eq. (5.29)

$$0 < -2a_{01} = \frac{c_3}{\langle\sigma^3\rangle} - \frac{c_0}{\langle\sigma^0\rangle} . \tag{5.32}$$

To simplify the discussion, the case $a_{\rho_2} \neq 0$ is only investigated in the chiral limit $c_0 = c_3 = 0$. Using Eq. (5.30) with $\langle\sigma^0\rangle \neq 0$, one immediately concludes that $a_{01} = 0$ implies $\langle\sigma^0\rangle = \langle\sigma^3\rangle$. In Nature, the latter is no option and therefore $a_{01} \neq 0$ can be concluded.

To conclude: Independent of the value of a_{ρ_2}, one cannot have both, vanishing a_{01} and

suppressed isospin breaking $\langle\sigma^3\rangle$ within the quark-meson model. As spontaneous chiral symmetry breaking demands a small $\langle\sigma^3\rangle$, one can conclude already at this stage that $a_{01} \neq 0$, without any input from the mesonic masses. In other words, this provides a connection between spontaneous chiral symmetry breaking and the strength of the 't Hoot determinant coupling.

5.2.2. Numerical Investigation

In this section numerical results for the quark-meson model in its two-flavor version with an effective potential of the form Eq. (5.15) are presented. Both, a mean-field treatment as described in Sec. 5.1.1 as well as the renormalization group method discussed in Sec. 5.1.2 will be used. The functional renormalization group equation is solved numerically on a two-dimensional grid and in a two-dimensional Taylor expansion through $\mathcal{O}(\Sigma^6)$ in chiral invariants, i.e. only $\tilde{U}_k$ is scale dependent. Further details concerning the numerical implementation can be found in App. C.2.1 and C.2.2. The model parameters are fixed as discussed in Sec. 5.1.1 and 5.1.2. Several scenarios are investigated in the following, where the physical mass point is referred to as the one with $m_q \approx 300$ MeV, $m_\pi \approx 138$ MeV and $m'_\eta \approx 980$ MeV. This may not be the correct η' mass with two flavors, as the real η' also contains strange contributions - see e.g. [255] for corresponding lattice calculations. In order to obtain a η' mass of this magnitude, already the initial anomaly $a_{01}(\Lambda)$ has to take a non-vanishing value, which means that the splitting between the η', a and σ, π-sector is already present at the UV-cutoff $\Lambda = 1500$ MeV. In principle, the initial strength of the $U(1)_A$ violating coupling $a_{01}(\Lambda)$ can be calculated from QCD, see e.g. [256]. Here the more phenomenological approach of fixing it to the desired $m_{\eta'}$ is taken. It is hard to evaluate the value of the explicit isospin breaking c_3 at the physical mass point within the quark-meson model. Therefore its value relative to the uniquely defined $c_0 = c_{phys}$ is specified for each of the calculations separately. Together with setting the pion decay constants to $\langle\sigma^0\rangle = f_\pi = 93.75$ MeV, the values of $h, c_0, a_{10}(\lambda), a_{01}(\Lambda)$ can therefore be fixed. The coupling $a_{20}(\Lambda)$, which provides an additional contribution to m_σ, is set to zero, since the mass of the σ-meson is not known precisely enough [8].

Temperature Dependence

The temperature dependence of the mesonic masses and condensates at the physical mass point is shown in Fig. 5.1. Independent of the technique, the FRG calculations show a reduction in the η' mass of approximately 200 MeV at temperatures around the chiral crossover, which is in accordance with recent experimental data [202]. The $\sigma, \vec{\pi}$-sector does not seem to be altered by the augmentation of the quark-meson model and behaves qualitatively as in the limit $(a_{10} - a_{01}) \rightarrow \infty$, i.e. the $O(4)$ quark-meson model (see e.g. [254]). The same figure also shows mean-field results, where one can observe that the chiral crossover becomes steeper if the mesonic fluctuations are not implemented. Furthermore the weakening of the anomalous mass-splitting between the $\sigma, \vec{\pi}$ and $\eta', \vec{a}$-sector around the crossover temperature is not reproduced in mean-field calculations. In the remainder of this section, only results obtained with the Taylor RG technique through $\mathcal{O}(\Sigma^6)$ will be shown, as it is computationally less expensive than the grid method.

The influence of explicit isospin breaking $c_3 \neq 0$ is investigated numerically in Fig. 5.2. Even for a change of c_3 by an order of magnitude, its effect on the meson masses is negligible.
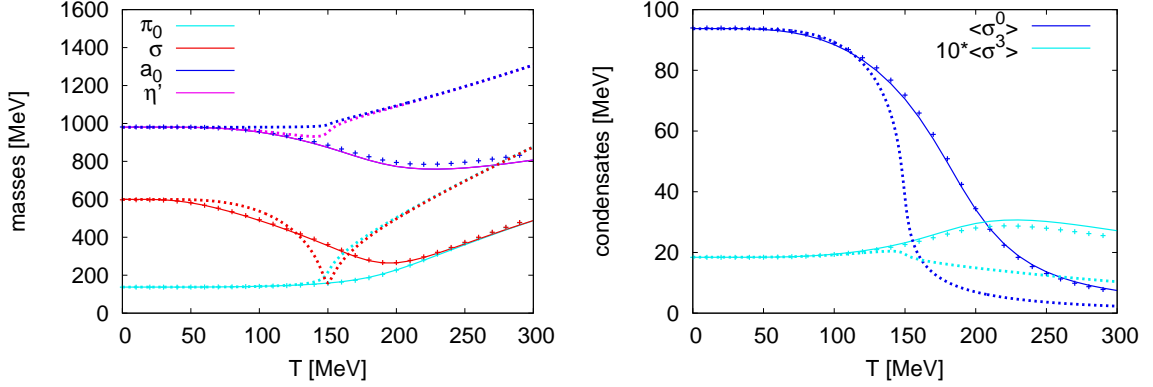
Figure 5.1.: Comparison of meson masses (left) and condensates (right) in mean-field approximation (dashed lines), with the RG calculation (solid lines: Taylor technique; crosses: grid) as a function of the temperature at the physical mass point ($c_0 = c_3 = c_{\mathrm{phys}}$). With the exception of the mean-field calculation the mass of η' and a_0 are degenerate.
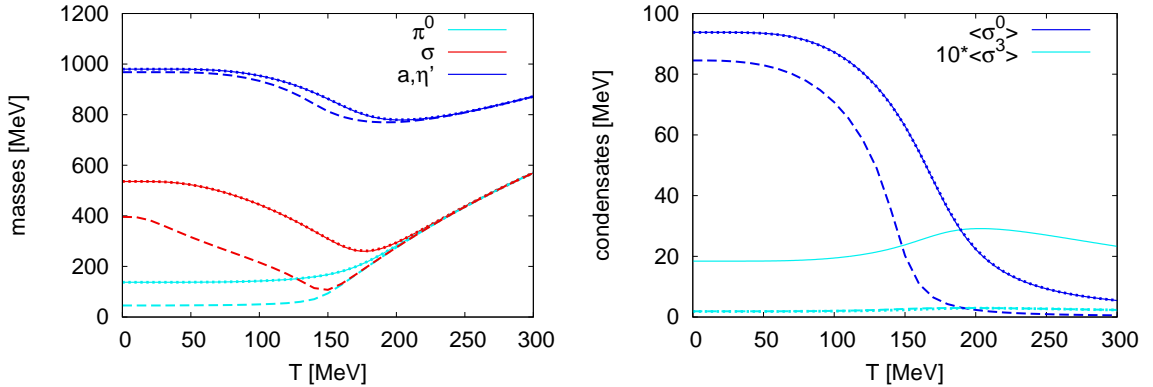

Figure 5.2.: Physical initial anomaly $a_{01}(\Lambda)$: masses (left panel) and condensates (right panel) for explicit breaking $c_0 = c_3 = c_{phys}$ (solid line), $c_0 = 10c_3 = c_{phys}$ (short dashed) and $c_0 = c_3 = c_{phys}/10$ (long dashed).

The only effect is on the trivial splitting between the two quark masses proportional $\langle \sigma^3 \rangle$. Also shown are results for symmetric explicit breaking terms $c_0 = c_3 = c_{phys}/10$, resulting in the typical quark-meson model behavior of $m_{\vec{\pi}}, m_\sigma$ and $\langle \sigma^0 \rangle$ close to the chiral limit [254], whereas the effect on the $\eta', \vec{a}$-sector is marginal.

Fig. 5.3 shows meson masses and condensates for almost vanishing initial anomalous coupling $a_{01}(\Lambda) = -(1 \text{ MeV})^2$ [1] and asymmetric explicit breaking parameters $c_0 = 10c_3 = c_{phys}$ as functions of temperature. Even though the anomalous splitting $|m_{\eta'} - m_{\vec{\pi}}| \propto |a_{01}|$ is taken to be practically vanishing at the initial scale Λ, the infrared $m_{\eta'}$ differs considerably from $m_{\vec{\pi}}$. Above the chiral transition temperature the degeneracy in the masses of η'-meson and

---

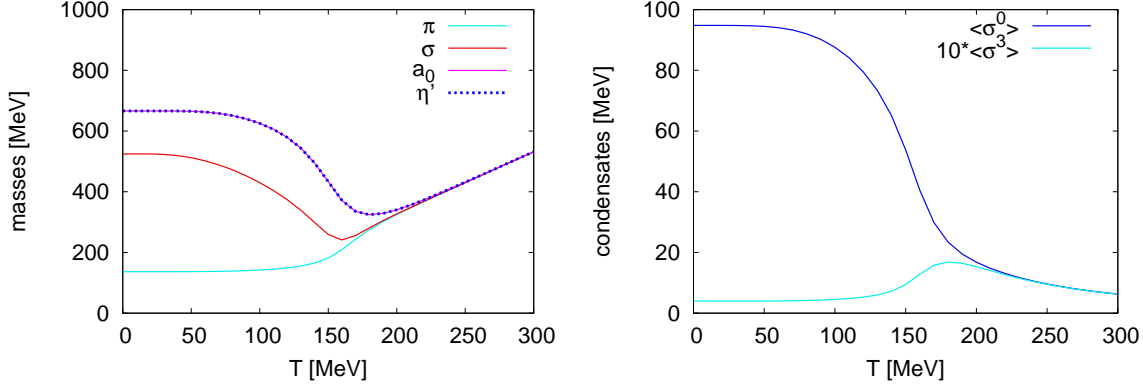[1]This has to be compared to $a_{01}(\Lambda) \approx -(450 \text{ MeV})^2$ in the previous calculations.

Figure 5.3.: Vanishing initial anomaly $a_{01}(\Lambda) = -(1\ \text{GeV})^2$ and explicit breaking $c_0 = 10c_3 = c_{phys}$: masses (left panel) and condensates (right panel) vs. temperature.

pions is restored again. This is in accordance with the connection between chiral symmetry breaking and the anomalous $m_{\eta'}$ in Eq. (5.32).

Spontaneous Breaking of Z_2

In order to gain a better understanding of the drop in the η' mass, it is instructive to examine some special limits away from the physical mass point. Recall from the discussion in App. B.3 that the Lagrangian can possess an additional Z_2 symmetry, if it only contains terms proportional to even powers of the 't Hooft determinant. This Z_2 symmetry is also respected by an explicit breaking term with $c_0 = c_3$, which is then an obvious choice for the corresponding investigations. This choice for the explicit breaking corresponds to maximal violation of isospin symmetry, i.e. one massive and one massless bare quark at the initial scale Λ.

Fig. 5.4 shows the scale dependence of the condensates and couplings for a UV-potential with very small $a_{01}(\Lambda) = -(1\ \text{MeV})^2$, for different choices of c_3. In case of $c_0 = c_3$ (solid line) Z_2 violating couplings remain suppressed above the scale of chiral symmetry breaking $k_\chi \in [500, 600]$ which is also reflected in the condensates $\langle \sigma^0 \rangle = \langle \sigma^3 \rangle$. Only together with spontaneous chiral symmetry breaking such Z_2 violating couplings are generated and $\langle \sigma^0 \rangle \neq \langle \sigma^3 \rangle$ is realized. Qualitatively this behavior even survives an explicit breaking of the Z_2 symmetry by setting $c_3 \neq c_0$. On the other hand, couplings which violate axial phase rotations but respect Z_2 are generated immediately below Λ.

In this special limit, the anomalous mass of the η' is therefore connected to spontaneous breaking of Z_2 at the scale of spontaneous chiral symmetry breaking. This can be seen as an explicit realization of Eq. (5.32). From this relation it is obvious that two massive quarks of approximately the same size imply a $\langle \sigma^0 \rangle$ that is considerably larger than $\langle \sigma^3 \rangle$, which can only be realized if a_{01} is large and negative.

Z_2 Phase Transition

Whenever a symmetry is spontaneously broken, there is the chance for a phase transition connected to its restoration. The finite temperature masses and condensates for Z_2 symmetric
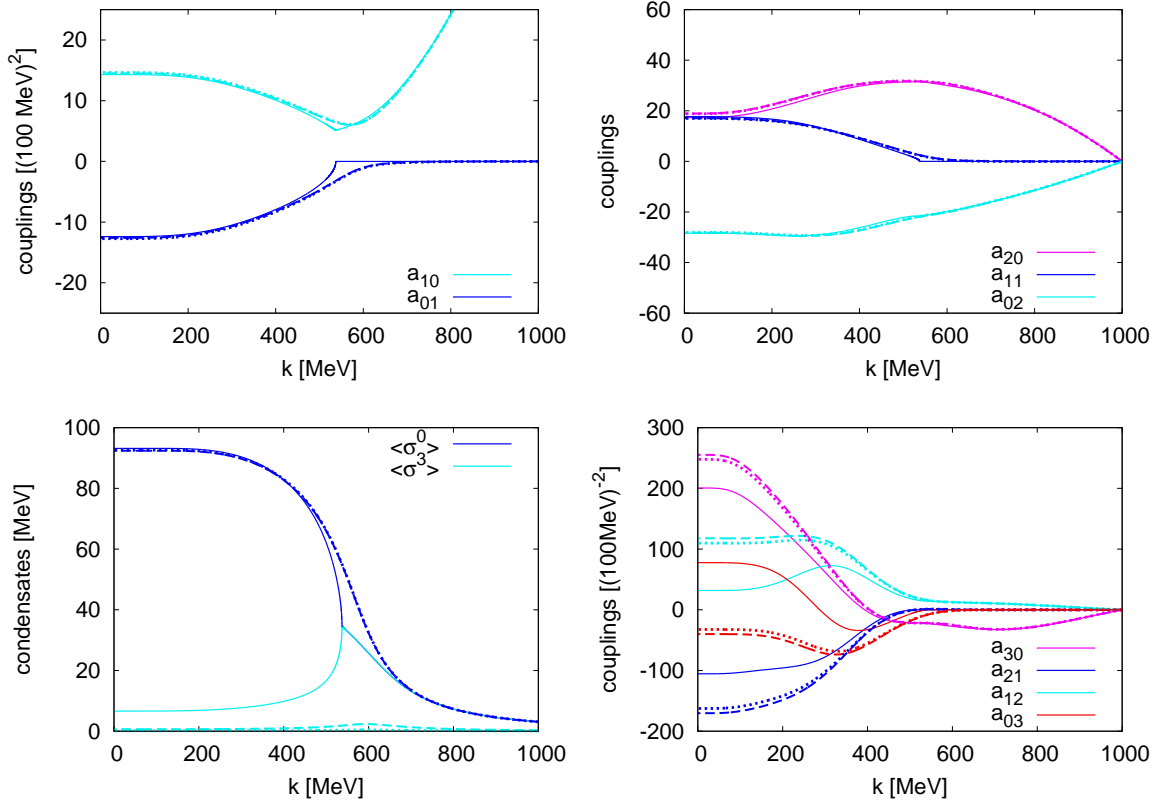
Figure 5.4.: Vanishing initial anomaly $a_{01}(\Lambda) = -(1\text{ GeV})^2$: $\mathcal{O}(\Sigma^2)$- (top left panel), $\mathcal{O}(\Sigma^4)$-couplings (top right panel), condensates (bottom left panel) and $\mathcal{O}(\Sigma^6)$-couplings (bottom right panel) vs. scale k. The solid line shows a calculation with explicit breaking parameters $c_0 = c_3 = c_{phys}$, the long dashed line with $c_0 = 10c_3 = c_{phys}$ and the short dashed line with $c_0 = 50c_3 = c_{phys}$.

explicit breaking parameters $c_0 = c_3 = c_{phys}$ are shown in Fig. 5.5. The $\eta', \vec{\pi}$ splitting vanishes at the chiral transition temperature and furthermore a perfect degeneracy in the condensates is restored. Also, all Z_2-violating couplings of odd powers of the 't Hooft determinant vanish at the transition temperature, as can be seen in Fig. 5.5. In contrast to this, Z_2 respecting couplings that violate the symmetry under general axial phase rotations remain non-vanishing above the chiral transition temperature. Therefore, the system experiences a phase transition, where Z_2 critical exponents are expected. The order parameter of the phase transition is given by $\sqrt{\xi_0}$ and the corresponding critical exponent $\beta = 0.366$. This can be compared to the three dimensional Ising universality class exponent of 0.326 [158]. The deviation can be explained by the fact that a leading order derivative expansion has been used. Furthermore the Taylor expansion in the effective potential has been performed only through $\mathcal{O}(\Sigma^6)$, which is known to give slightly higher results for the critical exponent ν and therefore also β [2] [257].

---

[2] The anomalous dimension vanishes in a leading order derivative expansion.
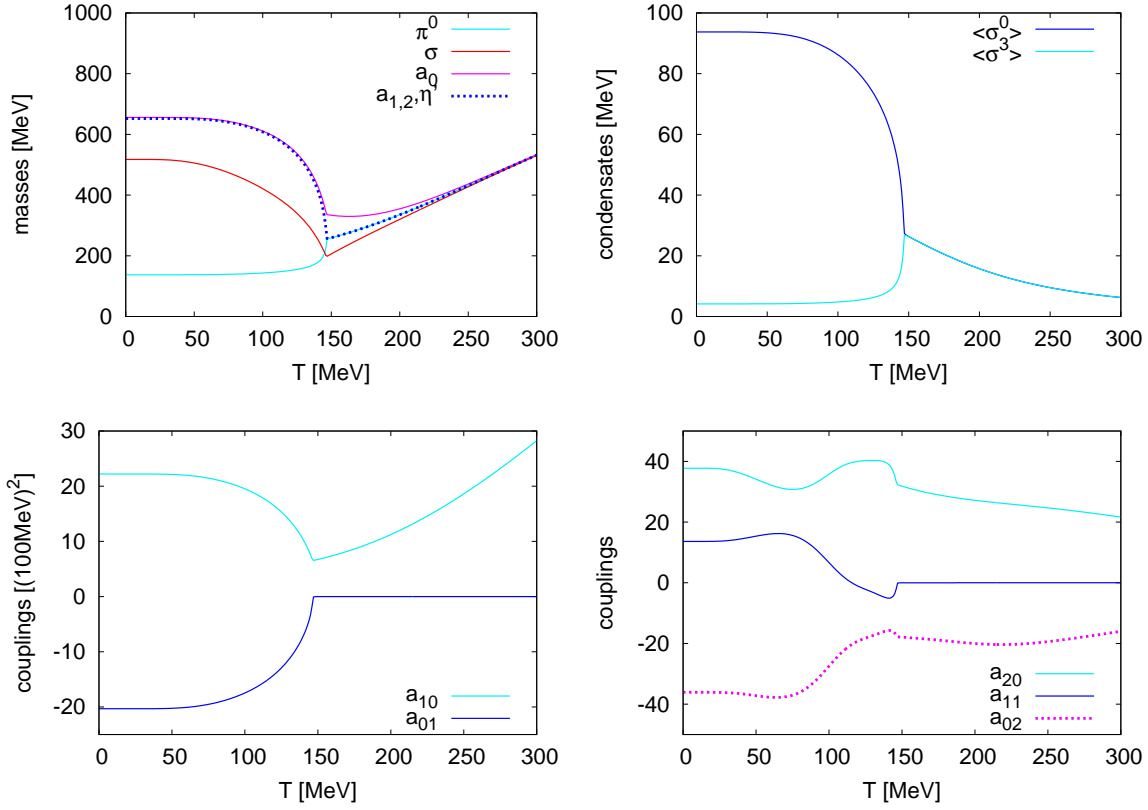
Figure 5.5.: Vanishing initial anomaly $a_{01}(\Lambda) = -(1 \text{ GeV})^2$ and explicit breaking $c_0 = c_3 = c_{phys}$: masses (top left panel), condensates (top right panel), $\mathcal{O}(\Sigma^2)$-couplings (bottom left panel) and $\mathcal{O}(\Sigma^4)$-couplings (bottom right panel) vs. temperature.

5.3. $N_f = 2 + 1$ and Light Chiral Limit

In this section the extension of the quark-meson model to three flavors is investigated [246]. The most general effective potential consistent with the symmetries is now given by [136]

$$U(\Sigma) = \tilde{U}(\rho_1, \rho_2, \rho_3, \xi) - \text{tr} \left[C(\Sigma + \Sigma^\dagger) \right] . \tag{5.33}$$

Again, the approximate nature of chiral symmetry has been taken into account by adding a diagonal explicit breaking matrix C.

The complex mesonic field is

$$\Sigma = (\sigma^a + i\pi^a)\frac{\lambda^a}{2} , \tag{5.34}$$

where $\lambda^0 = \sqrt{2/3}\, 1_{3\times 3}$ and λ^a are the Gell-Mann matrices for $a = 1, \ldots, 8$. Although mixing might occur, the field components can again be roughly related to particles [213]. In the scalar sector, σ^0 corresponds to the sigma meson $f_0(500)$ and $\sigma^{1,2,3}$ to the triplet $\vec{a}$ as in the two-flavor case. Additionally, the strange mesons $\sigma^{4,5,6,7}$ correspond to the κ quadruplet and σ^8 to the $f_0(1370)$. For the pseudoscalars, a mixing of π^0 and π^8 gives the η' and η mesons. The pions are represented by $\pi^{1,2,3}$ and the kaons correspond to $\pi^{4,5,6,7}$.

From the scalar and uncharged nature of the vacuum, only the fields $\sigma^0, \sigma^3, \sigma^8$ are allowed to obtain a non-vanishing expectation value, which takes the form

$$\langle \Sigma \rangle = \begin{pmatrix} \frac{\langle \sigma^0 \rangle}{\sqrt{6}} + \frac{\langle \sigma^8 \rangle}{2\sqrt{3}} + \frac{\langle \sigma^3 \rangle}{2} & 0 & 0 \\ 0 & \frac{\langle \sigma^0 \rangle}{\sqrt{6}} + \frac{\langle \sigma^8 \rangle}{2\sqrt{3}} - \frac{\langle \sigma^3 \rangle}{2} & 0 \\ 0 & 0 & \frac{\langle \sigma^0 \rangle}{\sqrt{6}} - \frac{\langle \sigma^8 \rangle}{\sqrt{3}} \end{pmatrix} . \tag{5.35}$$

Via the Yukawa interaction, these condensates can again be directly related to effective quark masses. Therefore, the order parameters for spontaneous chiral symmetry breaking are the three condensates $\langle \sigma^0 \rangle, \langle \sigma^3 \rangle, \langle \sigma^8 \rangle$.

5.3.1. The 2+1 Flavor Approximation

Interpreting the upper two entries of Eq. (5.35) as the light quark sector, the expectation value $\langle \sigma^3 \rangle$ describes isospin splitting as in the case of two flavors. The $2 + 1$ flavor approximation corresponds to ignoring isospin splitting and setting $\langle \sigma^3 \rangle = 0$ which results in two degenerate light quarks and one strange quark. It is convenient to rotate the remaining fields (σ^0, σ^8) to a strange-nonstrange basis [213]

$$\begin{pmatrix} \sigma_x \\ \sigma_y \end{pmatrix} = \frac{1}{\sqrt{3}} \begin{pmatrix} \sqrt{2} & 1 \\ 1 & -\sqrt{2} \end{pmatrix} \begin{pmatrix} \sigma^0 \\ \sigma^8 \end{pmatrix} . \tag{5.36}$$

5. Chiral Transition with Quarks and Mesons

The field can then take the expectation values

$$\langle \Sigma \rangle = \begin{pmatrix} \frac{\langle \sigma_x \rangle}{2} & 0 & 0 \\ 0 & \frac{\langle \sigma_x \rangle}{2} & 0 \\ 0 & 0 & \frac{\langle \sigma_y \rangle}{\sqrt{2}} \end{pmatrix} , \tag{5.37}$$

and the explicit breaking term translates to

$$\text{tr}\left[C(\Sigma + \Sigma^\dagger) \right] \to c_x \sigma_x + c_y \sigma_y . \tag{5.38}$$

As the transformation in Eq. (5.36) is unitary, the renormalization group equation is not affected by this basis change. The explicit symmetry breaking terms c_x and c_y control the bare light and strange quark masses, respectively.

The order parameters for spontaneous symmetry breaking are the condensates $\langle \sigma_x \rangle$ and $\langle \sigma_y \rangle$. Due to the explicit breaking, the latter is already large above the scale of chiral symmetry breaking. The explicit breaking term c_y breaks $SU(3)_L \times SU(3)_R$ to $SU(2)_L \times SU(2)_R$. The spontaneous symmetry breaking pattern in the light chiral limit $c_x \to 0$ is the same as in the case of two flavors and the light condensate $\langle \sigma_x \rangle$ is the order parameter for the spontaneous breaking pattern $SU(2)_L \times SU(2)_R \to SU(2)_{L+R}$.

The mesonic potential is taken as

$$U(\sigma_x, \sigma_y) = \tilde{U}(\rho_1, \tilde{\rho}_2) - c\xi - c_x \sigma_x - c_y \sigma_y , \tag{5.39}$$

with

$$\rho_1 = \frac{1}{2}(\sigma_x^2 + \sigma_y^2) , \tag{5.40a}$$

$$\tilde{\rho}_2 = \rho_2 - \frac{1}{3}\rho_1^2 = \frac{1}{24}(\sigma_x^2 - 2\sigma_y^2)^2 , \tag{5.40b}$$

and

$$\xi = \det \Sigma + \det \Sigma^\dagger = \frac{1}{2\sqrt{2}}\sigma_x^2 \sigma_y , \tag{5.41}$$

where more details can be found in App. B.4.2. The determinant ξ is included just as an explicit breaking, which will not depend on the temperature or scale in the renormalization group treatment. It would be desirable to go beyond this approximation in future investigations, which would require a three dimensional mesonic potential. The third invariant ρ_3, however, is not independent of $\rho_1, \tilde{\rho}_2$ and ξ in the $2 + 1$ flavor approximation.

The masses for the quarks are then given by the diagonal entries of $\langle \Sigma \rangle$ times the Yukawa coupling h

$$m_{q,x} = h\frac{\langle \sigma_x \rangle}{2} , \tag{5.42a}$$

$$m_{q,y} = h\frac{\langle \sigma_y \rangle}{\sqrt{2}} . \tag{5.42b}$$

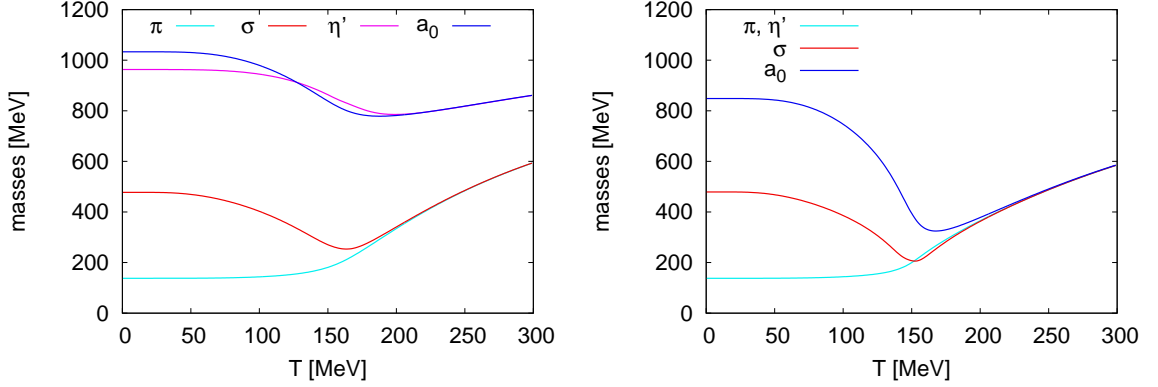To obtain the mesonic masses it is necessary to calculate the Hessian of the potential with

Figure 5.6.: Physical mass point: RG results for meson masses as functions of temperature with (left) and without (right) 't Hooft term.
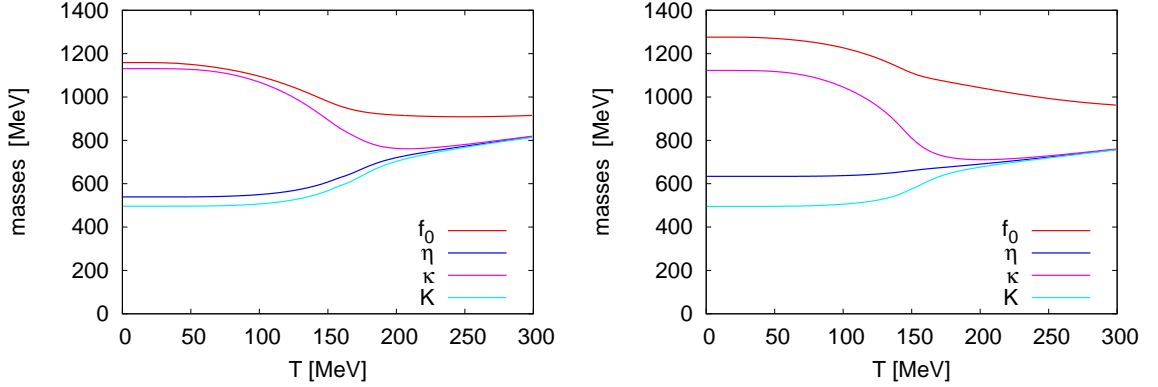

Figure 5.7.: As Fig. 5.6 for remaining mesons.

respect to Σ. The resulting matrix is block diagonal in the scalar and pseudoscalar part, i.e.

$$\nabla^2 U = \begin{pmatrix} m_s^2 & 0 \\ 0 & m_{ps}^2 \end{pmatrix} \; . \tag{5.43}$$

The only off-diagonal entries are in the 0 and 8 components of m_s^2 and m_{ps}^2 respectively, where e.g. the mixing angles of η, η' can be obtained from the corresponding matrix entries in m_{ps}^2 along the lines of [213]. The entries of the scalar and pseudoscalar mass matrix can then be expressed as functions of the derivatives $\tilde{U}_{\rho_1}, \tilde{U}_{\tilde{\rho}_2}, \tilde{U}_{\rho_1 \rho_1}, \tilde{U}_{\rho_1 \tilde{\rho}_2}, \tilde{U}_{\tilde{\rho}_2 \tilde{\rho}_2}$ and of σ_x, σ_y, where the exact expressions are very lengthy and given in App. B.5. In a mean field treatment one has additional contributions to this mass matrix from the fermionic fluctuations at $T \neq 0$ [213].

5.3.2. Numerical Investigation

Analogously to Sec. 5.2.2, in this section numerical results for the $2 + 1$ flavor quark-meson model are presented. The model parameters are the Yukawa coupling h, the two explicit breaking terms c_x, c_y and the 't Hooft determinant coupling c, with the same values as
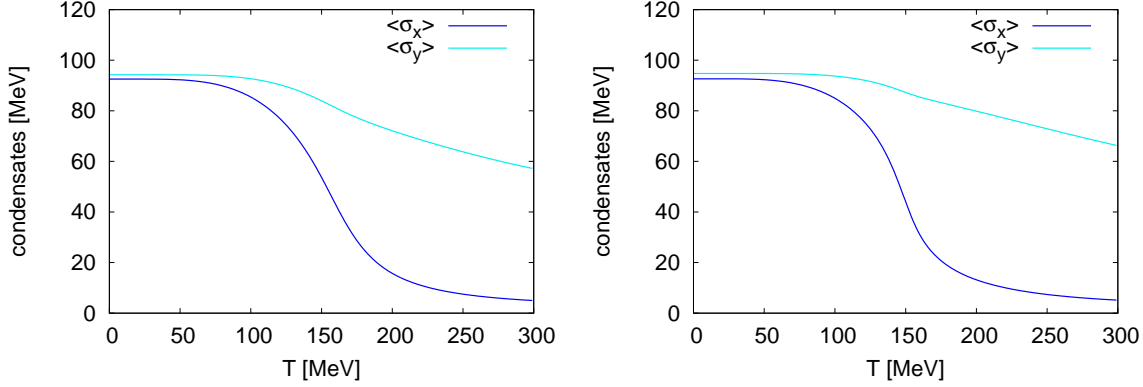
Figure 5.8.: As Fig. 5.6 for condensates.

in [213]. Additionally, the mesonic potential is defined in terms of its renormalizable terms as

$$U(\rho_1, \tilde{\rho}_2) = a_{10}\rho_1 + a_{01}\tilde{\rho}_2 + \frac{a_{20}}{2}\rho_1^2 \ . \tag{5.44}$$

In case of the renormalization group treatment this amounts to fixing the initial potential U_Λ.

Therefore at $T = 0$, seven parameters have to be fixed in total. The first four correspond to setting the values of the pion and kaon decay constant via $\langle\sigma_x\rangle$ and $\langle\sigma_y\rangle$, the η'-π mass splitting as well as the light constituent quark mass. The three parameters in the potential can then be used to adjust the mass of σ-meson, pion and kaon. The mass of the σ-meson is not very well known from experiments, which yield values in the range $400 - 1200$ MeV [8]. Its influence has e.g. been investigated in [213] in a mean-field treatment. In renormalization group studies there is usually a smaller window of allowed values for m_σ in the range of $400 - 600$ MeV. This restriction is due to the fact, that the initial potential U_Λ is used to fix the spectrum. Therefore, not necessarily all infrared potentials can be reached from the set of initial potentials.

As mentioned before, the coupling of the 't Hooft determinant is taken scale and temperature independent. Its influence will be investigated by comparing the $U(1)_A$ symmetric case $c = 0$ with the physical case $m_{\eta'} = 958$ MeV [8]. Several scenarios are investigated in the following, where the physical mass point refers to realistic $m_\pi = 138$ MeV and $m_K = 496$ MeV [8].

Physical Point

Results for the meson masses at the physical point from the grid FRG method are shown in Fig. 5.6 and 5.7. The left panel includes a physical 't Hooft term and the right panel shows results without $U(1)_A$ violation. At vanishing temperature, the 't Hooft term leads to the mixing of π^0 and π^8 and as a consequence to a suppression the mass of the η-meson, whereas the degeneracy in pion and η'-meson mass is lifted. Additionally, the a_0 and f_0 masses are enhanced by the determinant, which prevents a degeneracy of $\sigma, \vec{\pi}$ with the a_0 even in case of $\langle\sigma_x\rangle = 0$. The condensates, shown in Fig. 5.8, are not very susceptible to the determinant, although the slope of the light condensate is slightly steeper without it. Apart from this, the
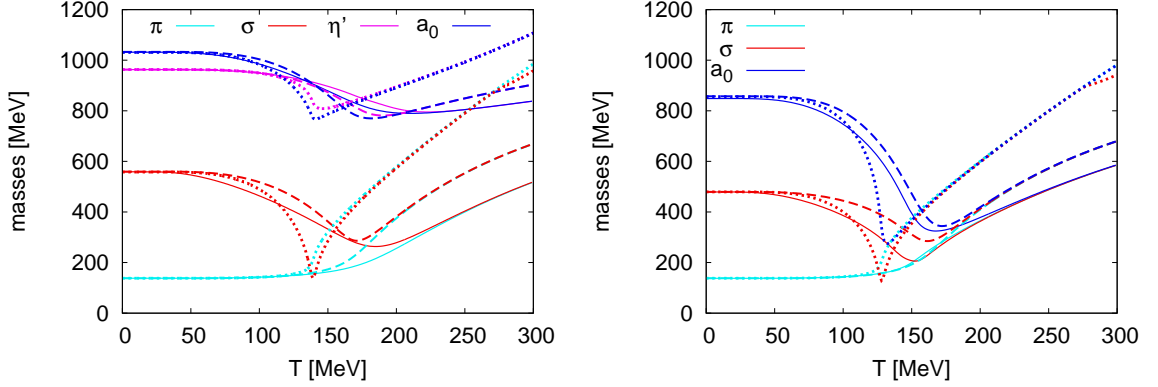
Figure 5.9.: Physical mass point: Comparison of RG (solid), RG without mesonic loop (long-dashed) and no-sea mean-field (short dashed) results for meson masses as functions of temperature with (left) and without (right) 't Hooft term.
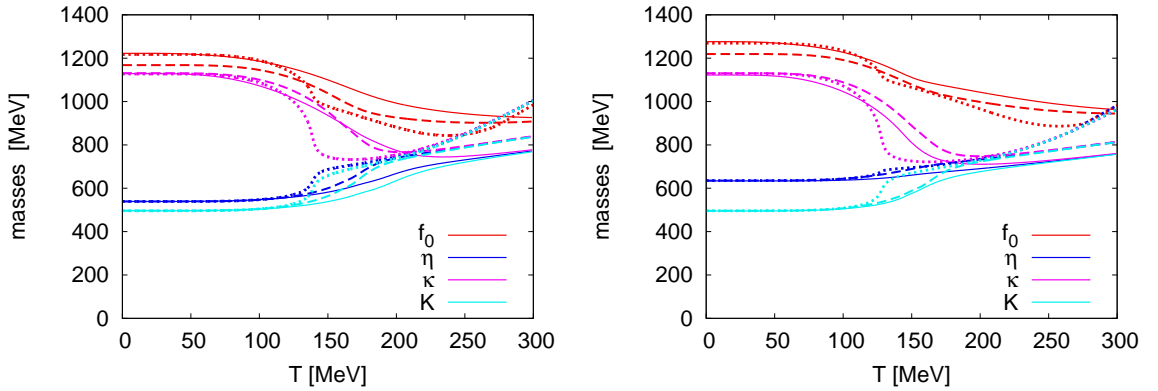

Figure 5.10.: As Fig. 5.9 for remaining mesons.

light sector seems to be largely unimpressed by the presence of strange degrees of freedom and behaves qualitatively similar to the $O(4)$-version of the quark-meson model [254]. Therefore the strange sector decouples to a large degree from the non-strange sector due to the large masses.

Additionally, the influence of mesonic fluctuations and the fermionic vacuum energy is investigated.Results for the masses and condensates with the full renormalization group (solid line), renormalization group without meson loop (long dashed line) and no-sea mean-field (short dashed line) are shown in Figs. 5.9, 5.10 and 5.11. Similar to the $O(4)$ quark-meson model (see e.g. [199]), the crossover is washed out by the inclusion of all fluctuations. This is also true independent of the presence of $U(1)_A$ violating terms. However, it is interesting that mesonic fluctuations do not wash out the transition without determinant. This is an indication that the physical point without determinant is closer to criticality.
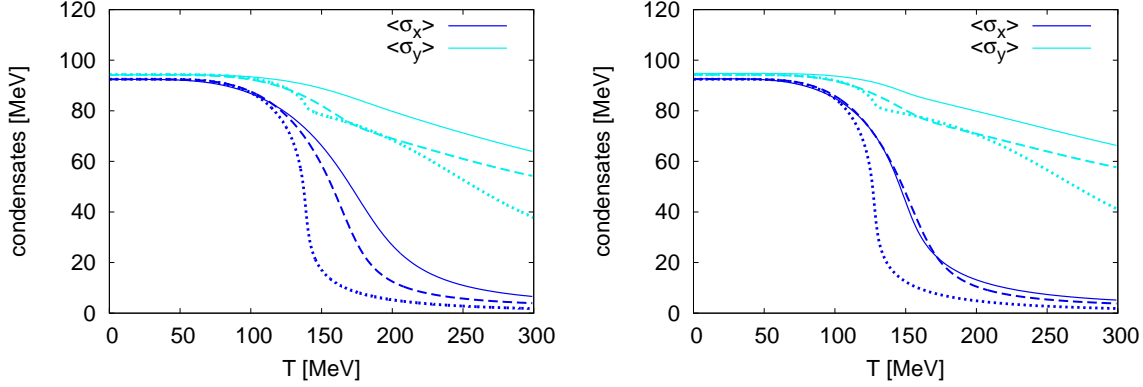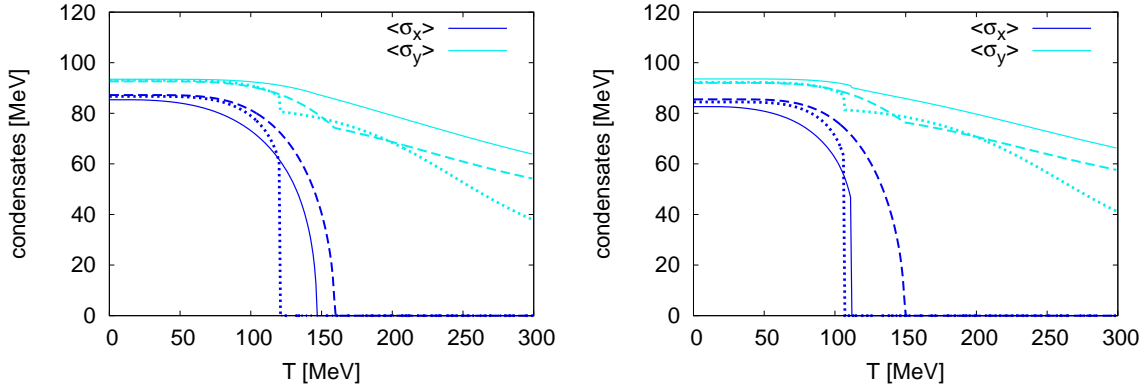
Figure 5.11.: As Fig. 5.9 for condensates.

Figure 5.12.: Light chiral limit: Comparison of RG (solid), RG without mesonic loop (long-dashed) and no-sea mean-field (short dashed) results for condensates as functions of temperature with (left) and without (right) 't Hooft term.

Light Chiral Limit

The influence of different kinds of fluctuations and the 't Hooft term become even more interesting when leaving the physical point. Fig. 5.12 shows the condensates in the light chiral limit $c_x = 0$, $c_y \neq 0$ as functions of the temperature. Again, the left panel is with 't Hooft determinant and the right panel without. As before, the solid line corresponds to full FRG results, the long dashed line to the FRG treatment without mesonic loop and the short dashed line to a no-sea mean-field treatment.

As reported previously [199], the chiral transition is of first order in the no-sea mean-field case independent of the 't Hooft term. Including the fermionic vacuum fluctuations via the FRG without mesonic loop changes the phase transition to second order, which is again independent of the presence of a 't Hooft determinant. Other, more detailed investigations of the influence of the vacuum term with three flavors include [258–262].

The 't Hooft term makes a difference, however, in the full FRG treatment with the mesonic loop. The transition is of second order with determinant and of first order without it. Ad-
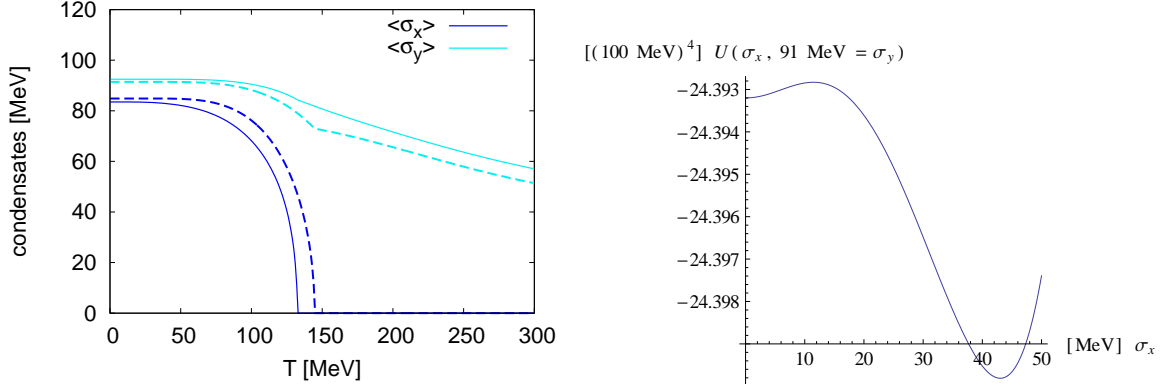
Figure 5.13.: Light chiral limit: RG results for condensates as functions of temperature (left) and effective potential as function of light condensates for fixed strange condensate $\sigma_y = \langle \sigma_y \rangle$ slightly below the transition temperature (right) with 't Hooft term.
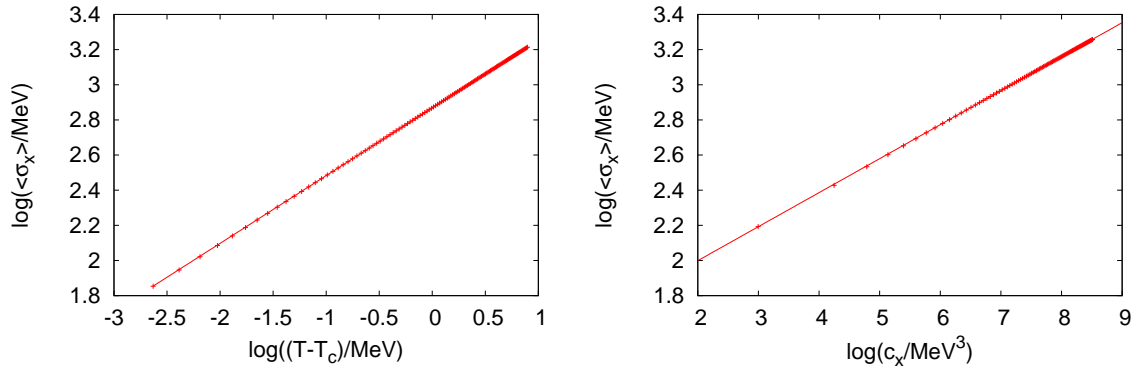

Figure 5.14.: Light chiral limit: Logarithmic plots and fit of the light condensate as function of temperature (left) and explicit breaking c_x (right) with 't Hooft determinant.

ditionally, the left panel of Fig. 5.12 shows the phase transition in the light chiral limit with 't Hooft term at lower m_σ than in the left panel of Fig. 5.12, which does not change the qualitative behavior of the transition.

To understand these findings, recall that in the chiral limit, the chiral transition for two flavors is expected to be of first order without and of second order with temperature independent 't Hooft term [214]. In the Columbia plot Fig. 2.7, this might lead to another first order region that is separated from the crossover region by a line of second-order transitions, as in case of the three flavor chiral limit. Leaving the two flavor chiral limit in direction of finite strange quark mass corresponds therefore to the light chiral limit for $N_f = 2 + 1$. For large strange quark masses, one would still expect a first-order transition. The presented results show, that at least at the physical strange quark mass there is still a first order transition. These findings are, however, also consistent with the possibility that the regions of first-order transitions of the two and three flavor chiral limit are connected.

From a Landau theory point of view it might come as a surprise that a term cubic in the field is responsible for a change from first to second order and not the other way around. In the $2 + 1$ flavor case this is actually a too simple picture, as there is more than one field component which acquires a non-vanishing expectation value. From the previous results it is clear that the strange condensate is almost unimpressed by the (order of the) transition. Therefore, only the potential at fixed σ_y, as shown in the right panel of Fig. 5.13, is relevant for the transition. The bump that would lead to a first-order transition comes from a positive quadratic term. The 't Hooft determinant is, however, proportional to $-\sigma_x^2 \sigma_y$, which provides a negative quadratic term in σ_x at fixed σ_y. Therefore, the bump, which is important for the first-order transition, is actually weakened by the 't Hooft determinant.

Finally, the two critical exponents β and δ are calculated in the light chiral limit with 't Hooft determinant. As critical phenomena are driven by the long-ranged mesonic fluctuations of the theory it is very important to set the infrared cutoff low enough, which has been taken as $k_{IR} = 2$ MeV. Fig. 5.14 shows the corresponding linear fit on a double logarithmic plot and the obtained exponents are

$$\beta = 0.39 \ , \qquad \delta = 5.2 \ . \tag{5.45}$$

Applying the same solution method to the $O(4)$ quark meson model, the results agree within a percent. These numbers are also compatible with other three-dimensional $O(4)$-universality class results obtained in the derivative expansion [257], where deviations can be attributed to the choice of the regulator. Deviations from the results obtained with other methods (see e.g. [158]) due to the derivative expansion.

Summary

The axial anomaly has been investigated close to the chiral transition with the quark-meson model in the functional renormalization group.

For two flavors, the temperature dependence of effective 't Hooft determinant interactions has been investigated. In accordance with recent experimental data, a drop in the anomalous mass of the η'-meson has been found around the chiral transition. Within the given effective description, this has been connected to a suppression of isospin breaking. Furthermore, a new Z_2 phase transition has been found in the limit of maximal isospin violation, i.e. one massive and one massless bare quark, and $U(1)_A$ symmetric initial theory. The anomalous η' mass has been interpreted as a consequence of the corresponding spontaneous breaking of Z_2. The drop in $m_{\eta'}$ at the chiral transition, however, corresponds then to a partial restoration of Z_2 instead of full $U(1)_A$.

Extending the quark-meson model to $2+1$ flavors, the influence of a temperature independent 't Hooft determinant has been investigated. For physical values of the mesons, a temperature independent determinant is already sufficient to reproduce a drop in the η'-mass due to its dependence on the light condensate. In the limit of vanishing up and down quark mass, a first-order transition is found in the full renormalization group treatment without axial anomaly. Including the anomaly via the 't Hooft term, this transition is changed to second order in the $O(4)$ universality class. This influence of the determinant on the order of the transition in the light chiral limit cannot be reproduced without mesonic fluctuations.

6. Conclusions and Outlook

In this thesis different aspects of strongly-interacting matter have been investigated. The focus has been put on the phenomena of confinement and spontaneous chiral symmetry breaking. In particular, at finite temperatures a rapid crossover from a confined phase of spontaneous chiral symmetry breaking to a deconfined and chirally symmetric phase - called quark-gluon plasma - occurs. Confinement at vanishing temperature in terms of a linearly rising potential has been investigated in Ch. 3, whereas Ch. 4 and Ch. 5 focus on the deconfinement and chiral transition at finite temperatures respectively. Investigations of these non-perturbative phenomena require appropriate methods. In this work, functional methods, i.e. the Dyson-Schwinger equations and the functional renormalization group, have been employed. Another important non-perturbative method would be lattice QCD which, however, requires a lot of numerical effort to implement chiral symmetry. Furthermore, it is often hard to extract simple qualitative pictures of physical phenomena from lattice calculations. Some aspects of strongly-interacting matter have been discussed in Ch. 2 to set the stage for the subsequent self-contained investigations.

In Ch. 3 the consequences of a hypothetical confining $1/k^4$ infrared singularity in the quark 4-point function have been investigated. Such a singularity violates cluster decomposition and results in a linearly rising static quark potential. A consistent set of similar infrared singularities has been found in all n-point functions with $n \geq 4$, whereas 3-point vertices and propagators are protected. A simple source for Casimir scaling has been identified in this picture of confinement. Furthermore, the presence of such a singularity in one kind of, possibly very heavy, fundamentally charged matter is sufficient to induce it in all other matter. This investigation shows that, if confinement is realized in terms of such singularities, it can probably be seen already on the level of 4-point functions. The absence of $1/k^4$ singularities on the level of 4-point functions, however, could be interpreted as bad news for the n-point function approach to confinement in terms of a linearly rising Landau gauge potential. In future investigations it would be desirable to show the absence of such long-ranged interactions between color singlets. Furthermore, it must be possible to see the absence of Van-der-Waals forces and derive the correct relative factors also for the asymptotic scaling of the linearly rising potential. If this picture of confinement is correct, these investigations would provide a basis for the construction of consistent truncations with confinement.

Confinement of fundamentally charged matter has been investigated in terms of center symmetry in Ch. 4. New order parameters that are accessible through matter propagators have been introduced. The solution of a truncated DSE for the matter propagator has been used to investigate the center transition. In fundamentally charged scalar QCD as well as real QCD a clear signal for the transition can be seen. In the latter case, the new order parameter compares well to the previously introduced dual chiral condensate with the advantage that no further regularization is necessary even away from the chiral limit. Unfortunately, the quality of the transition depends strongly on the model interaction between scalars and gluons which motivates a thorough investigation of the scalar-gluon vertex at non-vanishing temperatures.

6. Conclusions and Outlook

Scalar QCD can then provide a testing ground for investigations of the quark-gluon vertex of QCD at finite temperatures, which are complicated by a large number of tensor structures. In Ch. 5 the axial anomaly has been investigated close to the chiral transition in terms of quarks and mesons as effective degrees of freedom within the functional renormalization group. For two, as well as $2 + 1$ quark flavors, a recently reported drop in the anomalous mass of the η'-meson close to the chiral transition could be reproduced. In the case of two flavors, this requires a scale and temperature dependent $U(1)_A$ violating interaction in terms of a 't Hooft determinant. The drop in $m_{\eta'}$ close to the chiral transition could be connected to a partial restoration of an approximate Z_2 symmetry instead of full $U(1)_A$. The order of the chiral transition in the light chiral limit with $2 + 1$ flavors has been investigated in presence of a temperature independent 't Hooft determinant. With determinant a second-order transition in the $O(4)$ universality class has been found, whereas the transition is of first order without the 't Hooft term. These results motivate further studies of the temperature dependence of the determinant, especially with $2 + 1$ flavors, to check effects on the order of the transition in the light chiral limit. Additionally, it would be interesting to investigate the order of the transition in the two flavor chiral limit in the presence of additional relevant interactions. Finally, a calculation from first principles via the inclusion of the QCD flow for the 't Hooft determinant would be preferable. This could be augmented even further by employing dynamical rebosonization, which would take care of the change in the relevant degrees of freedom close to the chiral transition.

A. Conventions

In this appendix, some general conventions used throughout this thesis are summarized. All dimensionful quantities are characterized by their energy dimension, which is measured in electronvolt (eV). This resembles natural units, where Planck's constant $\hbar$, the speed of light c and the Boltzmann constant k_B are set to unity. Energy and momentum and temperature are measured in eV, whereas time and distance is measured in inverse eV. The most important conversion factors to SI units are

$$1\text{eV} = 1.78 \cdot 10^{-36} \text{ kg} , \tag{A.1a}$$

$$1\text{eV} = 1.16 \cdot 10^{4} \text{ K} , \tag{A.1b}$$

$$1\text{eV}^{-1} = 1.97 \cdot 10^{-7} \text{ m} , \tag{A.1c}$$

$$1\text{eV}^{-1} = 6.58 \cdot 10^{-16} \text{ s} . \tag{A.1d}$$

In flat Minkowski space, the metric $g_{\mu\nu}^M$ is defined via

$$x_\mu x^\mu = x^\nu g_{\mu\nu}^M x^\nu = x_0^2 - x_i x_i . \tag{A.2}$$

As demonstrated by this example, Einstein's summation convention is always assumed. A summation over all (space-like) components is indicated by Greek (Latin) letters.
The Euclidean metric is obtained by replacing $x_0 = ix_4$, which implies the completely negative signature

$$x_\mu x^\mu = -x_4^2 - x_i x_i \equiv -x^2 . \tag{A.3}$$

A.1. Dirac Matrices

Throughout this work, the chiral representation of the Dirac matrices

$$\gamma^0 = \begin{pmatrix} 0_{2\times2} & 1_{2\times2} \\ 1_{2\times2} & 0_{2\times2} \end{pmatrix} , \qquad \gamma^i = \begin{pmatrix} 0_{2\times2} & \tau^i \\ -\tau^i & 0_{2\times2} \end{pmatrix} , \qquad \gamma^5 = \begin{pmatrix} -1_{2\times2} & 0 \\ 0 & 1_{2\times2} \end{pmatrix} , \tag{A.4}$$

is used [6]. The corresponding Dirac matrices γ_μ can be obtained from these via $\gamma_\mu = g_{\mu\nu}\gamma^\nu$ and τ^i are the Hermitian Pauli-matrices

$$\tau^1 = \begin{pmatrix} 0 & 1 \\ 1 & 0 \end{pmatrix} , \qquad \tau^2 = \begin{pmatrix} 0 & -i \\ i & 0 \end{pmatrix} , \qquad \tau^3 = \begin{pmatrix} 1 & 0 \\ 0 & -1 \end{pmatrix} . \tag{A.5}$$

The Euclidean γ_4-matrix is defined by

$$-\gamma_4 = i\gamma_0 . \tag{A.6}$$

The Euclidean Dirac matrices have the properties

$$\{\gamma_\mu, \gamma_\nu\} = 2g_{\mu\nu}1_{4\times4}, \qquad \{\gamma^5, \gamma_\mu\} = 0_{4\times4} , \tag{A.7}$$
$$(\gamma_\mu)^\dagger = -\gamma_\mu , \qquad (\gamma^5)^\dagger = \gamma^5 ,$$

where $g_{\mu\nu} = -\delta_{\mu\nu}$ is the completely negative Euclidean metric.

A.2. Representations of $SU(N)$

Basic theorems concerning the generators of the fundamental and adjoint representations of $SU(N)$ are collected in this section. An explicit representation for the generators of $SU(3)$ in terms of the Gell-Mann matrices is given.

The $N-$dimensional fundamental representation is defined by its N^2-1 traceless generators $T^a = (T^a)^\dagger$ which have the properties

$$T^a T^b = \frac{1}{2N}\delta^{ab}I_{N\times N} + \frac{1}{2}\left(if^{abc} + d^{abc}\right)T^c , \tag{A.8a}$$

$$\left[T^a, T^b\right] = if^{abc}T^c , \tag{A.8b}$$

$$\left\{T^a, T^b\right\} = \frac{1}{N}\delta^{ab}I_{N\times N} + d^{abc}T^c , \tag{A.8c}$$

$$\mathrm{tr}\left[T^a T^b\right] = \frac{1}{2}\delta^{ab} , \tag{A.8d}$$

$$\mathrm{tr}\left[T^a T^b T^c\right] = \frac{1}{4}\left(if^{abc} + d^{abc}\right) , \tag{A.8e}$$

$$T^a_{mn}T^a_{op} = \frac{1}{2}\delta_{mp}\delta_{on} - \frac{1}{2N}\delta_{mn}\delta_{op} , \tag{A.8f}$$

$$T^a_{mn}T^a_{np} = \frac{N^2-1}{2N}\delta_{mp} . \tag{A.8g}$$

Here, (f^{abc}) d^{abc} are the totally (anti-)symmetric structure constants that define the Lie algebra. The second to last equation is due to the completeness relation obtained by noting that the N^2-1 generators together with the unit matrix span the N^2 dimensional vector space of complex matrices. The last equation defines the quadratic Casimir operator $C_F = (N^2-1)/(2N)$ of the fundamental representation.

The structure constants fulfill additionally the relations

$$d^{ace}d^{bce} = \frac{N^2-4}{N}\delta^{ab} , \tag{A.9a}$$

$$f^{ace}f^{bce} = N\delta^{ab} , \tag{A.9b}$$

$$f^{ace}d^{bce} = 0 , \tag{A.9c}$$

$$f^{abe}f^{cde} = \frac{2}{N}\left(\delta^{ac}\delta^{bd} - \delta^{ad}\delta^{bc}\right) + \left(d^{ace}d^{bde} - d^{ade}d^{bce}\right) , \tag{A.9d}$$

$$0 = f^{abe}f^{cde} + f^{ade}f^{bce} - f^{ace}f^{bde} , \tag{A.9e}$$

$$0 = f^{abe}d^{cde} - d^{ade}f^{bce} - d^{ace}f^{bde} . \tag{A.9f}$$

From the structure constants it is possible to construct the $(N^2 - 1)$-dimensional adjoint representation with $N^2 - 1$ traceless Hermitian generators

$$\left(\tilde{T}^a\right)^\dagger_{ij} = -if^{aij} \ . \tag{A.10}$$

These fulfill also the Lie algebra of $SU(N)$, but with different normalization

$$\left[\tilde{T}^a, \tilde{T}^b\right] = if^{abc}\tilde{T}^c \ , \tag{A.11a}$$

$$\text{tr}\left[\tilde{T}^a\tilde{T}^b\right] = N\delta^{ab} \ , \tag{A.11b}$$

$$\text{tr}\left[\tilde{T}^a\tilde{T}^b\tilde{T}^c\right] = i\frac{N}{2}f^{abc} \ , \tag{A.11c}$$

$$\tilde{T}^a_{mn}\tilde{T}^a_{np} = N\delta_{mp} \ , \tag{A.11d}$$

where the last line shows that the quadratic Casimir operator is also different for the adjoint representation, $C_A = N$.

In case of $N = 2$ an explicit representation of the fundamental generators is obtained from the Pauli-matrices Eq. (A.5) by $T^a = \tau^a/2$. There exists also a standard representation of the fundamental generators in case of $N = 3$, obtained from the Gell-Mann matrices

$$\lambda^1 = \begin{pmatrix} 0 & 1 & 0 \\ 1 & 0 & 0 \\ 0 & 0 & 0 \end{pmatrix} \ , \qquad \lambda^2 = \begin{pmatrix} 0 & -i & 0 \\ i & 0 & 0 \\ 0 & 0 & 0 \end{pmatrix} \ , \qquad \lambda^3 = \begin{pmatrix} 1 & 0 & 0 \\ 0 & -1 & 0 \\ 0 & 0 & 0 \end{pmatrix} \ , \tag{A.12}$$

$$\lambda^4 = \begin{pmatrix} 0 & 0 & 1 \\ 0 & 0 & 0 \\ 1 & 0 & 0 \end{pmatrix} \ , \qquad \lambda^5 = \begin{pmatrix} 0 & 0 & -i \\ 0 & 0 & 0 \\ i & 0 & 0 \end{pmatrix} \ ,$$

$$\lambda^6 = \begin{pmatrix} 0 & 0 & 0 \\ 0 & 0 & 1 \\ 0 & 1 & 0 \end{pmatrix} \ , \qquad \lambda^7 = \begin{pmatrix} 0 & 0 & 0 \\ 0 & 0 & -i \\ 0 & i & 0 \end{pmatrix} \ , \qquad \lambda^8 = \frac{1}{\sqrt{3}}\begin{pmatrix} 1 & 0 & 0 \\ 0 & 1 & 0 \\ 0 & 0 & -2 \end{pmatrix} \ ,$$

by $T^a = \lambda^a/2$. From this it is also immediately clear, that the first three Gell-Mann matrices fulfill also the algebra of $SU(2)$.

A.3. n-Point Functions

In general, the effective action or any other generating functional will depend one more than one field species. In case of anticommuting fields, the order of differentiation is important in the definition of n-point functions. In case of QCD, the notation

$$\Gamma^{(p,o,n,m,l)} = \frac{\delta^l}{\delta A^l}\frac{\delta^m}{\delta c^m}\frac{\delta^n}{\delta \bar{c}^n}\frac{\delta^o}{\delta q^o}\frac{\delta^p}{\delta \bar{q}^p}\Gamma \ , \tag{A.13}$$

A. Conventions

will be used. The conventions for scalar QCD are obtained from this by replacing $\bar{q} \to \phi^*$ and $q \to \phi$. For the quark-meson model

$$\Gamma^{(p,o,n)} = \frac{\delta^n}{\delta\Sigma^n} \frac{\delta^o}{\delta q^o} \frac{\delta^p}{\delta\bar{q}^p} \Gamma \ , \tag{A.14}$$

is used. The bare vertices $\Gamma_0^{(p,o,n,m,l)}$ and $\Gamma_0^{(p,o,n)}$ are defined analogously as derivatives of the action S. In case of only two derivatives, i.e. $p + o + n + m + l = 2$, the corresponding quantity is called (bare) propagator and denoted by (D_0) D.

The Fourier transform to momentum space is defined as

$$
\left(\tilde{\Gamma}^{(m_1,m_2,m_3,m_4,m_5)} \right) (p_1, \ldots, p_{m_1}, q_1, \ldots, q_{m_2}, r_1, \ldots, r_{m_3}, s_1, \ldots, s_{m_4}, t_1, \ldots, t_{m_5})
$$
$$
= \int\limits_{u_{i_1}, v_{i_2}, x_{i_3}, y_{i_4}, z_{i_5} \in \mathbb{R}^4} e^{i p_{i_1} \cdot u_{i_1}} e^{-i q_{i_2} \cdot v_{i_2}} e^{i r_{i_3} \cdot x_{i_3}} e^{-i s_{i_4} \cdot y_{i_4}} e^{i t_{i_5} \cdot z_{i_5}} \times
$$
$$
\times \left(\Gamma^{(m_1,m_2,m_3,m_4,m_5)} \right) (\{u_{i_1}\}, \{v_{i_2}\}, \{x_{i_3}\}, \{y_{i_4}\}, \{z_{i_5}\}) \ . \tag{A.15}
$$

In case of the quark-meson model, the quarks transform as defined here, whereas Σ transforms as the gauge field A.

A.3.1. Color Tensor Bases for n-Point Functions

Higher n-point functions have usually more than one color tensor structure consistent with conservation of color. The basis elements have been constructed along the lines of [263]. The legs of a n-point function can be classified according to the representation - fundamental or adjoint - of the corresponding field.

Propagators and 3-Point Functions

The case of propagators is trivial as color is conserved, giving the tensor structures (δ^{ab}) δ_{mn} for (adjoint) fundamental indices. For the 3-point functions one has either two fundamental and one adjoint index with tensor structure T_{mn}^a or three adjoint indices with tensor structures f^{abc}, d^{abc} as charge conservation allows only an even number of fundamental indices.

4-Point Functions

In case of four fundamental indices the allowed basis elements are given by $\delta_{mo}\delta_{np}$, $\delta_{mp}\delta_{no}$ and $\delta_{mn}\delta_{po}$ where one might be forbidden if the corresponding particles are not their own anti-particles. The case of two fundamental and two adjoint indices allows more basis elements given by

$$\left(T^a T^b \right)_{mn} \ , \quad \left(T^b T^a \right)_{mn} \ , \quad \delta^{ab}\delta_{mn} \ , \tag{A.16}$$

where all other possible combinations like $f^{abc}T_{mn}^c$ and $d^{abc}T_{mn}^c$ can be expressed in terms of the above via the (anti-)commutator relations Eq. (A.8).

Even more basis elements are possible in case of four adjoint indices

$$
\begin{gathered}
f^{abi}f^{cdi} \;, \quad f^{aci}f^{bdi} \;, \\
\delta^{ab}\delta^{cd} \;, \quad \delta^{ac}\delta^{bd} \;, \quad \delta^{ad}\delta^{bc} \;, \\
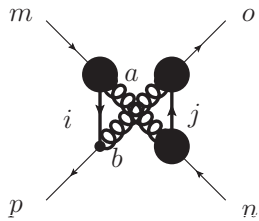f^{abe}d^{cde} \;, \quad f^{ace}d^{bde} \;, \quad f^{bce}d^{ade} \;,
\end{gathered}
\tag{A.17}
$$

where the $f^{adi}f^{bdi}$, the different permutations of $d^{abi}d^{cdi}$ and the remaining permutation of $f^{abe}d^{cde}$ can be expressed in terms of the above elements via the relations Eq. (A.9).

B. Calculations

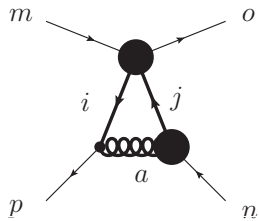In this appendix, some lengthy calculations, proofs and results are detailed.

B.1. Sources of Infrared Singularity

The simplest are the four "box-diagrams" where only 3-point functions - which have just one basis element for their color tensor structure - appear. These diagrams always contribute to a non-trivial combination of both tensor structures of the quark 4-point function as can be seen e.g. in
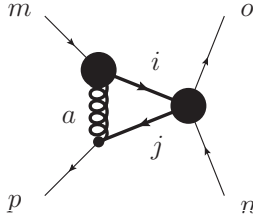
$$
\begin{aligned}
T^a_{mi} T^b_{io} T^a_{nj} T^b_{jp} \\
= \left(\frac{1}{2} \delta_{mj} \delta_{ni} - \frac{1}{2N} \delta_{mi} \delta_{nj} \right) \left(\frac{1}{2} \delta_{ip} \delta_{jo} - \frac{1}{2N} \delta_{io} \delta_{jp} \right) \\
= \left(\frac{N^2+1}{4N^2} \right) \delta_{mo} \delta_{np} + \left(-\frac{1}{2N} \right) \delta_{mp} \delta_{no} \ .
\end{aligned}
\tag{B.1}
$$

Consequently, contributions to $1/k^4$ cannot stem from these diagrams in either possible way. In the diagrams including the quark 4-point function, possible loop momentum independent contributions have already been identified in the previous section. To find possible loop integration dependent contributions it is useful, to calculate the contribution of a general tensor structure
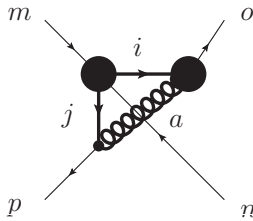
$$
\begin{aligned}
T^a_{ip} T^a_{nj} \left(F_1 \delta_{mo} \delta_{ji} + F_2 \delta_{mi} \delta_{jo} \right) \\
= \left(\frac{1}{2} \delta_{ij} \delta_{np} - \frac{1}{2N} \delta_{ip} \delta_{nj} \right) \left(F_1 \delta_{mo} \delta_{ji} + F_2 \delta_{mi} \delta_{jo} \right) \\
= F_1 \frac{N^2-1}{2N} \delta_{mo} \delta_{np} + F_2 \left(\frac{1}{2} \delta_{mo} \delta_{np} - \frac{1}{2N} \delta_{mp} \delta_{no} \right) \ ,
\end{aligned}
\tag{B.2}
$$

B. Calculations

$$T_{mi}^a T_{jp}^a \left(F_1 \delta_{no}\delta_{ij} + F_2\delta_{io}\delta_{nj}\right) \tag{B.3}$$

$$= \left(\frac{1}{2}\delta_{mp}\delta_{ij} - \frac{1}{2N}\delta_{mi}\delta_{jp}\right)\left(F_1\delta_{no}\delta_{ij} + F_2\delta_{io}\delta_{nj}\right)$$

$$= F_1\frac{N^2-1}{2N}\delta_{mp}\delta_{no} + F_2\left(\frac{1}{2}\delta_{mp}\delta_{no} - \frac{1}{2N}\delta_{mo}\delta_{np}\right) \ .$$
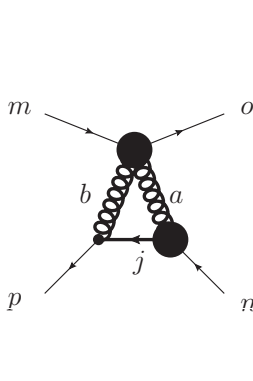
In the first diagram, the tensor structure $F_1 = -N/(N^2-1)F_2$ contributes only to $\delta_{mp}\delta_{no}$ and a possible singular contribution could arise from the loop integration. The same tensor structure contributes only to $\delta_{mo}\delta_{np}$ in the second diagram as required by symmetry. The third diagram containing the quark 4-point function can only contribute via loop integration. A general tensor structure yields

$$T_{io}^a T_{jp}^a \left(F_1 \delta_{mi}\delta_{nj} + F_2\delta_{mj}\delta_{ni}\right) \tag{B.4}$$

$$= \left(\frac{1}{2}\delta_{ip}\delta_{jo} - \frac{1}{2N}\delta_{io}\delta_{jp}\right)\left(F_1\delta_{mi}\delta_{nj} + F_2\delta_{mj}\delta_{ni}\right)$$

$$= F_1\left(\frac{1}{2}\delta_{mp}\delta_{no} - \frac{1}{2N}\delta_{mo}\delta_{np}\right) + F_2\left(\frac{1}{2}\delta_{mo}\delta_{np} - \frac{1}{2N}\delta_{mp}\delta_{no}\right) \ .$$
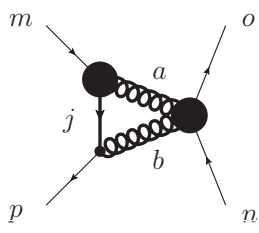
Therefore $F_1 = NF_2$ contributes to $\delta_{mp}\delta_{no}$, whereas $NF_1 = F_2$ contributes to $\delta_{mo}\delta_{np}$.

For diagrams containing the quark-gluon 4-point function one can do a similar analysis. The possible loop independent contributions have already been investigated in the previous section. A general tensor structure gives

$$T_{nj}^a T_{jp}^b \left(G_1 T_{mi}^a T_{io}^b + G_2 T_{mi}^b T_{io}^a\right) \tag{B.5}$$

$$= G_1\left(\frac{1}{2}\delta_{ni}\delta_{mj} - \frac{1}{2N}\delta_{nj}\delta_{mi}\right)\left(\frac{1}{2}\delta_{jo}\delta_{ip} - \frac{1}{2N}\delta_{io}\delta_{jp}\right)$$

$$+ G_2\left(\frac{1}{2}\delta_{no}\delta_{ij} - \frac{1}{2N}\delta_{nj}\delta_{io}\right)\left(\frac{1}{2}\delta_{ji}\delta_{mp} - \frac{1}{2N}\delta_{jp}\delta_{mi}\right)$$

$$= G_1\left(\frac{N^2+1}{4N^2}\delta_{mo}\delta_{np} - \frac{1}{2N}\delta_{mp}\delta_{no}\right)$$

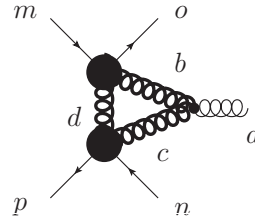$$+ G_2\left(\frac{1}{4N^2}\delta_{mo}\delta_{np} + \frac{N^2-2}{4N}\delta_{mp}\delta_{no}\right) \ ,$$

and similarly by interchanging $m \leftrightarrow n$

$$T_{mj}^a T_{jp}^b \left(G_1 T_{ni}^a T_{io}^b + G_2 T_{ni}^b T_{io}^a \right) \tag{B.6}$$

$$: \quad = G_1 \left(\frac{N^2+1}{4N^2}\delta_{mp}\delta_{no} - \frac{1}{2N}\delta_{mo}\delta_{np} \right)$$

$$+ G_2 \left(\frac{1}{4N^2}\delta_{mp}\delta_{no} + \frac{N^2-2}{4N}\delta_{mo}\delta_{np} \right) \ .$$

The tensor structure with $G_1(N^2+1) = -G_2$ contributes to $\delta_{mp}\delta_{no}$ in the first diagram and to $\delta_{mo}\delta_{np}$ in the second diagram. Similarly the tensor structure with $2G_1 = (N^2-2)G_2$ contributes to $\delta_{mo}\delta_{np}$ and $\delta_{mp}\delta_{no}$ respectively.

The last diagram contains a 5-point function, and it is first necessary to identify its possible tensor structures. Taking e.g. the diagram
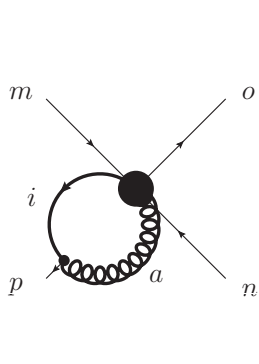
$$: \quad f^{abc}\Gamma_{mo}^{bd}\Gamma_{np}^{dc} \ , \tag{B.7}$$

contributing to its DSE gives at least the following tensor structures

$$\Gamma_{mnop}^a \propto c_1 T_{mp}^a \delta_{no} + c_2 T_{no}^a \delta_{mp} + c_3 T_{mo}^a \delta_{np} + c_4 T_{np}^a \delta_{mo} \tag{B.8}$$

$$+ i d_1 f^{abc} T_{mo}^b T_{np}^b + i d_2 f^{abc} T_{mp}^b T_{no}^b \ .$$

After a straightforward calculation one gets

$$\Gamma_{mnoi}^a T_{ip}^a \tag{B.9}$$

$$= c_1 \left(\frac{N^2-1}{2N} \right)\delta_{mp}\delta_{no}$$

$$+ \left(c_2 + d_2 \frac{N}{2} \right)\left(\frac{1}{2}\delta_{mo}\delta_{np} - \frac{1}{2N}\delta_{mp}\delta_{no} \right)$$

$$+ \left(c_3 - d_1 \frac{N}{2} \right)\left(\frac{1}{2}\delta_{mp}\delta_{no} - \frac{1}{2N}\delta_{mo}\delta_{np} \right)$$

$$+ c_4 \left(\frac{N^2-1}{2N} \right)\delta_{mo}\delta_{np} \ .$$

The tensor structures with coefficients c_1 and c_4 can contribute loop momentum independent $1/k^4$ singularities. Singular contributions arising from a loop integration can originate e.g. in the tensor structure $Nc_2 = c_3$, which contributes just to $\delta_{mp}\delta_{no}$ if all other c_i, d_i vanish.

Therefore, any of the possible loop momentum independent contributions to the singularity are proportional to the quadratic Casimir of the representation.

Additionally, it is interesting to investigate the tensor structures created by contributions

B. Calculations

from a skeleton expansion of the quark 4-point function. The first terms are given by [113]

$$\qquad\qquad\qquad\qquad\qquad\qquad\qquad\qquad\qquad\qquad (B.10)$$

where only one channel is shown. They contribute to the color structures

$$T^a_{mo}T^a_{np} = \frac{1}{2}\delta_{mp}\delta_{no} - \frac{1}{2N}\delta_{mo}\delta_{np} \ \text{ for } N = 2, \qquad\qquad (B.11)$$

and

$$T^a_{mj}T^b_{jo}T^a_{nl}T^b_{lp} = \left(\frac{1}{2}\delta_{ml}\delta_{nj} - \frac{1}{2N}\delta_{mj}\delta_{nl}\right)\left(\frac{1}{2}\delta_{jp}\delta_{ol} - \frac{1}{2N}\delta_{jo}\delta_{lp}\right) \qquad\qquad (B.12)$$

$$= \delta_{mp}\delta_{no}\frac{-1}{2N} + \delta_{mo}\delta_{np}\frac{N^2 + 1}{4N^2} \ .$$

This shows that a $1/k^4$ singularity in the $\delta_{mo}\delta_{np}$ tensor structure stemming from soft gluon divergences needs contributions from several diagrams in a skeleton expansion with non-trivial cancellations in $\delta_{mp}\delta_{no}$. In particular, the exchange of a single gluon cannot provide the correct color structure in the singularity.

B.2. Scalar QCD

Here some short calculations relevant for Ch. 4 are performed. In Eq. (4.12) the following calculation is useful

$$(p + t)_\mu P_{\mu\nu}(p - t)\Gamma_\nu(t, p) \qquad\qquad (B.13)$$

$$= (p + t)^\mu \left(\delta^{\mu\nu} - \frac{(p - t)^\mu(p - t)^\nu}{(p - t)^2}\right)$$

$$\times \left(A(t^2, p^2, z)(p + t)^\nu + B(t^2, p^2, z)\Big\{[p \cdot (p - t)]t^\mu - [t \cdot (p - t)p^\mu]\Big\}\right)$$

$$= A(t^2, p^2, z)\frac{(p + t)^2(p - t)^2 - [(p - t)^\mu(p + t)^\mu]^2}{(p - t)^2}$$

$$+ B(t^2, p^2, z)(p + t)^\mu\Big\{[p \cdot (p - t)]t^\mu - [t \cdot (p - t)p^\mu]\Big\}$$

$$= A(t^2, p^2, z)\frac{(p^2 + t^2 + 2p^\mu t^\mu)(p^2 + t^2 - 2p^\mu t^\mu) - (p^2 - t^2)^2}{(p - t)^2}$$

$$+ B(t^2, p^2, z)\Big\{[p^2 - p \cdot t][p \cdot t + t^2] - [t \cdot p - t^2][p^2 + p \cdot t]\Big\}$$

$$= A(t^2, p^2, z)\frac{(p^2 + t^2)^2 - 4(p^\mu t^\mu)^2 - (p^2 - t^2)^2}{(p - t)^2}$$

$$+ B(t^2, p^2, z)\Big\{2p^2t^2 - 2(t \cdot p)^2\Big\}$$

$$= 2 \left(2 \frac{A(t^2, p^2, z)}{(p-t)^2} + B(t^2, p^2, z) \right) \left(p^2 t^2 - (p^\mu t^\mu)^2 \right) \ .$$

In Eq. (4.38)

$$(p+q)^\mu \, P_{T,\mu\nu}(\vec{p} - \vec{q}, \omega_{m-n}) \, (q+p)^\nu \tag{B.14}$$

$$= (p+q)^\mu \left(\delta^{ij} - \frac{(p-q)^i \, (p-q)^j}{(\vec{p} - \vec{q})^2} \right) \delta^{i\mu} \delta^{j\nu} \, (q+p)^\nu$$

$$= \frac{(\vec{p} + \vec{q})^2 \, (\vec{p} - \vec{q})^2 - [(\vec{p} - \vec{q}) \cdot (\vec{p} + \vec{q})]^2}{(\vec{p} - \vec{q})^2}$$

$$= \frac{\left(\vec{p}^2 + 2\vec{p} \cdot \vec{q} + \vec{q}^2 \right) \left(\vec{p}^2 - 2\vec{p} \cdot \vec{q} + \vec{q}^2 \right) - \left(\vec{p}^2 - \vec{q}^2 \right)^2}{(\vec{p} - \vec{q})^2}$$

$$= 4 \frac{\vec{p}^2 \vec{q}^2 - (\vec{p} \cdot \vec{q})^2}{(\vec{p} - \vec{q})^2} \ ,$$

and

$$(p+q)^\mu \, P_{\mu\nu}(p-q)(p-q) \, (q+p)^\nu \tag{B.15}$$

$$= (p+q)^\mu \left(\delta^{\mu\nu} - \frac{(p-q)^\mu \, (p-q)^\nu}{(p-q)^2} \right) (q+p)^\nu$$

$$= 4 \frac{\left(\omega_m^2 + \vec{p}^2 \right) \left(\omega_n^2 + \vec{q}^2 \right) - \left(\omega_m \omega_n + \vec{p} \cdot \vec{q} \right)^2}{(\omega_m - \omega_n)^2 + (\vec{p} - \vec{q})^2} \ ,$$

have been used.

B.3. Chiral Symmetry and Axial Anomaly

This discussion of chiral symmetry and the axial anomaly in terms of the 't Hooft determinant Eq. (2.51) is performed for a general number of flavors N_f. The goal is to find the precise symmetry breaking induced by the 't Hooft term. For this it is useful to represent $U(N_f)_L \times U(N_f)_R$ in a (axial-)vector representation without double covering.

Different Chiral Symmetry Representations

Before starting the discussion it is crucial to recall how quarks in the chiral representation $q = (q_L \ q_R)^T$ transform under $U(N_f)_L \times U(N_f)_R$

$$q_{L,R} \to U_{L,R} q_{L,R} \ , \quad U_{L,R} \in U(N_f)_{L,R} \ . \tag{B.16}$$

The antiquark field is given by $\bar{q} = -iq^\dagger \gamma^4 = (q_R^\dagger \ q_L^\dagger)$ in this representation, whose components transform analogously as

$$q_{L,R}^\dagger \to q_{L,R}^\dagger U_{L,R}^\dagger \ , \quad U_{L,R} \in U(N_f)_{L,R} \ . \tag{B.17}$$

B. Calculations

The (axial-)vector representation, on the other hand, is defined on q via

$$q \to U_{V,A} q \ , \quad U_{V,A} \in U(N_f)_{V,A} \ , \tag{B.18a}$$

$$\bar{q} \to \bar{q} U_V^\dagger \ , \quad U_V \in U(N_f)_V \ , \tag{B.18b}$$

$$\bar{q} \to \bar{q} U_A \ , \quad U_A \in U(N_f)_A \ . \tag{B.18c}$$

A possible double covering has been ignored for the moment. This is also a symmetry of the kinetic term $\bar{q} \partial_\mu \gamma_\mu q$, if $U_A \gamma_\mu = \gamma_\mu U_A^\dagger$ for all γ_μ. This commutator rule is usually implemented with $U_A = \exp(i\alpha^a T^a \gamma^5)$, where T^a are the generators of $SU(N_f)$ and $\gamma^5 = \mathrm{diag}(-1,-1,1,1)$. With this definition one obtains the transformation of left and right handed spinors in the V, A representation

$$q_{L,R} \to U_V q_{L,R} \ , \quad U_V \in U(N_f)_V \ , \tag{B.19a}$$

$$q_L \to U_A^\dagger q_L \ , \quad U_A \in U(N_f)_A \ , \tag{B.19b}$$

$$q_R \to U_A q_R \ , \quad U_A \in U(N_f)_A \ , \tag{B.19c}$$

where $U_A = \exp(i\alpha^a T^a)$, without γ^5 in the exponential.

Up to this point everything is standard, but things get more involved if one wants to find a unique representation of every transformation $U_{L,R}$ in terms of V, A transformations. To understand the problem, note that any axial transformation fulfilling the relation $U_A = U_A^\dagger$ is doubly covered as it can also be represented by the vector transformation $U_V = U_A$.

As the axial anomaly affects only phase transformations, it will be sufficient to rewrite only the phase changes contained in $U(N_f)_L \times U(N_f)_R$ in a V, A representation. To do so, it is first necessary, to split these phase transformations off in the L, R language. Note that any unitary $N \times N$ matrix $UU^\dagger = 1$ fulfills

$$|\det(U)|^2 = 1 \ . \tag{B.20}$$

The determinant can therefore be written with a unique phase $\phi_U \in [0, 2\pi)$ as $\det(U) = \exp(i\phi_U)$. A unitary $N \times N$ matrix U can therefore be uniquely decomposed into a product of the matrix

$$\tilde{U} = U e^{-i\phi_U/N} \ \in SU(N) \ , \tag{B.21}$$

and a phase factor $\exp(i\phi_U/N)$ with $\phi_U \in [0, 2\pi)$. The phase factors can be represented by the factor group $U(1)/Z_N$ [1] where the cyclic group Z_N is given in terms of the Nth complex roots of unity. Finally, the chiral symmetry group can be rewritten as

$$U(N_f)_L \times U(N_f)_R = U(1)_L/Z_{N_f} \times SU(N_f)_L \times SU(N_f)_R \times U(1)_R/Z_{N_f} \ . \tag{B.22}$$

In the new representation, the quarks transform under the trivial modification of Eq. (B.16) as

$$q_{L,R} \to \hat{U}_{L,R} \tilde{U}_{L,R} q_{L,R} \ , \quad \hat{U}_{L,R} \in U(1)_{L,R}/Z_{N_f} \ , \quad \tilde{U}_{L,R} \in SU(N_f)_{L,R} \ . \tag{B.23}$$

---

[1]This factor group is obtained by identification of group elements that differ only by $z \in Z_N$

The next goal is to identify those vector and axial vector phases $\hat{U}_V$ and $\hat{U}_A$ that allow to represent Eq. (B.23) without double covering via

$$q_L \to \hat{U}_V \hat{U}_A^\dagger \tilde{U}_L q_L \ , \quad \tilde{U}_L \in SU(N_f)_L \ , \tag{B.24a}$$

$$q_R \to \hat{U}_V \hat{U}_A \tilde{U}_R q_R \ , \quad \tilde{U}_R \in SU(N_f)_L \ . \tag{B.24b}$$

Comparing Eq. (B.23) and Eq. (B.24) it is clear that only flavor independent phase transformations might be covered doubly by the latter. Therefore, the search for double covering can be restricted to $(\tilde{U}_L, \tilde{U}_R) \in Z_{N_f,L} \times Z_{N_f,R}$. As in the representation Eq. (B.23), any phase rotation $\hat{U}_V \in Z_{N_f}$ is already contained in $Z_{N_f,L} \times Z_{N_f,R}$, which leads to the restriction $\hat{U}_V \in U(1)_V/Z_{N_f}$. Finally, it is necessary to identify those axial transformations $\hat{U}_A$ that can be represented by combined transformations in $U(1)_V/Z_{N_f} \times Z_{N_f,L} \times Z_{N_f,R}$. With Eq. (B.24) this leads to the equations

$$\hat{U}_A^\dagger \to \hat{U}_V z_L \ , \quad \hat{U}_V \in U(1)_V/Z_{N_f} \ , \quad z_L \in Z_{N_f,L} \ , \tag{B.25a}$$

$$\hat{U}_A \to \hat{U}_V z_R \ , \quad \hat{U}_V \in U(1)_V/Z_{N_f} \ , \quad z_R \in Z_{N_f,R} \ . \tag{B.25b}$$

Combining both equations yields

$$\hat{U}_V^2 \, z_L^\dagger z_R^\dagger \in Z_{N_f} \ , \tag{B.26}$$

which has the solutions $\hat{U}_V \in Z_{2N_f}/Z_{N_f}$ represented by $\{1, e^{i\pi/N_f}\}$. Putting these solutions in Eq. (B.25) shows that any transformation $\hat{U}_A \in Z_{2N_f}$ can already be represented by combined transformations in $U(1)_V/Z_{N_f} \times Z_{N_f,L} \times Z_{N_f,R}$. Therefore, the final relation

$$U(N_f)_L \times U(N_f)_R = U(1)_V/Z_{N_f} \times SU(N_f)_L \times SU(N_f)_R \times U(1)_A/Z_{2N_f} \ , \tag{B.27}$$

is obtained.

Symmetries of 't Hooft Determinant

In the fermionic as well as bosonic representation the determinant is trivially invariant under $U(1)_V/Z_{N_f} \times SU(N_f)_L \times SU(N_f)_R$ but transforms as

$$\det \Sigma + \det \Sigma^\dagger \to (\hat{U}_A^\dagger)^{2N_f} \det \Sigma + \hat{U}_A^{2N_f} \det \Sigma^\dagger \ , \tag{B.28}$$

under $U(1)_A/Z_{2N_f}$. Invariance enforces $1 = (U_A^\dagger)^{2N_f} = U_A^{2N_f}$ which is only fulfilled by the trivial element of $U(1)_A/Z_{2N_f}$.

Additionally, it is interesting to investigate the symmetries of higher powers of the 't Hooft determinant. A general power $(2n + m)$, $n \in \mathbb{N}_0$, $m \in \{0, 1\}$ of the determinant transforms as

$$(\det \Sigma + \det \Sigma^\dagger)^{2n+m} \tag{B.29}$$
$$\to \sum_{j=0}^{2n+m} \binom{2n+m}{j} (U_A^\dagger)^{2N_f j} U_A^{2N_f(2n+m-j)} \det \Sigma^j \det \left(\Sigma^\dagger\right)^{2n+m-j} \ .$$

B. Calculations

This results in the invariance conditions

$$1 = (U_A^\dagger)^{2N_f j} U_A^{2N_f(2n+m-j)} = U_A^{2N_f(2(n-j)+m)}, \quad j \in \{0, \ldots, 2n+m\} . \tag{B.30}$$

For $m = 1$ one gets by setting $j = n$

$$1 = U_A^{2N_f} , \tag{B.31}$$

which is nothing but the statement that all odd powers of the determinant break $U(1)_A/Z_{2N_f}$ completely. In case of $m = 0$ the above condition results for any j at most in

$$1 = U_A^{4N_f} . \tag{B.32}$$

Therefore, all even powers of the determinant respect an additional Z_2 symmetry contained in $U(1)_A/Z_{2N_f}$.

B.4. Chiral Invariants

The effective potential of the quark-meson model can be expanded in chiral invariants shown in Eq. (2.72) and the 't Hooft determinant defined in Eq. (2.73). To obtain the mesonic screening masses, its second derivatives with respect to the full mesonic field Σ have to be calculated. In general this will require an inversion of the mapping from field components to chiral invariants. In case of a Taylor expansion of the effective potential around its scale-dependent minimum App. C.2.2, this inversion has to be differentiable. Furthermore, the set of values taken by the chiral invariants is usually very complicated. This poses problems, when approximating the mesonic potential by a discrete set of grid points, which are usually defined on a hypercubic lattice App. C.2.2. It is therefore desirable to map the domain of the chiral invariants smoothly to a simpler hypercubic domain.

B.4.1. Two Flavors

The chiral invariant ρ_1 and 't Hooft determinant ξ are obtained from the two fields σ^0 and σ^3 as

$$\rho_1 = \frac{(\sigma^0)^2 + (\sigma^3)^2}{2} , \tag{B.33a}$$

$$\xi \quad \frac{(\sigma^0)^2 - (\sigma^3)^2}{2} . \tag{B.33b}$$

Obviously this cannot be inverted uniquely as any quadrant in the (σ^0, σ^3) plane is mapped to the same values. Restricted to the first quadrant $\sigma^0, \sigma^3 \geq 0$ the equations

$$\rho_1 = \frac{1}{2}\left((\sigma^0)^2 + (\sigma^3)^2\right) \ \wedge \ \xi = \frac{1}{2}\left((\sigma^0)^2 - (\sigma^3)^2\right) , \tag{B.34}$$

have the unique solutions

$$\sigma^0(\rho_1, \xi) = \sqrt{\rho_1 + \xi} \, , \tag{B.35a}$$

$$\sigma^3(\rho_1, \xi) = \sqrt{\rho_1 - \xi} \, . \tag{B.35b}$$

This is differentiable as long as $\rho_1 > |\xi|$, which corresponds to $\sigma^0, \sigma^3 > 0$. Therefore, non-vanishing condensates are required, when applying the two dimensional Taylor technique with scale-dependent minimum App. C.2.2.A similar problem appears already in the one dimensional Taylor expansion of the $O(4)$ quark-meson model with scale-dependent minimum. In the latter case, the inversion of $2\rho_1 = \sigma^2$ is not differentiable at $\sigma = 0$ which can cause numerical problems. If the expansion point approaches $\sigma \to 0$ a change to the fixed expansion point $\sigma = 0$ is necessary, which avoids singular derivatives.
For the grid technique App. C.2.2, the form of the domain of the chiral invariants is relevant. From Eq. (B.33) it is clear, that the domain is not rectangular. Therefore, a grid is defined on the new coordinates

$$x(\rho_1, \xi) = \rho_1 + \xi \, , \tag{B.36a}$$

$$y(\rho_1, \xi) = \rho_1 - \xi \, . \tag{B.36b}$$

This linear map is smooth and derivatives of the effective potential with respect to ρ_1, ξ can be obtained from $U(x, y)$ by applying the chain rule.

B.4.2. $2 + 1$ Flavors

The chiral invariant ρ_1 and $\tilde{\rho}_2$ are obtained from the two fields σ_x and σ_y as

$$\rho_1 = \frac{\sigma_x^2 + \sigma_y^2}{2} \, , \tag{B.37a}$$

$$\tilde{\rho}_2 = \frac{\left(\sigma_x^2 - 2\sigma_y^2\right)^2}{24} \, . \tag{B.37b}$$

Again this cannot be inverted uniquely as any quadrant in the (σ_x, σ_y) plane is mapped to the same values. But even when restricting to the first quadrant $\sigma_x, \sigma_y \geq 0$ the equations

$$\rho_1 = \frac{1}{2}\left(\sigma_x^2 + \sigma_y^2\right) \, \wedge \, \tilde{\rho}_2 = \frac{1}{24}\left(\sigma_x^2 - 2\sigma_y^2\right)^2 \, , \tag{B.38}$$

have the solutions

$$\sigma_x(\rho_1, \tilde{\rho}_2) = \sqrt{\frac{2}{3}\left(2\rho_1 \mp \sqrt{6\tilde{\rho}_2}\right)} \, , \tag{B.39a}$$

$$\sigma_y(\rho_1, \tilde{\rho}_2) = \sqrt{\frac{2}{3}\left(\rho_1 \pm \sqrt{6\tilde{\rho}_2}\right)} \, . \tag{B.39b}$$

As $\rho_1, \tilde{\rho}_2 > 0$ the upper sign implies $\sigma_x \leq \sqrt{2}\sigma_y$ whereas the lower sign corresponds to $\sigma_x \geq \sqrt{2}\sigma_y$. Taking into account that the strange quark mass is larger than the light quark mass the only admissible solution is given by the upper sign. Similar to the previous case, the Taylor expansion App. C.2.2 with scale dependent minimum runs into numerical problems

whenever σ_x or σ_y vanishes.

Before applying the grid technique App. C.2.2, it is again necessary to map the complicated domain of ρ_1 and $\tilde{\rho}_2$ smoothly to a rectangular domain. From the restriction $\sigma_x \leq \sqrt{2}\sigma_y$ one obtains a rectangular grid with the coordinates

$$x = \sigma_x^2 \ , \tag{B.40a}$$

$$y = 2\sigma_y^2 - \sigma_x^2 \ . \tag{B.40b}$$

In terms of the chiral invariants, the grid coordinates become

$$x(\rho_1, \tilde{\rho}_2) = \frac{2}{3}\left(2\rho_1 - \sqrt{6\tilde{\rho}_2}\right) \ , \tag{B.41a}$$

$$y(\rho_1, \tilde{\rho}_2) = \sqrt{24\tilde{\rho}_2} \ . \tag{B.41b}$$

One disadvantage of these coordinates is, that they are not smooth at $\tilde{\rho}_2 = 0$. This corresponds to the limit of degenerate strange and light quark masses at $2\langle\sigma_y\rangle^2 = \langle\sigma_x\rangle^2$. On the other hand, these coordinates are smooth in the light chiral limit $\sigma_x = 0$ as long as $\sigma_y > 0$. In order to handle the limit $2\sigma_y^2 = \sigma_x^2$ it is necessary to expand the potential in a set of variables $\tilde{x}, \tilde{y}$ which are differentiable as functions of ρ_1 and $\tilde{\rho}_2$ at $\tilde{\rho}_2 = 0$. The main problem in the previous case is the appearance of the square root of the second chiral invariant. This can be avoided if $\tilde{x}, \tilde{y}$ are taken quartic in the mesonic field. In order to map the cone $2\sigma_y^2 \geq \sigma_x^2$, $\sigma_y, \sigma_x \geq 0$ to a rectangle, the following variables are taken

$$\tilde{x}(\rho_1, \tilde{\rho}_2) = \rho_1^2 - \frac{3}{2}\tilde{\rho}_2 \ , \tag{B.42a}$$

$$\tilde{y}(\rho_1, \tilde{\rho}_2) = \tilde{\rho}_2 \ . \tag{B.42b}$$

This is everywhere smooth and the line $2\sigma_y^2 = \sigma_x^2$ corresponds to $\tilde{y} = 0$, whereas the light chiral limit $\sigma_x = 0$ is represented by $\tilde{x} = 0$.

B.5. $2 + 1$ Flavor Meson Masses

This section gives explicit expression for the mesonic screening masses as obtained from a potential of the form

$$U(\Sigma) = \tilde{U}(\rho_1, \tilde{\rho}_2) - c\xi - c_x\sigma_x - c_y\sigma_y \ , \tag{B.43}$$

$$\tilde{U}(\rho_1, \tilde{\rho}_2) = a_{10}\rho_1 + a_{01}\tilde{\rho}_2 + \frac{a_{20}}{2}\rho_1^2 + a_{11}\rho_1\tilde{\rho}_2 + \frac{a_{02}}{2}\tilde{\rho}_2^2 \ .$$

The squared masses are obtained by diagonalizing the Hessian matrix of the effective potential evaluated at its minimum. In a mean-field treatment there is an additional contribution to the effective potential from the quarks which also modifies the Hessian [213]. Here, only the contribution from the mesonic part of the effective potential will be shown.

The Hessian splits into a (pseudo)scalar (9×9)-mass matrix M_s^2 and M_{ps}^2

$$\nabla_\Sigma^2 U_k = \begin{pmatrix} M_s^2 & 0 \\ 0 & M_{ps}^2 \end{pmatrix} \ . \tag{B.44}$$

Explicitly, the non-vanishing entries defining the nine scalar meson masses read

$$(M_s)_{11} = \frac{1}{54}\Big(54a_{10} + 12a_{01}\sigma_x^2 + 36a_{20}\sigma_x^2 + 12a_{11}\sigma_x^4 + a_{02}\sigma_x^6 - 24\sqrt{2}a_{01}\sigma_x\sigma_y \qquad \text{(B.45a)}$$
$$+36\sqrt{2}a_{20}\sigma_x\sigma_y - 6\sqrt{2}a_{11}\sigma_x^3\sigma_y - 2\sqrt{2}a_{02}\sigma_x^5\sigma_y + 24a_{01}\sigma_y^2 + 18a_{20}\sigma_y^2$$
$$-36a_{11}\sigma_x^2\sigma_y^2 - 2a_{02}\sigma_x^4\sigma_y^2 + 12\sqrt{2}a_{11}\sigma_x\sigma_y^3 + 8\sqrt{2}a_{02}\sigma_x^3\sigma_y^3 + 24a_{11}\sigma_y^4$$
$$-4a_{02}\sigma_x^2\sigma_y^4 - 8\sqrt{2}a_{02}\sigma_x\sigma_y^5 + 8a_{02}\sigma_y^6 - 18c(2\sigma_x + \sqrt{2}\sigma_y) \Big) \,,$$

$$(M_s)_{19} = \frac{1}{108}\Big(36\sqrt{2}a_{20}\sigma_x^2 + 12\sqrt{2}a_{11}\sigma_x^4 + \sqrt{2}a_{02}\sigma_x^6 + 18c(\sqrt{2}\sigma_x - 2\sigma_y) \qquad \text{(B.45b)}$$
$$-36a_{20}\sigma_x\sigma_y + 6a_{11}\sigma_x^3\sigma_y + 2a_{02}\sigma_x^5\sigma_y - 36\sqrt{2}a_{20}\sigma_y^2 - 8\sqrt{2}a_{02}\sigma_x^4\sigma_y^2$$
$$-12a_{11}\sigma_x\sigma_y^3 - 8a_{02}\sigma_x^3\sigma_y^3 - 48\sqrt{2}a_{11}\sigma_y^4 + 20\sqrt{2}a_{02}\sigma_x^2\sigma_y^4 + 8a_{02}\sigma_x\sigma_y^5$$
$$-16\sqrt{2}a_{02}\sigma_y^6 + 6a_{01}(5\sqrt{2}\sigma_x^2 + 4\sigma_x\sigma_y - 14\sqrt{2}\sigma_y^2) \Big) \,,$$

$$(M_s)_{99} = \frac{1}{108}\Big(108a_{10} + 72c\sigma_x - 6a_{01}\sigma_x^2 + 36a_{20}\sigma_x^2 + 12a_{11}\sigma_x^4 + a_{02}\sigma_x^6 - 18\sqrt{2}c\sigma_y \quad \text{(B.45c)}$$
$$+48\sqrt{2}a_{01}\sigma_x\sigma_y - 72\sqrt{2}a_{20}\sigma_x\sigma_y + 12\sqrt{2}a_{11}\sigma_x^3\sigma_y + 4\sqrt{2}a_{02}\sigma_x^5\sigma_y$$
$$+132a_{01}\sigma_y^2 + 72a_{20}\sigma_y^2 - 72a_{11}\sigma_x^2\sigma_y^2 + 4a_{02}\sigma_x^4\sigma_y^2 - 24\sqrt{2}a_{11}\sigma_x\sigma_y^3$$
$$-16\sqrt{2}a_{02}\sigma_x^3\sigma_y^3 + 96a_{11}\sigma_y^4 - 28a_{02}\sigma_x^2\sigma_y^4 + 16\sqrt{2}a_{02}\sigma_x\sigma_y^5 + 32a_{02}\sigma_y^6 \Big) \,,$$

$$(M_s)_{ii} = a_{10} + \frac{1}{6}(7a_{01}\sigma_x^2) + \frac{1}{\sqrt{2}}(c\sigma_y) - \frac{1}{3}(a_{01}\sigma_y^2) \,, \quad i = 2,3,4 \,, \qquad \text{(B.45d)}$$

$$(M_s)_{ii} = \frac{1}{6}\Big(6a_{10} + 3c\sigma_x + a_{01}(\sigma_x^2 + 3\sqrt{2}\sigma_x\sigma_y + 4\sigma_y^2) \Big) \,, \quad i = 5,\ldots,8 \qquad \text{(B.45e)}$$

Correspondingly the pseudoscalar masses are obtained from

$$(M_{ps})_{11} = a_{10} + \frac{1}{3}c\Big(2\sigma_x + \sqrt{2}\sigma_y \Big) \,, \qquad \text{(B.46a)}$$

$$(M_{ps})_{19} = \frac{1}{6}\Big(c(-\sqrt{2}\sigma_x + 2\sigma_y) + \sqrt{2}a_{01}(\sigma_x^2 - 2\sigma_y^2) \Big) \,, \qquad \text{(B.46b)}$$

$$(M_{ps})_{99} = \frac{1}{6}\Big(6a_{10} - 4c\sigma_x - a_{01}\sigma_x^2 + \sqrt{2}c\sigma_y + 2a_{01}\sigma_y^2 \Big) \,, \qquad \text{(B.46c)}$$

$$(M_{ps})_{ii} = \frac{1}{6}\Big(6a_{10} - 3\sqrt{2}c\sigma_y + a_{01}(\sigma_x^2 - 2\sigma_y^2) \Big) \,, \quad i = 2,3,4 \,, \qquad \text{(B.46d)}$$

$$(M_{ps})_{ii} = \frac{1}{6}\Big(6a_{10} - 3c\sigma_x + a_{01}(\sigma_x^2 - 3\sqrt{2}\sigma_x\sigma_y + 4\sigma_y^2) \Big) \,, \quad i = 5,\ldots,8 \,. \qquad \text{(B.46e)}$$

C. Numerical Implementation

In this appendix, the numerical methods employed in the solution of the Dyson-Schwinger equation for the scalar propagator at vanishing (Eq. (4.16)) and finite temperature (Eq. (4.40)) as well as the mean-field approximation (Eq. (5.6)) and flow equation (Eq. (5.9)) for the effective potential in two and $2 + 1$ flavor are described.

C.1. Scalar Propagator DSE

The same methods introduced and discussed in detail in ref. [264] are used for the numerical solution of the scalar propagator DSE. The momentum integral in Eq. (4.16) is approximated by a logarithmically remapped Gauss-Legendre quadrature rule (see e.g. [244]). For the angular integration, a Gauss-Chebyshev quadrature is employed [265], and the result is stored since it does not depend on the dressing function Z_S. With this approximation, only a finite number of values of the dressing function Z_S at the momentum quadrature nodes are needed. The integral equation becomes therefore a non-linear equation on $\mathbb{R}^n$, where n is the number of momentum quadrature nodes. The approximate equation is solved by fixed point iteration, where in every step the renormalization conditions Eq. (4.26) or Eq. (4.29) are enforced.

In the finite temperature equation Eq. (4.40), the $\vec{p}^2$ integral is approximated as in the vacuum case. Additionally, it is necessary to sum over the Matsubara modes. This sum is performed explicitly only up to a fixed number, and the remaining Matsubara sum up to the cutoff $\sqrt{\Lambda_c^2 - \vec{p}^2}$ is approximated by a Gauss-Legendre integration. This is justified by the fact, that the Matsubara sum resembles a Riemann sum. The angular integrand is singular at the boundaries, and a double exponential quadrature (see e.g. [244]) is used. The renormalization constants, of the corresponding vacuum solution are used and the equation is solved iteratively, where the result of the angular integration is stored again. Note, that storing the result of the angular integration requires several GB of memory. Therefore, a parallelized code has been used, where each node stores only the relevant result of this angular integration.

C.2. Mesonic Effective Potential

The mesonic effective potential is calculated with three different methods, whose numerical implementation is specified in this section.

C.2.1. Mean-Field Calculations

For the calculation of the mean-field potential, it is necessary to evaluate the integral in Eq. (5.6). Furthermore, the evaluation of the mesonic masses, requires its derivative with respect to the mesonic field which has to be integrated as well. The integral is split into two integrations over $[0, \Lambda]$ and $[\Lambda, \infty)$ with varying Λ. The second integration is mapped to

C. Numerical Implementation

[0, 1/Λ] by replacing $y \to 1/y$. These two integrals are performed with the doubly-adaptive *CQUAD* routine of the GNU Scientific Library (GSL). Additionally, it is necessary to minimize the obtained potential. After a coarse search for the valley containing the minimum with a grid, the minimization routines of the GSL are used.

C.2.2. Wetterich RG in Leading Order Derivative Expansion

The Wetterich equation for the effective potential Eq. (5.9) is a non-linear partial differential equation. By specifying a finite dimensional approximation for the effective potential, this is turned into a system of ordinary differential equations for the expansion coefficients, which can be solved with standard Runge-Kutta methods. Two different sets of basis elements have been used in this work.

Taylor Expansion in Invariants

All the physically relevant information is contained in the effective potential close to its minimum. Therefore a Taylor expansion in general invariants $\rho \equiv (\rho_1, \ldots, \rho_n)$ is performed around the scale-dependent minimum $\rho_0(k)$

$$U_k(\Sigma) = \tilde{U}_k(\rho(\Sigma)) - c_i \sigma^i , \tag{C.1}$$

$$\tilde{U}_k(\rho) = \sum_{\alpha \in \mathbb{N}_0^n}^{|\alpha| \leq N} \frac{a_\alpha(k)}{\alpha!} (\rho - \rho_0(k))^\alpha .$$

Here, the c^i are explicit breaking terms and $\alpha = (\alpha_1, \ldots, \alpha_n)$ is a multi-index with

$$|\alpha| = \sum_{i=1}^n \alpha_i , \qquad \alpha! = \prod_{i=1}^n (\alpha_i!) , \qquad \rho^\alpha = \rho_1^{\alpha_1} \cdots \rho_n^{\alpha_n} . \tag{C.2a}$$

By plugging Eq. (C.1) in the flow equation, one can compare coefficients to obtain the flow of the expansion coefficients and the minimum.
The condition, that $\rho_0(k)$ is the minimum is implemented via

$$0 = \nabla_\rho U_k(\rho)\big|_{\rho=\rho_0(k)} \tag{C.3}$$
$$= a_1(k) - c_i \nabla_\rho \sigma^i(\rho_0(k)) .$$

This relation allows to express the linear expansion coefficients

$$a_1(k) = (a_{10\cdots0},\ a_{010\cdots0},\ \ldots,\ a_{0\cdots01}) , \tag{C.4}$$

in terms of the scale-dependent minimum $\rho_0(k)$, where it is crucial that the $\sigma^i(\rho)$ are differentiable at the minimum. Note, that Eq. (C.3) is only a necessary condition, if the minimum $\rho_0(k)$ is not at the boundary of the domain of ρ. Furthermore, in case of a first order transition it can happen, that the minimum turns into a saddle point or maximum.
In case of the two flavor calculations, the vector $\rho = (\rho_1, \xi)$ as specified in App. B.4.1 has been taken, whereas $\rho = (\rho_1, \tilde{\rho}_2)$ from App. B.4.2 has been taken for the $2+1$ flavor calculations.

In the latter case, also the 't Hooft term is taken as an explicit breaking term, which modifies the condition Eq. (C.3).

Effective Potentials on Multidimensional Grids

Another possibility of approximating the effective potential is to put it on a discrete lattice. Again, the effective potential is taken as a function of the chiral invariants $\rho \equiv (\rho_1, \ldots, \rho_n)$

$$U_k(\Sigma) = \tilde{U}_k(\rho(\Sigma)) - c_i \sigma^i \ , \tag{C.5}$$

where $\tilde{U}_k(\rho)$ represents a discrete approximation of the potential. In general, the domain in the chiral invariants ρ is very complicated and does not allow a cubic lattice - as e.g. in the $2 + 1$ flavor case App. B.4.2.

Therefore, a smooth map from a hypercube K to the domain of the chiral invariants Ω_ρ has to be defined

$$F : K \to \Omega_\rho \ , \tag{C.6}$$

which allows to approximate the effective potential $\hat{U}_k$ by a lattice on the hypercube K. The derivatives of $\hat{U}_k$ are calculated with multi-dimensional clamped cubic splines, where the value of the derivative at the boundary is obtained from forward and backward finite differences respectively.

The derivatives of $\tilde{U}_k(\rho)$ can be obtained from the relation $\tilde{U}_k(\rho) = \hat{U}(F^{-1}(\rho))$ via the chain rule

$$\nabla_\rho \tilde{U} = \left(\nabla_i \hat{U} \right) \left(\nabla_\rho F_i^{-1} \right) \tag{C.7a}$$

$$\nabla_\rho^2 \tilde{U} = \left(\nabla_\rho^T F_i^{-1} \right) \left(\nabla_{ij}^2 \hat{U} \right) \left(\nabla_\rho F_j^{-1} \right) + \left(\nabla_i \hat{U} \right) \left(\nabla_\rho^2 F_i^{-1} \right) \ , \tag{C.7b}$$

where the gradient is by default a column vector. From this is it obvious, that F^{-1} has to be at least two times differentiable on all grid points.

In contrast to the Taylor expansion, it is necessary to diagonalize the Hessian of $U_k(\Sigma)$ also away from its minimum. This can be done by invoking the chain rule once more

$$\nabla_\Sigma U = \left(\nabla_{\rho_i} \tilde{U} \right) \left(\nabla_\Sigma \rho_i \right) \tag{C.8a}$$

$$\nabla_\Sigma^2 U = \left(\nabla_\Sigma^T \rho_i \right) \left(\nabla_{\rho_i \rho_j}^2 \tilde{U} \right) \left(\nabla_\Sigma \rho_j \right) + \left(\nabla_{\rho_i} \tilde{U} \right) \left(\nabla_\Sigma^2 \rho_i \right) \ . \tag{C.8b}$$

Bibliography

[1] W. J. Marciano and H. Pagels, Phys. Rept. **36**, 137 (1978).

[2] S. Weinberg, *The Quantum theory of fields. Vol. 1: Foundations* (Cambridge University Press, 1995),

[3] S. Weinberg, *The quantum theory of fields. Vol. 2: Modern applications* (Cambridge University Press, 1996),

[4] D. Gross and F. Wilczek, Phys.Rev.Lett. **30**, 1343 (1973).

[5] H. D. Politzer, Phys.Rev.Lett. **30**, 1346 (1973).

[6] M. E. Peskin and D. V. Schroeder, *An Introduction to quantum field theory* (Perseus Books, 1995), ISBN-9780201503975 ETC.;

[7] J. Greensite, Lect.Notes Phys. **821**, 1 (2011).

[8] J. Beringer et al. (Particle Data Group), Phys.Rev. **D86**, 010001 (2012).

[9] Y. Nambu, Phys.Rev.Lett. **4**, 380 (1960).

[10] J. Goldstone, Nuovo Cim. **19**, 154 (1961).

[11] J. Goldstone, A. Salam, and S. Weinberg, Phys.Rev. **127**, 965 (1962).

[12] M. Stephanov, PoS **LAT2006**, 024 (2006).

[13] R. Streater and A. Wightman, *PCT, spin and statistics, and all that* (Princeton University Press, 2000),

[14] R. Haag, *Local quantum physics: Fields, particles, algebras* (Springer, 1992).

[15] J. Glimm and A. M. Jaffe, *Quantum Physics. A Functional Integral Point of View* (Springer-Verlag, 1987),

[16] K. Osterwalder and R. Schrader, Commun.Math.Phys. **31**, 83 (1973).

[17] K. Osterwalder and R. Schrader, Commun.Math.Phys. **42**, 281 (1975).

[18] M. Creutz, Cambridge University Press (1984).

[19] H. Rothe, *Lattice gauge theories: An Introduction*, vol. 43 (World Sci.Lect.Notes Phys., 1992),

[20] I. Montvay and G. Munster, *Quantum fields on a lattice* (Cambridge University Press, 1994),

BIBLIOGRAPHY

[21] J. Smit, *Introduction to quantum fields on a lattice: A robust mate*, vol. 15 (Cambridge Lect.Notes Phys., 2002),

[22] T. DeGrand and C. E. Detar, *Lattice methods for quantum chromodynamics* (World Scientific, 2006), INSPIRE-739893;

[23] C. Gattringer and C. B. Lang, *Quantum chromodynamics on the lattice*, vol. 788 (Springer, 2010),

[24] F. J. Dyson, Phys. Rev. **75**, 1736 (1949).

[25] J. S. Schwinger, Proc. Nat. Acad. Sci. **37**, 452 (1951a).

[26] J. S. Schwinger, Proc. Nat. Acad. Sci. **37**, 455 (1951b).

[27] C. D. Roberts and A. G. Williams, Prog.Part.Nucl.Phys. **33**, 477 (1994).

[28] R. Alkofer and L. von Smekal, Phys.Rept. **353**, 281 (2001).

[29] C. S. Fischer, J.Phys. **G32**, R253 (2006).

[30] K. G. Wilson and J. B. Kogut, Phys. Rept. **12**, 75 (1974).

[31] F. J. Wegner and A. Houghton, Phys.Rev. **A8**, 401 (1973).

[32] J. Nicoll and T. Chang, Phys.Lett. **A62**, 287 (1977).

[33] J. Polchinski, Nucl.Phys. **B231**, 269 (1984).

[34] B. J. Warr, Annals Phys. **183**, 1 (1988).

[35] T. Hurd, Commun.Math.Phys. **124**, 153 (1989).

[36] G. Keller, C. Kopper, and M. Salmhofer, Helv.Phys.Acta **65**, 32 (1992).

[37] C. Wetterich, Phys. Lett. **B301**, 90 (1993).

[38] M. Bonini, M. D'Attanasio, and G. Marchesini, Nucl.Phys. **B409**, 441 (1993).

[39] U. Ellwanger, Z.Phys. **C62**, 503 (1994).

[40] T. R. Morris, Int.J.Mod.Phys. **A9**, 2411 (1994).

[41] S.-B. Liao, Phys. Rev. **D53**, 2020 (1996).

[42] M. Fisher, Rev.Mod.Phys. **70**, 653 (1998).

[43] K. Aoki, Int.J.Mod.Phys. **B14**, 1249 (2000).

[44] C. Bagnuls and C. Bervillier, Phys.Rept. **348**, 91 (2001).

[45] J. Berges, N. Tetradis, and C. Wetterich, Phys. Rept. **363**, 223 (2002).

[46] J. Polonyi, Central Eur.J.Phys. **1**, 1 (2003).

[47] M. Salmhofer and C. Honerkamp, Prog.Theor.Phys. **105**, 1 (2001).

[48] B. Delamotte, D. Mouhanna, and M. Tissier, Phys.Rev. **B69**, 134413 (2004).

[49] J. M. Pawlowski, Annals Phys. **322**, 2831 (2007).

[50] H. Gies, arXiv:0611146 [hep-ph] (2006).

[51] B. Delamotte, arXiv:0702365 [cond-mat] (2007).

[52] O. J. Rosten, Phys.Rept. **511**, 177 (2012).

[53] T. Appelquist and J. Carazzone, Phys. Rev. **D11**, 2856 (1975).

[54] B. Friman, C. Hohne, S. Knoll, Jornand Leupold, J. Randrup, et al., Lect.Notes Phys. **814**, 1 (2011).

[55] D. F. Litim, Phys. Lett. **B486**, 92 (2000).

[56] D. F. Litim, Phys. Rev. **D64**, 105007 (2001).

[57] J.-P. Blaizot, R. Mendez-Galain, and N. Wschebor, Phys.Rev. **E74**, 051116 (2006a).

[58] J.-P. Blaizot, R. Mendez Galain, and N. Wschebor, Phys.Lett. **B632**, 571 (2006b).

[59] J. Berges, Nucl.Phys. **A699**, 847 (2002).

[60] M. Nakahara, *Geometry, topology and physics* (Institute of Physics Publishing, 1990),

[61] R. Rivers, *Path Integral Methods In Quantum Field Theory* (Cambridge University Press, 1987),

[62] N. Vandersickel, D. Zwanziger, and D. Zwanziger, arXiv:1202.1491 [hep-th] (2012).

[63] V. Gribov, Nucl.Phys. **B139**, 1 (1978).

[64] D. Zwanziger, Nucl.Phys. **B209**, 336 (1982).

[65] G. Dell'Antonio and D. Zwanziger, Commun.Math.Phys. **138**, 291 (1991).

[66] M. Semenov-Tyan-Shanskii and V. Franke, Zap. Nauchn. Sem. LOMI **120**, 159 (1982).

[67] P. van Baal, Nucl.Phys. **B369**, 259 (1992).

[68] A. Slavnov, Theor.Math.Phys. **10**, 99 (1972).

[69] J. Taylor, Nucl.Phys. **B33**, 436 (1971).

[70] J. C. Ward, Phys.Rev. **78**, 182 (1950).

[71] Y. Takahashi, Nuovo Cim. **6**, 371 (1957).

[72] T. Brauner, Symmetry **2**, 609 (2010).

[73] Wikimedia Commons (http://commons.wikimedia.org/wiki/Main_Page) (2012).

BIBLIOGRAPHY

[74] A. V. Smilga, *Lectures on quantum chromodynamics* (World Scientific, 2001), INSPIRE-572018;

[75] S. Weinberg, Phys.Rev. **D11**, 3583 (1975).

[76] J. Bell and R. Jackiw, Nuovo Cim. **A60**, 47 (1969).

[77] S. L. Adler, Phys.Rev. **177**, 2426 (1969).

[78] S. L. Adler and W. A. Bardeen, Phys.Rev. **182**, 1517 (1969).

[79] K. Fujikawa, Phys. Rev. Lett. **42**, 1195 (1979).

[80] E. Witten, Nucl. Phys. **B156**, 269 (1979).

[81] G. Veneziano, Nucl. Phys. **B159**, 213 (1979).

[82] N. Christ, C. Dawson, T. Izubuchi, C. Jung, Q. Liu, et al., Phys.Rev.Lett. **105**, 241601 (2010).

[83] R. Alkofer, C. S. Fischer, and R. Williams, Eur.Phys.J. **A38**, 53 (2008).

[84] G. 't Hooft, Phys. Rev. Lett. **37**, 8 (1976).

[85] G. 't Hooft, Phys. Rept. **142**, 357 (1986).

[86] V. Baluni, Phys.Rev. **D19**, 2227 (1979).

[87] R. Crewther, P. Di Vecchia, G. Veneziano, and E. Witten, Phys.Lett. **B88**, 123 (1979).

[88] S. Elitzur, Phys.Rev. **D12**, 3978 (1975).

[89] C. Becchi, A. Rouet, and R. Stora, Commun.Math.Phys. **42**, 127 (1975).

[90] I. V. Tyutin, Lebedev Institute Preprint **39** (1985).

[91] T. Kugo and I. Ojima, Prog.Theor.Phys.Suppl. **66**, 1 (1979).

[92] N. Nakanishi and I. Ojima, World Sci.Lect.Notes Phys. **27**, 1 (1990).

[93] K. Holland and U.-J. Wiese, arXiv:0011193 [hep-ph] (2000).

[94] J. Greensite, Prog.Part.Nucl.Phys. **51**, 1 (2003).

[95] J. Braun, L. M. Haas, F. Marhauser, and J. M. Pawlowski, Phys.Rev.Lett. **106**, 022002 (2011).

[96] A. M. Polyakov, Phys.Lett. **B59**, 82 (1975).

[97] A. M. Polyakov, Phys.Lett. **B72**, 477 (1978).

[98] K. G. Wilson, Phys.Rev. **D10**, 2445 (1974).

[99] G. S. Bali, H. Neff, T. Duessel, T. Lippert, and K. Schilling (SESAM Collaboration), Phys.Rev. **D71**, 114513 (2005).

[100] D. Gromes, Zeit. Phys. **C11**, 147 (1981).

[101] L. von Smekal, R. Alkofer, and A. Hauck, Phys.Rev.Lett. **79**, 3591 (1997).

[102] C. Lerche and L. von Smekal, Phys.Rev. **D65**, 125006 (2002).

[103] J. M. Pawlowski, D. F. Litim, S. Nedelko, and L. von Smekal, Phys.Rev.Lett. **93**, 152002 (2004).

[104] R. Alkofer, C. S. Fischer, and F. J. Llanes-Estrada, Phys.Lett. **B611**, 279 (2005).

[105] A. Aguilar, D. Binosi, and J. Papavassiliou, Phys.Rev. **D78**, 025010 (2008).

[106] C. S. Fischer, A. Maas, and J. M. Pawlowski, Annals Phys. **324**, 2408 (2009).

[107] A. Cucchieri and T. Mendes, Phys.Rev.Lett. **100**, 241601 (2008a).

[108] A. Cucchieri and T. Mendes, Phys.Rev. **D78**, 094503 (2008b).

[109] A. Maas, Phys. Lett. **B689**, 107 (2010).

[110] A. Sternbeck and M. Müller-Preussker, in *Xth Quark Confinement and the Hadron Spectrum, Munich 2012* (2012).

[111] N. Alkofer and R. Alkofer, Phys.Lett. **B702**, 158 (2011).

[112] M. Flory, R. C. Helling, and C. Sluka, arXiv:1201.2714 [math-ph] (2012).

[113] R. Alkofer, C. S. Fischer, F. J. Llanes-Estrada, and K. Schwenzer, Annals Phys. **324**, 106 (2009a).

[114] L. Fister, R. Alkofer, and K. Schwenzer, Phys. Lett. **B688**, 237 (2010).

[115] M. Hopfer, Master's thesis, University of Graz (2011).

[116] D. Zwanziger, Nucl.Phys. **B378**, 525 (1992).

[117] D. Zwanziger, Nucl.Phys. **B399**, 477 (1993).

[118] D. Zwanziger, Phys.Lett. **B257**, 168 (1991).

[119] G. Kallen, Helv.Phys.Acta **25**, 417 (1952).

[120] H. Lehmann, Nuovo Cim. **11**, 342 (1954).

[121] G. 't Hooft, Nucl.Phys. **B138**, 1 (1978).

[122] G. Mack, DESY **03** (1980).

[123] H. B. Nielsen and P. Olesen, Nucl.Phys. **B160**, 380 (1979).

[124] J. Ambjorn and P. Olesen, Nucl.Phys. **B170**, 265 (1980).

[125] J. M. Cornwall, Nucl.Phys. **B157**, 392 (1979).

BIBLIOGRAPHY

[126] R. P. Feynman, Nucl.Phys. **B188**, 479 (1981).

[127] H. Shiba and T. Suzuki, Phys.Lett. **B333**, 461 (1994).

[128] G. Tiktopoulos, Phys.Lett. **B66**, 271 (1977).

[129] J. Greensite and C. B. Thorn, JHEP **0202**, 014 (2002).

[130] D. Zwanziger, Phys.Rev.Lett. **90**, 102001 (2003).

[131] L. Susskind, Phys.Rev. **D20**, 2610 (1979).

[132] J. Gasser and H. Leutwyler, Annals Phys. **158**, 142 (1984).

[133] J. Gasser and H. Leutwyler, Nucl.Phys. **B250**, 465 (1985).

[134] Y. Nambu and G. Jona-Lasinio, Phys.Rev. **122**, 345 (1961).

[135] M. Buballa, Phys. Rept. **407**, 205 (2005).

[136] D. U. Jungnickel and C. Wetterich, Phys. Rev. **D53**, 5142 (1996).

[137] R. D. Pisarski, Phys.Rev. **D62**, 111501 (2000).

[138] K. Fukushima and K. Ohta, J.Phys. **G26**, 1397 (2000).

[139] P. N. Meisinger and M. C. Ogilvie, Phys.Lett. **B379**, 163 (1996).

[140] P. N. Meisinger, T. R. Miller, and M. C. Ogilvie, Nucl.Phys.Proc.Suppl. **119**, 511 (2003).

[141] P. N. Meisinger, T. R. Miller, and M. C. Ogilvie, Nucl.Phys.Proc.Suppl. **129**, 563 (2004).

[142] K. Fukushima, Phys.Lett. **B591**, 277 (2004).

[143] E. Megias, E. Ruiz Arriola, and L. Salcedo, Phys.Rev. **D74**, 065005 (2006).

[144] C. Ratti, M. A. Thaler, and W. Weise, Phys.Rev. **D73**, 014019 (2006).

[145] S. K. Ghosh, T. K. Mukherjee, M. G. Mustafa, and R. Ray, Phys.Rev. **D73**, 114007 (2006).

[146] C. Sasaki, B. Friman, and K. Redlich, Phys.Rev. **D75**, 074013 (2007).

[147] B.-J. Schaefer, J. M. Pawlowski, and J. Wambach, Phys.Rev. **D76**, 074023 (2007).

[148] T. K. Herbst, J. M. Pawlowski, and B.-J. Schaefer, Phys.Lett. **B696**, 58 (2011).

[149] H. Gies and C. Wetterich, Phys.Rev. **D65**, 065001 (2002).

[150] S. Floerchinger and C. Wetterich, Phys.Lett. **B680**, 371 (2009).

[151] S. Floerchinger, Eur.Phys.J. **C69**, 119 (2010).

124

[152] H. Gies and C. Wetterich, Phys.Rev. **D69**, 025001 (2004).

[153] R. L. Stratonovich, Dokl. Akad., Nauk. SSR **115**, 1097 (1957).

[154] J. Hubbard, Phys.Rev.Lett. **3**, 77 (1959).

[155] J. Braun, L. Fister, L. Haas, and J. M. Pawlowski, in *ERG 2012, Aussois, France* (2012).

[156] J. Kapusta and C. Gale, *Finite-temperature field theory: Principles and applications* (Cambridge University Press, 2006),

[157] J. Zinn-Justin, Int.Ser.Monogr.Phys. **113**, 1 (2002).

[158] A. Pelissetto and E. Vicari, Phys. Rept. **368**, 549 (2002).

[159] B.-J. Schaefer and M. Wagner, arXiv:0812.2855 [hep-ph] (2008).

[160] K. Fukushima and T. Hatsuda, Rept.Prog.Phys. **74**, 014001 (2011).

[161] J. M. Pawlowski, AIP Conf.Proc. **1343**, 75 (2011).

[162] C. S. Fischer, A. Maas, and J. A. Muller, Eur.Phys.J. **C68**, 165 (2010).

[163] D. B. Kaplan, Lectures given at the Ecole d'Ete de Physique Theorique des Houches pp. 223–272 (2009).

[164] A. Bazavov, T. Bhattacharya, M. I. Buchoff, M. Cheng, N. H. Christ, H.-T. Ding, R. Gupta, P. Hegde, C. Jung, F. Karsch, et al. (HotQCD Collaboration) (2012a).

[165] G. Cossu, S. Aoki, S. Hashimoto, T. Kaneko, H. Matsufuru, et al., PoS **LATTICE2011**, 188 (2011).

[166] P. de Forcrand and O. Philipsen, Nucl.Phys. **B642**, 290 (2002).

[167] Y. Aoki, Z. Fodor, S. Katz, and K. Szabo, Phys.Lett. **B643**, 46 (2006).

[168] S. Borsanyi, G. Endrodi, Z. Fodor, C. Hoelbling, S. Katz, et al., J.Phys.Conf.Ser. **316**, 012020 (2011).

[169] A. Bazavov, T. Bhattacharya, M. Cheng, C. DeTar, H. Ding, et al., Phys.Rev. **D85**, 054503 (2012b).

[170] J. Braun and H. Gies, JHEP **0606**, 024 (2006).

[171] J. Braun and H. Gies, Phys.Lett. **B645**, 53 (2007).

[172] J. Braun, Eur.Phys.J. **C64**, 459 (2009).

[173] J. Braun and A. Janot, Phys.Rev. **D84**, 114022 (2011).

[174] J. Braun and T. K. Herbst, arXiv:1205.0779 [hep-ph] (2012).

[175] P. Chomaz, arXiv:0410024 [nucl-ex] (2004).

[176] M. Asakawa and K. Yazaki, Nucl.Phys. **A504**, 668 (1989).

[177] A. Barducci, R. Casalbuoni, S. De Curtis, R. Gatto, and G. Pettini, Phys.Lett. **B231**, 463 (1989).

[178] F. Wilczek, Int.J.Mod.Phys. **A7**, 3911 (1992).

[179] J. Berges and K. Rajagopal, Nucl.Phys. **B538**, 215 (1999).

[180] N. Strodthoff, B.-J. Schaefer, and L. von Smekal, Phys.Rev. **D85**, 074007 (2012).

[181] N. Khan, J. M. Pawlowski, F. Rennecke, and M. Scherer, in *ERG 2012, Aussois, France* (2012).

[182] S. Cotter, P. Giudice, S. Hands, and J.-I. Skullerud, arXiv:1210.4496 [hep-lat] (2012).

[183] M. G. Alford, A. Schmitt, K. Rajagopal, and T. Schafer, Rev.Mod.Phys. **80**, 1455 (2008).

[184] D. Nickel, J. Wambach, and R. Alkofer, Phys.Rev. **D73**, 114028 (2006a).

[185] D. Nickel, R. Alkofer, and J. Wambach, Phys.Rev. **D74**, 114015 (2006b).

[186] D. Nickel, R. Alkofer, and J. Wambach, Phys.Rev. **D77**, 114010 (2008).

[187] L. McLerran and R. D. Pisarski, Nucl.Phys. **A796**, 83 (2007).

[188] C. S. Fischer, J. Luecker, and J. A. Mueller, Phys.Lett. **B702**, 438 (2011).

[189] C. S. Fischer, J. Luecker, and J. Luecker, arXiv:1206.5191 [hep-ph] (2012).

[190] H. Heiselberg and M. Hjorth-Jensen, Phys.Rept. **328**, 237 (2000).

[191] M. D'Elia and M.-P. Lombardo, Phys.Rev. **D67**, 014505 (2003).

[192] P. de Forcrand and O. Philipsen, Nucl.Phys. **B673**, 170 (2003).

[193] P. de Forcrand and O. Philipsen, JHEP **0701**, 077 (2007).

[194] Z. Fodor and S. Katz, Phys.Lett. **B534**, 87 (2002).

[195] F. Karsch, C. Allton, S. Ejiri, S. Hands, O. Kaczmarek, et al., Nucl.Phys.Proc.Suppl. **129**, 614 (2004).

[196] Z. Fodor and S. Katz, JHEP **0404**, 050 (2004).

[197] Z. Fodor, C. Guse, S. D. Katz, and K. K. Szabo, PoS **LAT2007**, 189 (2007).

[198] R. Gavai and S. Gupta, Phys.Rev. **D78**, 114503 (2008).

[199] B.-J. Schaefer and J. Wambach, Phys.Rev. **D75**, 085015 (2007).

[200] C. S. Fischer and J. A. Mueller, Phys.Rev. **D84**, 054013 (2011).

[201] M. Hopfer, private communication, 2012.

[202] T. Csorgo, R. Vertesi, and J. Sziklai, Phys. Rev. Lett. **105**, 182301 (2010).

[203] E. V. Shuryak, Comments Nucl.Part.Phys. **21**, 235 (1994).

[204] S. Benic, D. Horvatic, D. Kekez, and D. Klabucar, Phys.Rev. **D84**, 016006 (2011).

[205] M. Cheng, S. Datta, A. Francis, J. van der Heide, C. Jung, et al., Eur.Phys.J. **C71**, 1564 (2011).

[206] H. Ohno, U. Heller, F. Karsch, and S. Mukherjee, PoS **LATTICE2011**, 210 (2011).

[207] J. I. Kapusta, D. Kharzeev, and L. D. McLerran, Phys.Rev. **D53**, 5028 (1996).

[208] C. Manuel and M. H. Tytgat, Phys.Lett. **B479**, 190 (2000).

[209] D. Son, M. A. Stephanov, and A. Zhitnitsky, Phys.Lett. **B510**, 167 (2001).

[210] T. Schafer, Phys.Rev. **D65**, 094033 (2002).

[211] T. Schafer, Phys.Rev. **D67**, 074502 (2003).

[212] J.-W. Chen, K. Fukushima, H. Kohyama, K. Ohnishi, and U. Raha, Phys. Rev. **D80**, 054012 (2009).

[213] B.-J. Schaefer and M. Wagner, Phys. Rev. **D79**, 014018 (2009).

[214] R. D. Pisarski and F. Wilczek, Phys. Rev. **D29**, 338 (1984).

[215] P. Bak, S. Krinsky, and D. Mukamel, Phys. Rev. Lett. **36**, 52 (1976).

[216] K. Fukushima, K. Kamikado, and B. Klein, Phys.Rev. **D83**, 116005 (2011).

[217] C. Alexandrou, A. Borici, A. Feo, P. de Forcrand, A. Galli, et al., Phys.Rev. **D60**, 034504 (1999).

[218] A. Dumitru, D. Roder, and J. Ruppert, Phys.Rev. **D70**, 074001 (2004).

[219] F. Karsch, E. Laermann, and C. Schmidt, Phys.Lett. **B520**, 41 (2001).

[220] M. Mitter and R. Alkofer, in preparation (2012).

[221] K. Osterwalder and E. Seiler, Annals Phys. **110**, 440 (1978).

[222] E. H. Fradkin and S. H. Shenker, Phys.Rev. **D19**, 3682 (1979).

[223] R. Alkofer, M. Q. Huber, and K. Schwenzer, Comput.Phys.Commun. **180**, 965 (2009b).

[224] M. Q. Huber and J. Braun, Comput.Phys.Commun. **183**, 1290 (2012).

[225] M. Q. Huber, K. Schwenzer, and R. Alkofer, Eur.Phys.J. **C68**, 581 (2010).

[226] V. Macher, A. Maas, and R. Alkofer, Int.J.Mod.Phys. **A27**, 1250098 (2012).

[227] L. Del Debbio, M. Faber, J. Greensite, and S. Olejnik, Phys.Rev. **D53**, 5891 (1996).

BIBLIOGRAPHY

[228] P. Cvitanovic, *Group theory: Birdtracks, Lie's and exceptional groups* (Princeton University Press, 2008),

[229] M. Hopfer, M. Mitter, B.-J. Schaefer, and R. Alkofer, arXiv:1211.0166 [hep-ph] (2012a).

[230] M. Mitter, M. Hopfer, B.-J. Schaefer, and R. Alkofer, in preparation (2012a).

[231] C. Gattringer, Phys. Rev. Lett. **97**, 032003 (2006).

[232] E. Bilgici, F. Bruckmann, C. Gattringer, and C. Hagen, Phys. Rev. **D77**, 094007 (2008).

[233] C. S. Fischer, Phys. Rev. Lett. **103**, 052003 (2009).

[234] C. S. Fischer and J. A. Mueller, Phys.Rev. **D80**, 074029 (2009).

[235] F. Synatschke, A. Wipf, and C. Wozar, Phys. Rev. **D75**, 114003 (2007).

[236] F. Synatschke, A. Wipf, and K. Langfeld, Phys. Rev. **D77**, 114018 (2008).

[237] J. S. Ball and T.-W. Chiu, Phys. Rev. **D22**, 2542 (1980).

[238] M. Hopfer, A. Windisch, and R. Alkofer, in *Xth Quark Confinement and the Hadron Spectrum, Munich* (2012b).

[239] A. Maas, J. Wambach, and R. Alkofer, Eur.Phys.J. **C42**, 93 (2005).

[240] A. Maas, arXiv:1106.3942 [hep-ph], Habilitation Thesis (2011).

[241] L. Fister and J. M. Pawlowski, arXiv:1112.5440 [hep-ph] (2011).

[242] C. S. Fischer and R. Alkofer, Phys. Rev. **D67**, 094020 (2003).

[243] C. S. Fischer, Ph.D. thesis, University of Tübingen (2003).

[244] M. Q. Huber and M. Mitter, Comput.Phys.Commun. **183**, 2441 (2012).

[245] M. Mitter, B.-J. Schaefer, N. Strodthoff, and L. von Smekal, in preparation (2012b).

[246] M. Mitter and B.-J. Schaefer, in preparation (2012).

[247] T. K. Herbst, Master's thesis, University of Graz (2009).

[248] M. Wagner, Ph.D. thesis, TU Darmstadt (2009).

[249] V. Skokov, B. Friman, E. Nakano, K. Redlich, and B.-J. Schaefer, Phys. Rev. **D82**, 034029 (2010).

[250] J. O. Andersen, R. Khan, and L. T. Kyllingstad, arXiv:1102.2779 [hep-ph] (2011).

[251] U. S. Gupta and V. K. Tiwari, Phys.Rev. **D85**, 014010 (2012).

[252] B.-J. Schaefer and J. Wambach, Phys. Part. Nucl. **39**, 1025 (2008).

[253] S. Weinberg, Phys. Rev. Lett. **18**, 188 (1967).

[254] J. Berges, D. U. Jungnickel, and C. Wetterich, Phys. Rev. **D59**, 034010 (1999).

[255] K. Hashimoto and T. Izubuchi, Prog. Theor. Phys. **119**, 599 (2008).

[256] J. M. Pawlowski, Phys. Rev. **D58**, 045011 (1998).

[257] D. F. Litim, Nucl. Phys. **B631**, 128 (2002).

[258] B.-J. Schaefer, M. Wagner, and J. Wambach, Phys.Rev. **D81**, 074013 (2010).

[259] H. Mao, J. Jin, and M. Huang, J.Phys.G **G37**, 035001 (2010).

[260] U. S. Gupta and V. K. Tiwari, Phys.Rev. **D81**, 054019 (2010).

[261] S. Chatterjee and K. A. Mohan, Phys.Rev. **D85**, 074018 (2012).

[262] B. Schaefer and M. Wagner, Phys.Rev. **D85**, 034027 (2012).

[263] V. Macher, A. Maas, and R. Alkofer, arXiv:1106.5381 [hep-ph] (2011).

[264] J. C. Bloch, PhD Thesis, University of Durham (1995).

[265] P. Deuflhard and A. Hohmann, *Numerische Mathematik I, Eine algorithmisch orientierte Einführung* (Gruyter, 2008).

Acknowledgments